NASA CR-132650

PROPAGATION SOUND AT MODERATE AND HIGH INTENSITIES IN ABSORBENT AND HARD-WALLED CYLINDRICAL DUCTS

by Oliver Herbert McDaniel

Prepared under Grant No. NGL 39-009-121 by
PENNSYLVANIA STATE UNIVERSITY
University Park, Pennsylvania

for

NATIONAL AERONAUTICS AND SPACE ADMINISTRATION

The Pennsylvania State University

The Graduate School

Propagation of Sound at Moderate and High Intensities in Absorbent and Hard-Walled Cylindrical Ducts

A Thesis in

Engineering Acoustics

by

Oliver Herbert McDaniel

Submitted in Partial Fulfillment
of the Requirements
for the Degree of

Doctor of Philosophy

March, 1975

Date of Approval:

_____

Gerhard Reethof
Alcoa Professor of Mechanical Engineering
Chairman of Committee
Thesis Advisor

_____

Jiri Tichy
Associate Professor of Architectural Engineering
Chairman of the Committee on Engineering Acoustics

ABSTRACT

The propagation of plane wave and higher order acoustic modes in both hard-walled and absorbent cylindrical ducts has been studied at moderate sound intensities where the linear wave equation is valid and at high intensities where nonlinear effects can be observed. The experiments were conducted with an anechoically terminated twelve-inch inside-diameter transite pipe. Various types of sound sources were mounted at one end of the duct to generate the desired acoustic fields within the duct. Arrays of conventional loudspeakers were used to generate plane waves and higher order acoustic modes at moderate intensities and an array of four high intensity electro-pneumatic sound sources were used for the experiments in the nonlinear region.

The attenuation of absorbent liners made of several different materials was obtained at moderate intensities for both plane waves and higher order modes and it was found that the characteristics of the liners studied did not change appreciably at high intensities. High intensity plane waves for the hard-walled case exhibited the familiar wave steepening effect in agreement with the Bessel-Fubini solution to the nonlinear plane wave equation. The harmonic frequencies of the sawtooth waves remained plane despite the fact that their frequencies were above the cutoff frequencies of many higher order modes. Wave steepening did not occur for higher order modes up to the maximum sound pressure level available of 175 dB re 0.0002 μ bar. The wave steepening is prevented by the dispersive nature of higher order mode propagation.

ACKNOWLEDGEMENTS

The author would first like to acknowledge the considerable assistance and encouragement provided by the Chairman of his Doctoral Committee, Dr. Gerhard Reethof. He is also grateful for the advice given to him by Drs. Eugen Skudrzyk and Jiri Tichy, whose knowledge and experience in the field of Acoustics have been of considerable assistance. He is especially indebted to Dr. Miles Pigott, who has given advice and encouragement throughout the Doctoral program and served as advisor in the first two years of study. The assistance given to him by Dr. John M. Seiner on many special problems deserves many thanks. He would also like to thank Mr. Robert Owens who provided considerable technical assistance and many helpful suggestions in the experimental phase of the program. The assistance of Mr. Ray Clark of the Brunswick Corporation in providing generous supplies of fiber metal materials is also gratefully acknowledged.

The research reported in this thesis has been predominantly supported by a grant from the National Science Foundation. The initial phases of the research were sponsored by the Naval Ordnance Systems Command and by the Langley Research Center of the National Aeronautics and Space Administration.

TABLE OF CONTENTS

LIST OF FIGURES

LIST OF FIGURES (CONTINUED)

LIST OF FIGURES (CONTINUED)

LIST OF FIGURES (CONTINUED)

CHAPTER I

INTRODUCTION

The radiation of undesirable acoustic energy from ducts is a frequently encountered noise control problem. Typical examples are the noise emitted from air conditioning ducts and from jet engine inlet and exhaust ducts. A frequent solution to these problems is to install acoustically absorbent liners in the ducts in order to attenuate the sound before it is radiated from the duct outlet.

The basic objective of this project is to study the attenuation characteristics of absorbent duct liners at moderate sound intensities where linear behavior can be expected and at high amplitudes where departures from linearity can occur. The initial phase of the research was to study the characteristics of absorbing materials suitable for use as duct liners. This included extensive measurements of a variety of materials using the impedance tube method to obtain normal incidence behavior and by a free-field method to obtain oblique incidence characteristics. A significant portion of the measurements included fiber metal materials suitable for jet engine noise control applications since the early phases of the project were sponsored by the National Aeronautics and Space Administration. These studies of the basic characteristics of sound absorbing materials were considerably extended by Kilmer and Wyerman and their results are reported in their Master's theses in References 1 and 2.

Much of the research on sound absorbing materials is applicable to such areas as architectural acoustics and machinery noise control;

however, the basic effort has been directed towards the use of these materials as duct liners. The most obvious applications are in air conditioning ducts, the intake and exhaust ducts of jet engines and in dissipative mufflers.

The analysis of the behavior of sound waves confined in a duct can present some challenging problems. The simplest case, that of an infinite, rigid-walled frictionless duct of uniform cross-section and diameter small compared to the wavelength has a solution familiar to everyone in the acoustics field. The result is the plane wave which travels at the velocity of sound with constant amplitude. We can add fluid losses (viscosity, heat conduction, molecular relaxation, and wall friction) and easily obtain a solution which predicts a plane wave with an additional exponential damping term. We can eliminate the long wavelength assumption and again relatively easily get an analytic solution which predicts plane wave and higher order mode propagation. We can eliminate the basic assumption of small amplitudes used in deriving the linear plane wave equation and, although somewhat complicated, can obtain approximate solutions to predict the nonlinear behavior of plane sound waves in a duct (assuming, of course, that the wavelength is long compared to the duct diameter). It is also relatively easy to analyze the propagation of sound in ducts of variable cross-sectional area provided that the area varies in certain specific ways; that is, exponential, square, and catenoidal area variation with distance down the duct. In this case, long wavelength and small amplitude assumptions are necessary.

Serious theoretical complications arise if any of the following situations exist:

1. When the wall has a finite impedance (a duct lined with absorbing material).
2. When the amplitude is high and the wavelength is of the order of the duct diameter or smaller.
3. If there are variations in duct cross-sectional area other than the simple cases mentioned above.
4. When there are bends or other discontinuities in the duct.
5. In the presence of flow in the duct.

The situation is further complicated if two or more of the above situations exist simultaneously. For the case of a jet engine inlet or exhaust duct with acoustic treatment,we are faced with all of the complications. The aircraft industry has conducted numerous research projects which attempt to combine all of these effects and the interpretation of the results is understandably difficult. We have taken the opposite approach in that we are studying each effect separately. The effort of the research reported in this thesis is directed toward the first two complications; that is,the effects of finite wall impedance and high amplitudes in the presence of higher order modes. The two phenomena have also been studied in combination. The effects of variable geometry (items 3 and 4 above) are being studied extensively by another member of the Noise Control Laboratory Staff (Roger Richards). It is hoped that the effects of flow will be the subject of a future research project.

In the following sections of this thesis, we will present the theory necessary to understand acoustic wave propagation in cylindrical ducts of finite wall impedance, examine in detail the theoretical aspects of high amplitude sound wave propagation and then discuss the

properties of sound absorbing materials. The experimental results of this study will then be presented and will include measurements in hard walled and lined ducts for plane waves and higher order modes in both the linear and nonlinear regions.

The research topic presented in this introduction is broad in scope and, as stated above, is the subject of several other thesis research efforts at this University. The topic has also been extensively explored by many other research organizations. It is therefore appropriate at this point to state the specific experimental goals of this thesis effort as follows:

1. The development of a method for determining the attenuation of duct liners which includes a realistic comparison with theoretical treatment.
2. The design and construction of a facility for generation of high amplitude acoustic waves in large cylindrical ducts.
3. The extension of both of the above experimental techniques to higher order duct modes.
4. The verification of plane wave finite amplitude theory for large ducts.
5. An investigation into the behavior of higher order modes at high intensities.
6. An experimental determination of the behavior of several duct liners at high intensities for both plane waves and higher order modes.

CHAPTER II

LINEAR WAVEGUIDE THEORY

It is well known that higher order acoustic modes exist in hollow ducts above certain frequencies (known as cut-off frequencies) and that these frequencies are a function of the cross-sectional dimensions of the duct. These higher order modes can be obtained from the results of the solution of the three-dimensional wave equation in the particular coordinate system appropriate to the duct geometry. This study is restricted to constant diameter cylindrical ducts and we will use cylindrical polar coordinates as shown in Figure 1.

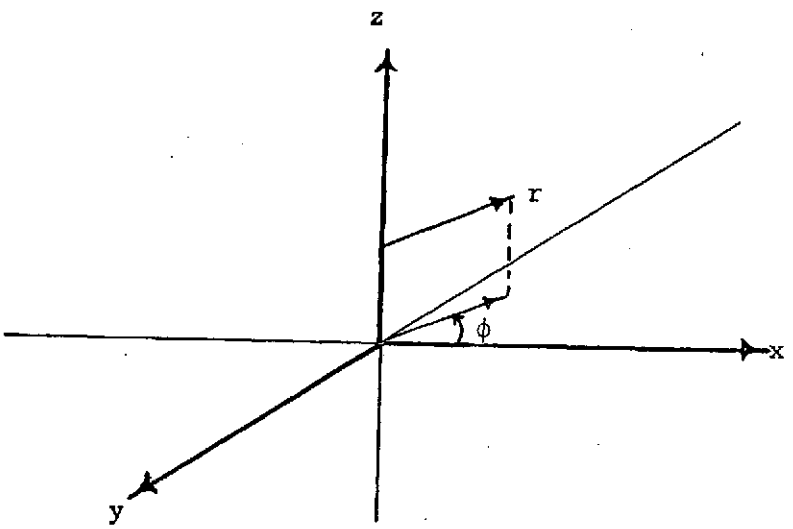

Figure 1 Cylindrical Coordinate System

In our case, the z-axis will be the axis of the cylinder. The three-dimensional wave equation in cylindrical polar coordinates is as follows:

$$\frac{\partial^2 p}{\partial r^2} + \frac{1}{r}\frac{\partial p}{\partial r} + \frac{1}{r^2}\frac{\partial^2 p}{\partial \phi^2} + \frac{\partial^2 p}{\partial z^2} = \frac{1}{c^2}\frac{\partial^2 p}{\partial t^2} \quad , \tag{2-1}$$

where p is the sound pressure, r, ϕ and z are the coordinates defined in Figure 1 and t is time. This equation is readily solved by the method of separation of variables (see Reference 3, page 429) yielding a solution of the form

$$p = R(r)\, Z(z)\, \Phi(\phi)\, T(t) \quad , \tag{2-2}$$

where the functions R, Z, Φ, and T are determined from the following partial differential equations:

$$\frac{\partial^2 T}{\partial t^2} = -\omega^2 T \quad , \tag{2-3}$$

$$\frac{\partial^2 Z}{\partial z^2} = -k_z^2 Z \quad , \tag{2-4}$$

$$\frac{\partial^2 \Phi}{\partial \phi^2} = -m^2 \psi \tag{2-5}$$

and

$$\frac{1}{R}\left(\frac{\partial^2 R}{\partial r^2} + \frac{1}{r}\frac{\partial R}{\partial r}\right) + k_r^2 - \frac{m^2}{r^2} = 0 \quad , \tag{2-6}$$

where ω = angular frequency, and

m = a constant.

The constants k_z and k_r are wave numbers related as follows:

$$k^2 = \frac{\omega^2}{c^2} = k_z^2 + k_r^2 \quad , \tag{2-7}$$

where c is the velocity of sound.

Equations (2-3)-(2-5) are all forms of the Helmholtz equation and for a <u>single</u> progressive wave have solutions of the form

$$T = \bar{A}\, e^{j\omega t} , \tag{2-8}$$

$$Z = \bar{B}\, e^{-jk_z z} \tag{2-9}$$

and

$$\Phi = \bar{C}\, e^{jm\phi} . \tag{2-10}$$

$\bar{A}$, $\bar{B}$, and $\bar{C}$ are constants and the bar denotes that they may be complex.

Equation (2-6) is Bessel's equation. Solutions to Bessel's equation (see Reference 4, Chapter XII) are the Bessel functions of the first, second and third kinds which are also called Bessel functions, Neumann functions and Hankel functions, respectively. The functions are defined by infinite series resulting from solutions to Bessel's equation by the method of infinite series. These functions are extensively tabulated in mathematical handbooks. Solutions can, of course, also be linear combinations of any of the three kinds of Bessel functions. The choice of the kind of function in any particular problem is based on physical arguments. We can easily show that, for our case, the Bessel function of the first kind, J_m, is the proper choice. The Bessel function of the second kind, (or Neumann function) N_m, is excluded since it is infinite at the origin. It could not be excluded if, for example, we had an annular duct. The two types of Hankel functions $H_m^{(1)}$ and $H_m^{(2)}$ are excluded for the same reason since

$$H_m^{(1)} = J_m - jN_m \tag{2-11}$$

and

$$H_m^{(2)} = J_m + jN_m . \tag{2-12}$$

It is interesting to note that the same solution, Equation (2-2), applies to the sound field exterior to a rigid infinite cylinder; however, in this case, the solution is given by Hankel functions since the origin is excluded and these functions have the proper behavior for large argument.

The solution appropriate for our problem can now be written from Equations (2-2), (2-8), (2-9) and (2-10) as follows:

$$p = P_m J_m(k_r r)\, e^{j(\omega t - k_z z + m\phi)} \quad . \tag{2-13}$$

We will see later that Equation (2-13) must be in the form of a double infinite series.

There is no requirement in the solution to Bessel's equation that m be of integer value or even real; however, we can argue on physical grounds that this must be the case here. The value of p must be the same for successive 360° rotations in ϕ if r and z are fixed. This must be true since in each case we are returning to the same point in space. The variable m must therefore be an integer number. For the same reason, m must also be real.

The quantities r, ϕ, z and t must, of course, be real but there is no such restriction on p_m, k_r or k_z and we will see later that these quantities can be complex and that J_m can therefore have a complex argument. The variable m can have any integer value from zero to infinity so that Equation (2-13) becomes:

$$p = \sum_{m=0}^{\infty} P_m J_m(k_r r)\, e^{j(\omega t - k_z z + m\phi)} \quad . \tag{2-14}$$

We can show that k_r and, hence, k_z also have an infinite number of values by applying the boundary condition of a rigid duct wall.

Under this condition, the normal component of the sound particle velocity at the wall is zero. The relationship between sound pressure and sound particle velocity is

$$\bar{v} = \frac{j}{k\rho c} \nabla p \quad , \tag{2-15}$$

where $\bar{v}$ = sound particle velocity,

$k = \omega/c$,

ρ = density,

c = velocity of sound

and ∇ = gradient operator.

The normal component for our case is given by

$$\bar{v}_n = \frac{j}{k\rho c} \frac{\partial p}{\partial r} \quad . \tag{2-16}$$

From Equation (2-13) and our boundary condition,

$$\frac{\partial}{\partial r} J_m(k_r r)\Big|_{r=r_o} = 0 \quad , \tag{2-17}$$

where r_o is the duct radius.

The properties of several of the Bessel functions are shown in Figure 2.

For each function, there is a series of oscillations about the kr axis and Equation (2-17) is satisfied at each point where the slope of J_m is zero. A value for k_r therefore exists at each of these zero slope points for each J_m. It is therefore appropriate to introduce another integer running index, n, to specify which of the succeeding slope points is taken and to change k_r to k_{mn}. Since there are an infinite number of zero slope points, Equation (2-14) is actually a double infinite series and becomes:

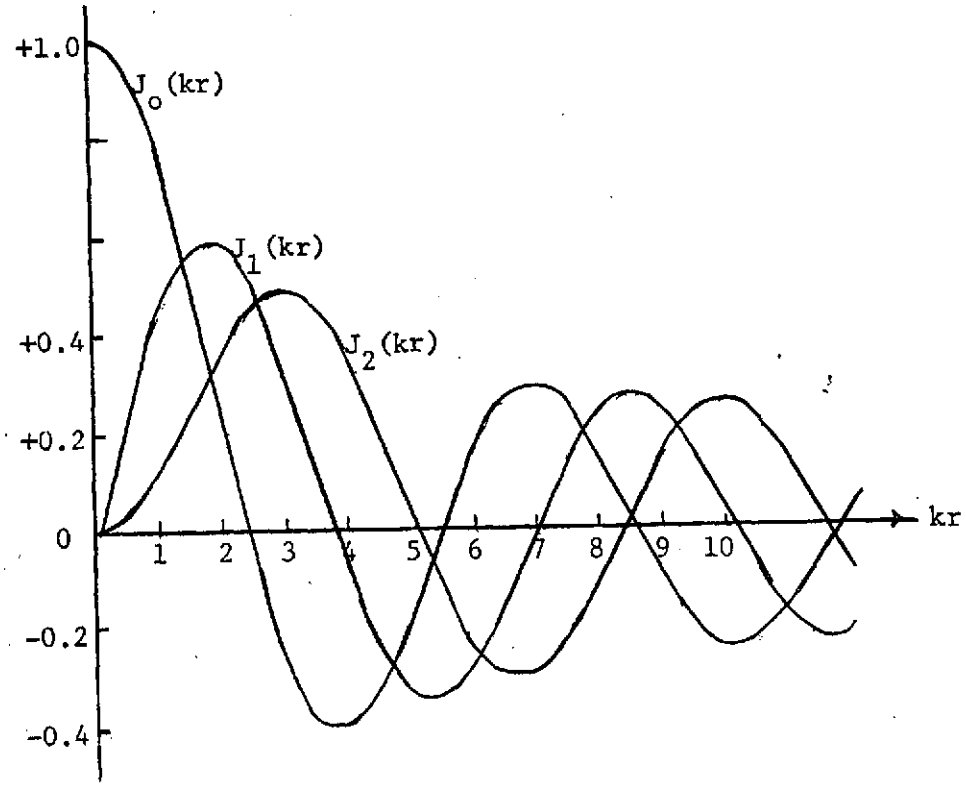

Figure 2 Properties of Several Bessel Functions of the First Kind

$$p = \sum_{m=0}^{\infty} \sum_{n=0}^{\infty} P_{mn} J_m(k_{mn} r) e^{j(\omega t - k_z z + m\phi)} . \qquad (2\text{-}18)$$

Each integer pair mn defines a particular mode of the solution. The m determines which of the J_m functions is specified and the n determines which of the succeeding zero slope points is specified; thus, determining what k_{mn} will be. Since

$$k_z = \sqrt{k^2 - k_{mn}^2} . \qquad (2\text{-}19)$$

both k_z and k_{mn} are uniquely determined, for a given r_o, by m and n.

From Figure 2, J_o has zero slope and a finite value at the origin and therefore represents a solution. In this case, $k_{mn} r_o = 0$ and therefore $k_{mn} = 0$. This is the m=0, n=0 mode. In this case, $k_z = k$ and the solution is

$$p = P_o e^{j(\omega t - k_z)} ,$$

which is the familiar plane wave. This is the only solution for $k_{mn} r_o = 0$ since J_1 has finite slope at the origin and although J_m for m=2, 3,..., ∞, have zero slope at the origin, the values of the functions there are zero and represent trivial solutions (i.e., p=0). This means that there are no higher modes without a radial amplitude dependence.

There is some confusion in the literature concerning the labeling of modes for n=0 and n=1. Often n is specified as zero for the first non-trivial solution. The various modes are easier to visualize if we specify n=1 for the first mode in each case with radial amplitude dependence. This means that the m=1, n=0 mode does

not exist and that the m=2, 3,..., ∞, n=0 modes are trivial solutions. In this way, the value of n will be equal to the number of nodes between r=0 and $r=r_o$. Several mode shapes (sound pressure amplitude as a function of r for fixed z, ϕ, t) are shown in Figure 3.

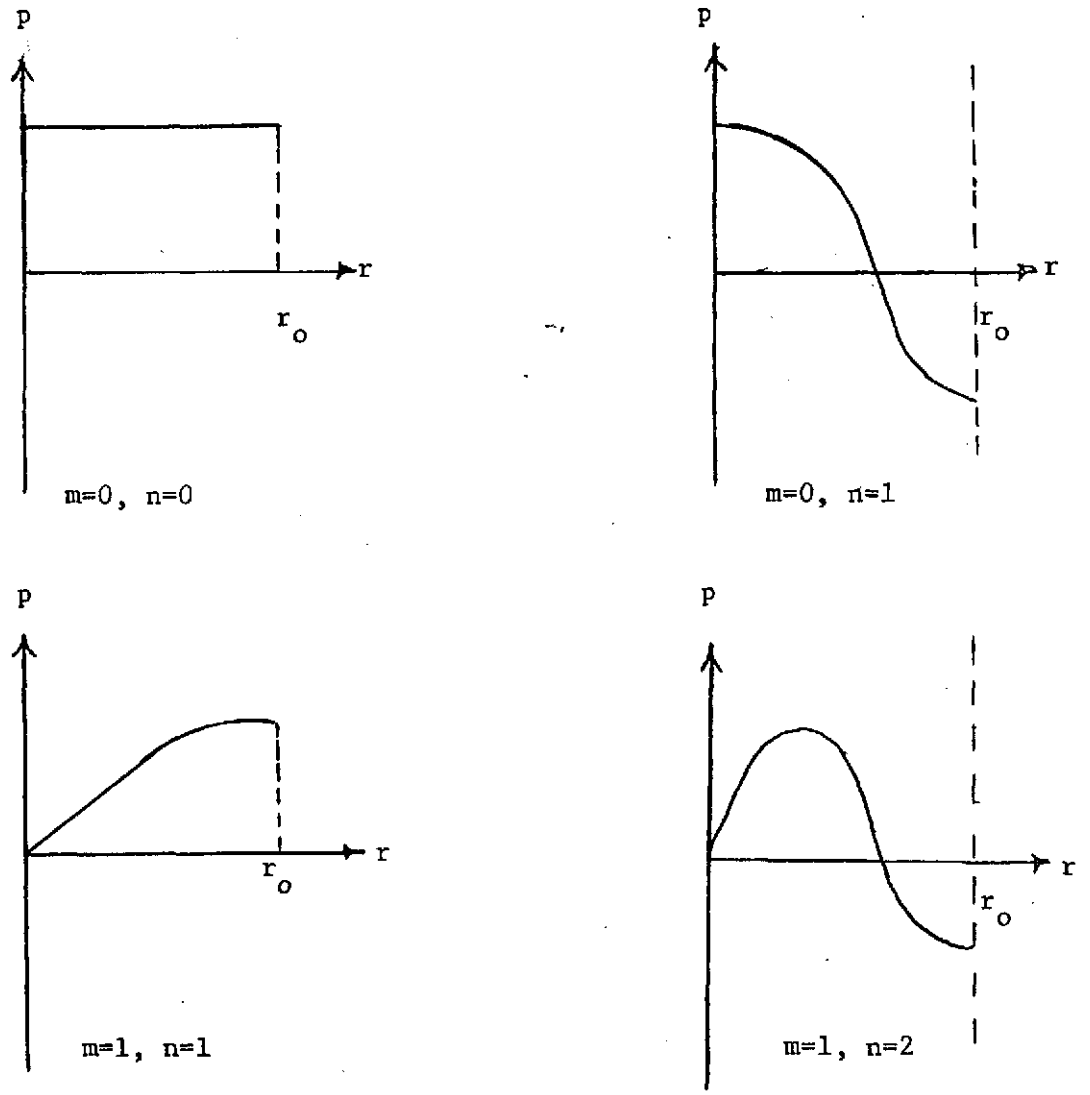

Figure 3 Mode Shapes of Several Higher Order Cylindrical Modes

It can be seen from the solution, Equation (2-18), and the characteristics of the Bessel functions in Figure 2 that there are three distinct types of modes. First, there is the plane wave case (and there is, of course, only one mode of this type [m=0, n=0]) which has no radial or circumferential dependence. Then, there are all of the modes for which m=0 and n=1, ..., ∞. All of these modes have a maximum at r=0 and one or more node lines between r=0 and $r=r_o$. These modes have no circumferential phase dependence. The third type of modes are where m=1, 2,..., ∞ and n=1, 2, ..., ∞. They always have a node at $r=r_o$ and n-1 nodes in the region $0 < r < r_o$. They also have a circumferential phase dependence (see Equation [2-18]), and are frequently called "spinning" or spiral modes. All of the modes, except for the plane wave, are referred to as higher order modes.

The wavenumber k_z determines the nature of propagation in the z direction. From Equation (2-19),

$$k_z = \sqrt{\frac{\omega^2}{c^2} - k_{mn}^2} \quad . \tag{2-20}$$

For a given k_{mn} and for sufficiently small ω, k_z will be imaginary and, from Equation (2-18), the wave will be exponentially damped. This is the region where $\frac{\omega^2}{c^2} < k_{mn}^2$. When $\frac{\omega^2}{c^2} = k_{mn}^2$, $k_z = 0$, and the wave has no z dependence. The frequency at which this occurs is called the cut-off frequency f_c and is given by

$$f_c = \frac{\omega_c}{2\pi} = \frac{ck_{mn}}{2\pi} \quad . \tag{2-21}$$

Each mode has an associated cut-off frequency. Each cut-off frequency is a function of the duct diameter and the value of m and n. The cut-off frequency increases with increasing values of m and n.

For a given mode, k_z is real above f_c and there is undamped wave propagation. The propagation is, however, dispersive; that is, the phase and group velocities in the z direction are frequency dependent. This can be seen from Equation (2-20). The phase velocity c_p which is the velocity at which points of constant phase travel in the z direction is given by

$$c_p = \frac{\omega}{k_z} = \frac{\omega}{\sqrt{\frac{\omega^2}{c^2} - k_{mn}^2}} \quad . \tag{2-22}$$

At cut-off, the phase velocity is infinite and if we re-arrange Equation (2-22)

$$c_p = \frac{1}{\sqrt{\frac{1}{c^2} - \frac{k_{mn}^2}{\omega^2}}} \quad , \tag{2-23}$$

it can be seen that as $\omega \to \infty$, c_p approaches the ordinary sound velocity c. Infinite phase velocity does not imply that we are violating the laws of relativity since it does not describe the velocity of energy transport. This is described (see Reference 5, page 110) by the group velocity c_g where

$$c_g = \frac{\partial \omega}{\partial k_z} \quad . \tag{2-24}$$

If we rearrange Equation (2-22), perform the derivative indicated in Equation (2-24), and do some algebraic manipulation, we obtain an expression for the group velocity as follows:

$$c_g = c \sqrt{1 - \frac{c^2}{\omega^2} k_{mn}^2} \quad . \tag{2-25}$$

From Equation (2-25), we can see that at cut-off where $k_z=0$ or $k_{mn} = \frac{\omega}{c}$ the group velocity is zero and from Equation (2-25) that as $\omega \to \infty$, c_g approaches c. The behavior of the phase and group velocities is shown in Figure 4.

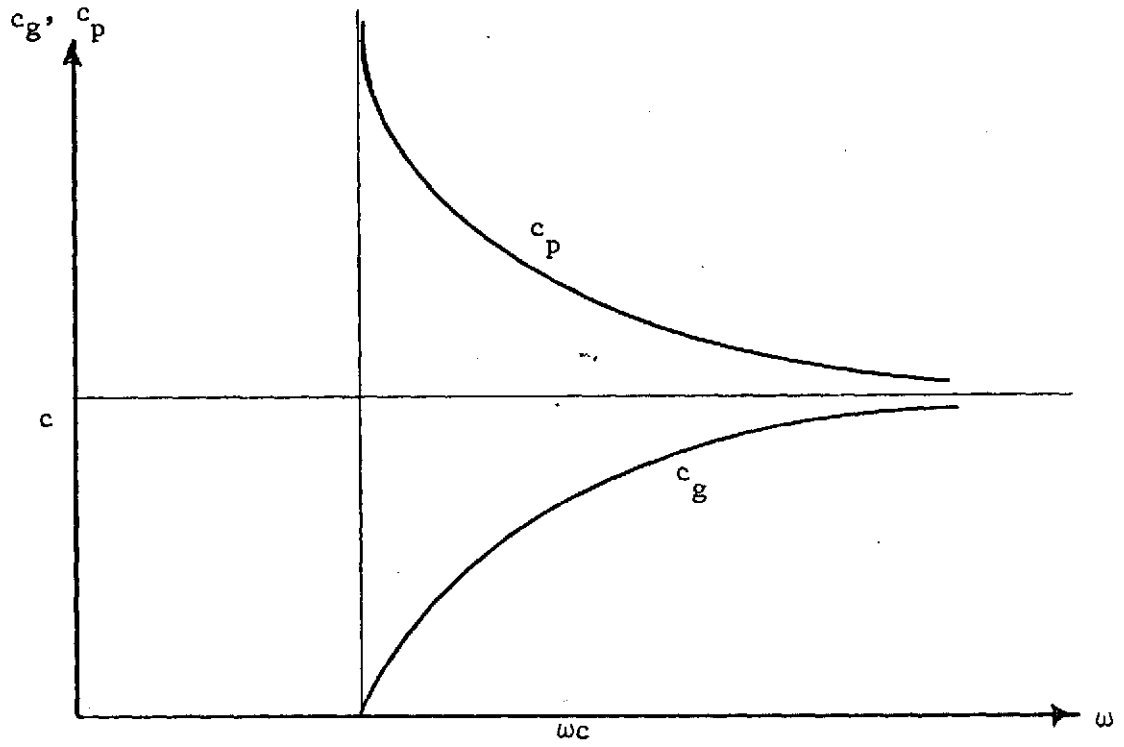

Figure 4 Dispersion of a Higher Order Mode

At cut-off, there is no net transport of energy and the waves remain in the duct in the form of a standing wave. Without dissipative effects the acoustic energy is pure reactive. Intuitively, it is obvious that high energy absorption will occur at cut-off if the duct walls are absorptive.

Many modes can exist simultaneously and the modal distribution is a function of the duct diameter and the frequency and spacial phase and amplitude of the source exciting the sound wave in the duct. As an example, Figure 5 illustrates the frequency regions in which several modes can propagate in a 12-inch diameter rigid walled duct.

It can be seen from Figure 5 that there are frequency regions where only a few modes can exist and other regions where many modes can exist simultaneously.

All of the above discussion following Equation (2-14) pertains to a rigid walled duct; however, Equation (2-14) and the development preceding it are valid without regard to specification of the nature of the wall impedance. If a duct is lined with absorbing material,we cannot use the simple boundary condition that the normal components of the particle velocity is zero at the wall. The problem of finding the wave-numbers now becomes considerably more complicated. At this point,we no longer have the clear proof that n is an integer but it will be assumed for now that this is still true. This implies that we still have discrete solutions for the wavenumbers. It is clear that m must still be an integer. Another important assumption will be made; that is, that the absorptive lining is locally reacting. This means that the behavior of the material is completely determined from its normal impedance, Z_n, where Z_n is defined by

$$Z_n = \frac{p}{v_n} \quad , \tag{2-26}$$

where $Z_n = R + jX$,

R = the resistive component of Z_n, and

X = the reactive component of Z_n.

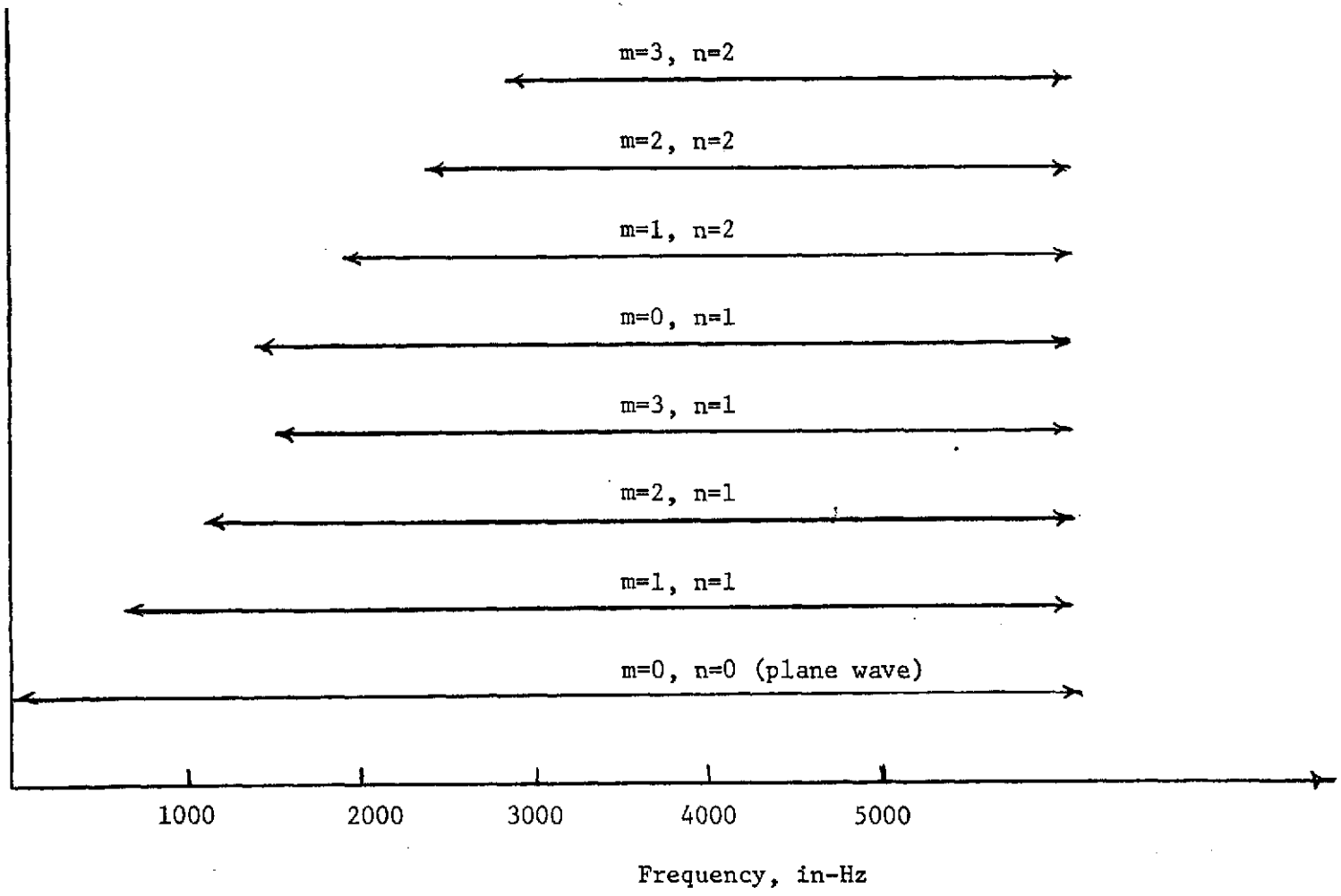

Figure 5 Frequency Regions of Allowed Propagation for Various Modes

From Equations (2-14) and (2-15), the new boundary conditions is

$$\frac{p}{v_n} = \left.\frac{k\rho c\, J_m(k_{mn}r)}{j\,\frac{\partial}{\partial r} J_m(k_{mn}r)}\right|_{r=r_o} = Z_n \quad . \tag{2-27}$$

Derivatives of the Bessel Function J_m have the following property (see Reference 6, page 188) for integer m:

$$\frac{d}{dx} J_m(ax) = \frac{1}{2a}\left[J_{m-1}(ax) - J_{m+1}(ax)\right] \quad . \tag{2-28}$$

Equation (2-28) can be simplified by the use of the relation below:

$$J_{m-1}(x) + J_{m+1}(x) = \frac{2m}{x} J_m(x) \quad . \tag{2-29}$$

Combining Equations (2-28) and (2-29),

$$\frac{d}{dx} J_m(ax) = \frac{1}{a}\left[\frac{m}{ax} J_m(ax) - J_{m+1}(ax)\right] \quad . \tag{2-30}$$

The above expression can be substituted into Equation (2-27) yielding the boundary condition

$$\frac{kk_{mn}\rho c\, J_m(k_{mn}r_o)}{j\left[\frac{m}{k_{mn}r} J_m(k_{mn}r_o) - J_{m+1}(k_{mn}r_o)\right]} = Z_n \quad . \tag{2-31}$$

For a given k, ρ, c, r_o, and Z_n k_{mn} is the only unknown in Equation (2-31) and represents the eigenvalues of the problem. Since Z_n is, in general complex, k_{mn} and J_m will be complex. The major consequence of J_m being complex is that the mode shape, the dependence of p on r, will be different from the hard walled case. The fact that k_{mn} is complex has an additional important consequence

since k_z is a function of k_{mn} and will therefore be complex as

$$\bar{k}_z = k_z + j\alpha_z , \tag{2-32}$$

where $\bar{k}_z$ = complex longitudinal wave number

k_z = real part of $\bar{k}_z$

α_z = imaginary part of $\bar{k}_z$.

Since p has the following z dependence

$$p(z) = Ae^{-j\bar{k}_z z} \tag{2-33}$$

α_z represents a damping term and must always have a negative sign to provide an exponentially decreasing rather than increasing value of p with increasing z. It is obvious that α_z represents the liner attenuation. This is the quantity with which we are most concerned and can be found by solving Equation (2-31). This equation has no exact solution and approximate solutions to this boundary value problem will be the subject of a later study.

CHAPTER III

NONLINEAR ACOUSTICS

Wave equations used in acoustics are derived from three equations from Fluid Mechanics and Thermodynamics and all of these equations are usually nonlinear. The three equations required are:

1. An equation of motion.
2. A continuity equation.
3. An equation which describes the proper relationship between pressure and density applicable to the problem.

The arguments used in elementary textbooks in acoustics to linearize these equations is quite familiar and will be briefly discussed later. There are many situations where these equations cannot be linearized and this gives rise to three distinct nonlinear acoustic phenomena:

1. Cavitation.
2. Acoustic Streaming.
3. Finite Amplitude Waves.

Acoustic cavitation is a phenomena restricted to liquids and occurs when the intensity of the acoustic wave is sufficiently high to cause stresses which exceed the liquid's tensile strength. The liquid ruptures forming cavities filled with the fluid in its gaseous state. These cavities continuously form and collapse with the oscillations of the acoustic wave. Cavitation is of no concern in the present study since we are restricted to air as our acoustic medium. It has, however, been the subject of extensive research primarily in the ultrasonic region (see, for example, Reference 7).

Streaming can occur in liquids and gases and is often observed with high intensity sound waves. It is characterized by a net flow of the fluid in the direction of wave propagation. The resulting flow velocities are small and are of little importance in this study since our ultimate application is towards liners for situations where the mean flow is much greater than the flow due to streaming. This interesting subject has also been extensively studied and an excellent summary is contained in Reference 8.

The third phenomenon, finite amplitude waves, is of significant importance in this research since sound levels are encountered in situations such as a jet engine inlet and internal combustion engine exhaust where the effect can be quite pronounced. The term finite amplitude is used to denote acoustic waves of sufficiently high amplitude where a certain nonlinear effect occurs as opposed to infinitesimal waves where linear behavior is observed.

A thorough summary of plane lossless finite amplitude waves is given by Blackstock in Reference 9. In this paper, Blackstock points out that, although the subject has been given relatively little attention in modern times, the theoretical foundation which explains the phenomena was discovered early in the nineteenth century by Poisson, Stokes and others.

Finite amplitude waves result from the following fact: An initially sinusoidal plane progressive sound wave of any intensity will not retain its sinusoidal shape in a dissipationless medium. This can be shown by a purely physical argument with the aid of Figure 6.

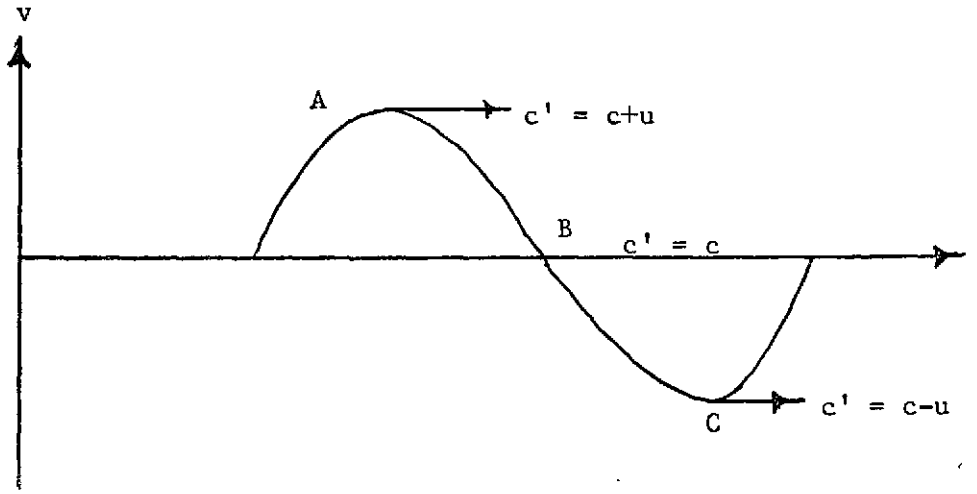

Figure 6 Distortion of a Finite Amplitude Wave

c' = instantaneous phase velocity

c = velocity of sound

u = peak velocity of a piston source x=0。

The sound velocity in a fluid is given by the relation

$$c^2 = \left(\frac{\partial p}{\partial \rho}\right)_S \quad , \tag{3-1}$$

where p = pressure,

ρ = density,

and S = entropy.

For an isentropic process in an ideal gas,the pressure density relationship

$$\frac{p}{p_o} = \left(\frac{\rho}{\rho_o}\right)^{\gamma} \tag{3-2}$$

is nonlinear and c_1 therefore varies with the instantaneous amplitude of the wave. The constant γ is the ratio of specific heats and p_o and ρ_o are the equilibrium values of the pressure and density. The exact manner in which c varies is found by substituting Equation (3-2) into Equation (3-1) yielding,

$$c^2 = \frac{\gamma p_o}{\rho^\gamma} \rho^{\gamma-1} \qquad (3-3)$$

Since γ is always greater than unity the sound speed at constant temperature always increases with increasing density and pressure. This means that the peak of a sound wave travels faster than the trough resulting in a progressive distortion and steepening of the waveform.

There is also an additional distortion mechanism. The initial particle velocity, u, causes the peak of the wave to move faster than the mean sound velocity and the trough to move slower. This can be considered as a convection effect but should not be confused with streaming since there is no net motion of the fluid. Lighthill (Reference 10) has somewhat incorrectly referred to the combined effect (the nonlinear p, ρ relationship and the convection effect) as "convection of sound."

Referring to Figure 6, the peak of the wave (point A) is accelerated since c' is increased due to an increase in c and the addition of u. At the trough (point C) the wave is retarded since c decreases and u is subtracted. In region B, $\rho=\rho_o$ and $c^2 = c_o^2 = \frac{\gamma p_o}{\rho_o}$ which is the ordinary infinitesimal sound speed. The group velocity of the wave is therefore c_o.

The distortion process is cumulative; that is, the wave becomes more and more distorted with each cycle. We could continue the argument to a point where the wave becomes multivalued as shown in Figure 7 but this is physically impossible.

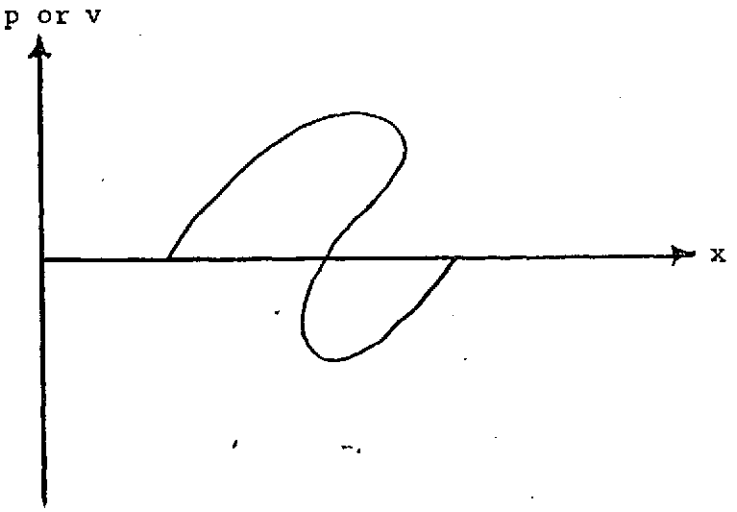

Figure 7 Multi-Valued Distortion

Solutions to the exact dissipationless plane wave equation also yield physically impossible solutions at large distances. In order to predict the correct behavior at large distances, the dissipationless assumption must be discarded and losses in the fluid due to viscosity, heat conduction and molecular relaxation must be taken into account. There are many regions of interest, however, where the dissipationless assumption is valid.

In order to obtain solutions which theoretically predict the behavior of finite amplitude waves, one must derive wave equations from the hydrodynamic equations in their original non-linearized form. The exact plane wave equation for an ideal gas can be easily derived (see Reference 11) from the continuity equation,

$$\rho = \rho_o \left(1 + \frac{\partial \xi}{\partial x}\right)^{-1} \quad , \tag{3-4}$$

Euler's equation

$$\frac{\partial^2 \xi}{\partial t^2} + \frac{1}{} \frac{\partial p}{\partial x} = 0 \quad , \tag{3-5}$$

and the adiabatic pressure-density relationship

$$\frac{p}{p_o} = \left(\frac{\rho}{\rho_o}\right)^{\gamma} \quad , \tag{3-2}$$

where ξ = particle displacement, and

x = spacial coordinate.

First substitute Equation (3-4) into Equation (3-2):

$$\frac{p}{p_o} = \left[\left(1 + \frac{\partial \xi}{\partial x}\right)^{-1}\right]^{\gamma}$$

or

$$p = p_o \left(1 + \frac{\partial \xi}{\partial x}\right)^{-\gamma} \quad . \tag{3-6}$$

Next substitute Equation (3-6) into Equation (3-5),

$$\rho_o \frac{\partial^2 \xi}{\partial t^2} = - \frac{\partial}{\partial x} p_o \left(1 + \frac{\partial \xi}{\partial x}\right)^{-\gamma} = p_o \gamma \frac{\partial^2 \xi}{\partial x^2} \left(1 + \frac{\partial \xi}{\partial x}\right)^{-\gamma-1} \quad .$$

Rearranging and substituting $c_o^2 = \frac{p_o \gamma}{\rho_o}$ results in the exact plane wave equation for an ideal gas,

$$\frac{\partial^2 \xi}{\partial x^2} = \frac{\left(1 + \frac{\partial \xi}{\partial x}\right)^{\gamma+1}}{c_o^2} \frac{\partial^2 \xi}{\partial t^2} \quad . \tag{3-7}$$

If we substitute

$$c^2 = \frac{c_o^2}{\left(1 + \frac{\partial \xi}{\partial x}\right)^{\gamma+1}} \quad , \tag{3-8}$$

Equation (2-7) becomes:

$$\frac{\partial^2 \xi}{\partial x^2} = \frac{1}{c^2} \frac{\partial^2 \xi}{\partial t^2} \quad , \tag{3-9}$$

which has the same form as the ordinary linear plane wave equation except that c, in this case is varying in time and space. This is in keeping with our earlier physical argument that the instantaneous phase velocity is varying over the cycle resulting in progressive distortion. Solutions to Equation (3-7) predict progressive distortion up to a value of x where the solution is discontinuous. This distance is known as the discontinuity distance $\bar{x}$ and corresponds to the point in our physical argument where the wave becomes multi-valued. The value of $\bar{x}$ is a function of the initial amplitude and frequency of the wave. The solution is invalid beyond the discontinuity distance.

A good physical analogy to a finite amplitude wave is a water wave propagating towards a shallow beach. Due to the proximity of the bottom, the trough of the wave travels with a lower velocity than the crest. In this case, the shape of the wave actually becomes double valued, overtakes itself and forms a "breaker." In the case of a distorting sound wave, a shock wave eventually forms. This occurs at the discontinuity distance. At this point, the wave has a sawtooth or N shape. Dissipative effects exactly balance the distortion producing mechanism and the wave travels as a stable

sawtooth. Beyond this region the sawtooth shape eventually decays to a sine wave at reduced amplitude.

As stated before, Equation (3-7) will not predict the behavior beyond $\bar{x}$ and a more complicated equation must be used which accounts for dissipative effects.

Equation (3-7) predicts progressive distortion regardless of initial amplitude provided that the distance from the source is sufficiently great. Recall that $\bar{x}$ increases linearly with decreasing initial amplitude. It therefore, appears at first that for a large enough x, the linear wave equation

$$\frac{\partial^2 \xi}{\partial x^2} = \frac{1}{c_o^2} \frac{\partial^2 \xi}{\partial t^2} \tag{3-10}$$

is never correct for large distances even at very small amplitudes. Dissipative effect (present in all real fluids), however, gets us out of this difficulty. These effects are due to viscosity, heat conduction and molecular relaxation. The subject is discussed in detail in Chapters 9 and 12 of Reference 5 by Lindsay. The dissipative effects result in an exponential damping of the sound wave with distance and result from the fact that our original assumptions in deriving lossless wave equations is slightly incorrect. These assumptions are:

1. That the thermodynamic process is adiabatic.
2. That there are no shear forces.
3. That the sound wave is not affected by the molecular structure of the fluid.

If we assume that we have a viscous, heat conducting medium and have measured these properties, then we can modify the thermodynamic

process equation, Euler's equation, for example, Equations (3-5) and (3-6), and obtain a wave equation which takes these factors into account. The equations can be linearized and a linear solution which is exponentially damped with distance results. The damping constant or "absorption coefficient" is a function of the shear viscosity, the heat conduction coefficient, and the square of the frequency. The solution is in agreement with measurements for a few fluids but predicts a coefficient much too small for the majority of fluids. The excess absorption is not due, in this case, to nonlinear effects but to the above mentioned molecular relaxation. This additional absorption mechanism can be accounted for by adding a "bulk viscosity" term but must usually be determined by measurement of actual absorption coefficients versus frequency for the fluid of interest. The absorption due to viscosity and heat conduction are known as "classical absorption" and the effect of molecular relaxation is to increase the actual absorption coefficient at all frequencies near or below the relaxation frequency of the particular molecular process. Above the relaxation frequency, the absorption coefficient returns to the classical absorption value. At sufficiently low amplitudes, sound waves obey the modified linear wave equation which accounts for dissipation and no indication of progressive distortion occurs regardless of propagation distance. For sufficiently small amplitudes and long propagating distances, the absorption of the harmonics produced by finite amplitude effects counterbalances their growth and the harmonics cannot be observed. Since the absorption coefficient is proportional to $(\omega^2 x)$, the medium acts like a low-pass filter and the wave remains sinusoidal. At high amplitudes, the growth of the harmonics is so rapid with

distance that the absorption mechanism which is proportional to distance cannot act on the wave to prevent the sawtooth formation. The role of absorption for the high amplitude case is, as stated before, to act in the shock region (beyond $x=\bar{x}$) to provide a stable decoying sawtooth in the region where solutions to the exact dissipationless wave equation are invalid. It is apparent from the above discussion that the usual justification of the linearizing of Equation (3-7) by assuming $\frac{\partial \xi}{\partial x}$ small is only valid if we add the stipulation that $x << \bar{x}$. In summary of the above discussion, we can say that solutions to Equation (3-7) predict high amplitude behavior in the region where $x < \bar{x}$, that dissipative effects account for the stable sawtooth behavior beyond $x = \bar{x}$ where (3-7) is invalid, that the usual linear wave equation is only valid at relatively short distances and low amplitudes (where the majority of past problems of practical interest lie) and that the linear dissipative wave equation is valid at low amplitudes regardless of propagation distance.

In any problem with nonlinearities, we must determine the range of values of various parameters for which a linear approximation can be used and the range over which a nonlinear analyses must be undertaken. Some difficulties involved in nonlinear analysis are discussed later in this chapter. In a typical problem with a term $\left(1 + \frac{\partial \xi}{\partial x}\right)^{\gamma+1}$ such as appears in Equation (3-7) one would assume that if $\frac{\partial \xi}{\partial x}$ is "small" compared to unity that the term could be neglected. For example, we could state that if

$$\frac{\partial \xi}{\partial x} < 10^{-2} \quad ,$$

the linearized equation would result. We have, however, previously pointed out that it is improper to linearize Equation (3-7) in this manner due to the cumulative distortion effect. We can prove our point with the following example:

We can assume that close to the origin ξ has the form

$$\xi \simeq \xi_o \, e^{j(\omega t - kx)} \tag{3-11}$$

and

$$\frac{\partial \xi}{\partial x} = - jk\xi \quad . \tag{3-12}$$

Also

$$v = \frac{\partial \xi}{\partial t} = j\omega\xi \tag{3-13}$$

Combining Equations (3-12) and (3-13),

$$\frac{\partial \xi}{\partial x} = \frac{v}{c_o} \, . \tag{3-14}$$

The initial magnitude of $\frac{\partial \xi}{\partial x}$ is equal to the magnitude of the particle velocity divided by the speed of sound which we will call the acoustic Mach number M_A,

$$M_A = \frac{v_o}{c_o} \quad , \tag{3-15}$$

where $v = v_o \, e^{j(\omega t - kx)}$ near the origin.

As our example, consider an initial sound pressure level of 150 dB re 2×10^{-4} dynes/cm^2 in air. This corresponds to a peak sound pressure of 10^4 dynes/cm^2. The corresponding sound particle velocity amplitude is 2.41×10^2 cm/sec and the resulting acoustic

Mach number is 0.7×10^{-2}, a "small" number compared to unity. In spite of this fact, strong nonlinear effects are observed at levels of 1500 dB. Examples similar to that given above are presented by Beyer in Reference 12.

The following question is therefore frequently asked: When is a wave finite? The answer is that a wave can be considered a finite amplitude wave when the frequency, initial amplitude and propagation distance are such that progressive distortion or finite amplitude effects can be observed.

The first explicit solution to Equation (3-7) appearing in the literature of acoustics was obtained by Fubini in 1935 (Reference 13). Blackstock points out in Reference 9 that a mathematically identical solution was obtained by Bessel in his analysis of Kepler's second law of planetary motion. Blackstock has therefore aptly referred to the analysis as the Bessel-Fubini solution. The solution is in the form of a Fourier series and can be expressed in terms of the sound pressure (ignoring phase factors of the harmonics) as follows:

$$p(x, t) = \sum_{n=1}^{\infty} \sqrt{2}\, P_n\, e^{nj(\omega t - kx)} , \qquad (3\text{-}16)$$

where n = an integer

ω_o = angular frequency of initially sinusoidal wave,

$k = \omega / c_o$,

and Pn = RMS amplitude of the nth harmonic.

It would be appropriate here to clarify what is meant by the nth harmonic since this is frequently a confusing issue. If we define $f_o = \frac{\omega_o}{2\pi}$ as the fundamental or the frequency of the initially sinusoidal wave, then the frequency of the nth harmonic is defined as

$n f_o$. This is a widely accepted convention and the confusion arises from the also widely accepted convention in expressing harmonics in terms of "overtones" usually used in connection with music. The first overtone is two times the fundamental. The first harmonic is therefore equal to f_o; however, the first overtone is equal to $2f_o$. We will avoid use of the term "overtone" here and use our definition above for the various harmonics.

The Fourier coefficients P_n are functions of the initial amplitude and frequency of the wave, the propagation distance, and the properties of the gas. They are given in terms of the ratios of Bessel functions as follows:

$$P_n = P_o \frac{J_n(n\sigma)}{n\, J_1(\sigma)} \quad , \tag{3-17}$$

where

$$\sigma = \frac{x}{\bar{x}} = \frac{(\gamma+1)\, \omega_o\, P_o x}{\sqrt{2}\, \rho_o\, c_o^3} \quad , \tag{3-18}$$

and p_o = initial RMS amplitude of the fundamental,

J_n = nth order; Bessel function of the first kind.

and $\bar{x}$ = discontinuity or shock formation distance.

It is immediately apparent that the solution is an approximation since it predicts that $P_1 = P_o$ for any x while the harmonics are growing in intensity with distance. The fundamental P_1 actually decreases in intensity in accord with the total increase in intensity of the harmonics and this could be accounted for separately if necessary. The behavior of the solution at the origin is proper since, although $J_1(\sigma) = 0$ at $\sigma = 0$,

$$\lim_{\sigma \to 0} \frac{J_n(n\sigma)}{J_1(\sigma)} = 0 \quad . \tag{3-19}$$

The solution becomes infinite at other successive zeros of the function $J_1(\sigma)$ but this always occurs in the region where $\sigma > 1$ and the solution is invalid there for other previously stated reasons; that is, x exceeds the shock formation distance.

The solution can be simplified for small σ with the aid of the power series expansion of $J_n(\sigma)$ of integer order where

$$J_n(\sigma) = \sum_{j=0}^{\infty} \frac{(-1)^j \left(\frac{\sigma}{2}\right)^{2j+n}}{j!(n+j)!} \quad . \tag{3-20}$$

Expressions can be obtained for $J_1(\sigma)$ and $J_n(n\sigma)$ from Equation (3-20) as follows:

$$J_1(\sigma) = \frac{\sigma}{2}\left[1 - \frac{\sigma^2}{8} + \frac{\sigma^4}{192} - \ldots\right] , \tag{3-21}$$

$$J_2(2\sigma) = \frac{\sigma^2}{2}\left[1 - \frac{\sigma^2}{3} + \frac{\sigma^4}{24} - \ldots\right] , \text{ and} \tag{3-22}$$

$$J_3(3\sigma) = \frac{9\sigma^3}{16}\left[1 - \frac{9\sigma^2}{16} + \frac{81\sigma^4}{640} - \ldots\right] . \tag{3-23}$$

We can express Equation (3-17) in terms of the ratios of the various harmonics to the fundamental as follows:

$$\frac{P_n}{P_o} = \frac{J_n(n\sigma)}{n\, J_1(\sigma)} \quad . \tag{3-24}$$

We can substitute Equations (3-21), (3-22), and (3-23) into Equation (3-24) and perform the indicated division (since all of the series are absolutely convergent for $\sigma < 1$) and obtain expressions for the ratios of the second and third harmonics to the fundamental where

$$\frac{P_2}{P_o} = \frac{\sigma}{2}\left[1 - \frac{5\sigma^2}{24} + \frac{\sigma^4}{96} - \ldots\right] \tag{3-25}$$

and

$$\frac{P_3}{P_o} = \frac{3\sigma^2}{8}\left[1 - \frac{7\sigma^2}{16} + \frac{\sigma^4}{15} - \ldots\right] . \tag{3-26}$$

It can be determined by inspection that Equations (3-25) and (3-26) are rapidly convergent for sufficiently small σ and that for many cases the first term is sufficient. For $\sigma = 0.6$, the first term determines P_2/P_o within 7 percent and P_3/P_o within 15 percent of the correct value. The percentage error decreases rapidly from these values for σ smaller than 0.6. A computer program has been written for use in this study which takes into account the first three terms and is sufficient for all practical regions of interest where $\sigma < 1$.

For sufficiently small σ, Equations (3-25) and (3-26) reduce to

$$\frac{P_2}{P_o} = \frac{\sigma}{2}$$

and

$$\frac{P_3}{P_o} = \frac{3\sigma^2}{8} .$$

Substituting Equation (3-18) into these expressions yields:

$$\frac{P_2}{P_o} = \frac{(\gamma+1)\ \omega\ P_o x}{2\sqrt{2}\ \rho_o\ c_o{}^3} \tag{3-27}$$

and

$$\frac{P_3}{P_o} = \frac{3}{8}\left[\frac{(\gamma+1)\ \omega\ P_o x}{\sqrt{2}\ \rho\ c_o{}^3}\right] . \tag{3-28}$$

Thuras, Jenkins and O'Neil and Black (References 14 and 15), who were unaware of Fubini's work, obtained Equations (3-27) and (3-28) as approximate solutions to the problem by entirely different methods from that used in the Bessel-Fubini solution. Reference 14 contains the first published experimental measurements of finite amplitude distortion and their data agree with theory within 3 dB.

The value of x for which $\sigma=1$, that is, the discontinuity distance is a good measure of the importance of finite amplitude effects in a given situation. If, for example, the discontinuity distance is of the order of a kilometer, then observation of nonlinear effects is in most cases unlikely. We can set $\sigma=1$ in Equation (3-18) and rearrange it solving for $\bar{x}$:

$$x = \bar{x} = \frac{\sqrt{2}\,(\rho_o\, c_o)\, c_o^2}{(\gamma+1)\; 2\pi\; f_o\; P_o} \quad , \tag{3-29}$$

and since, in this case, we are concerned with air, we can add the following constants in CGS units:

$$\gamma = 1.4 \quad ,$$

$$\rho_o c_o = 41.5 \text{ cgs RAYLS} \quad ,$$

and $$c_o = 3.43 \times 10^4 \text{ cm/sec.}$$

Substituting these into Equation (3-29) yields

$$\bar{x} = \frac{4.75 \times 10^9}{f_o\, P_o} \quad . \tag{3-30}$$

For a frequency of 1 kHz,

$$\bar{x} = \frac{4.75 \times 10^6}{P_o} \quad . \tag{3-31}$$

Equation (3-31) was used to obtain the graph shown in Figure 8. This is a plot of discontinuity distance versus sound pressure level in dB re 0.0002 dynes/cm^2 for a frequency of 1 kHz. Since $\bar{x}$ is inversely proportional to frequency, the overall level of the curve would drop 6 dB for a doubling of frequency and would rise 6 dB if the frequency were halved. Since sound waves are rarely confined to ducts of longer than 10-20 meters in most practical situations, we can see from Figure 8 that nonlinear effects in the middle audio frequency range are usually of importance only above about 140 dB. This gives us a crude answer to the question posed earlier as to when a sound wave becomes nonlinear. A level of 140 dB corresponds to an acoustic Mach number of about 2×10^{-3}. Typical sound pressure levels in the inlets of jet engines and large stationary gas turbines are frequently 150 to 160 dB which is well into the nonlinear region.

The discussion has been limited so far to plane finite amplitude waves; however, there are many situations where other types of waves of large amplitudes are encountered. Examples are high amplitude higher order modes propagating in ducts which is of most interest to us here and high amplitude spherically diverging waves which are of interest for underwater sonar applications. An exact solution for the case of higher order mode propagation would require that the equation of motion, continuity equation and pressure-density relationship be used to obtain a three-dimensional wave equation, in this case, in cylindrical coordinates, and that the resulting wave equation be exactly solved by some method. This appears to be impossible. It would therefore be desirable if the Bessel-Fubini

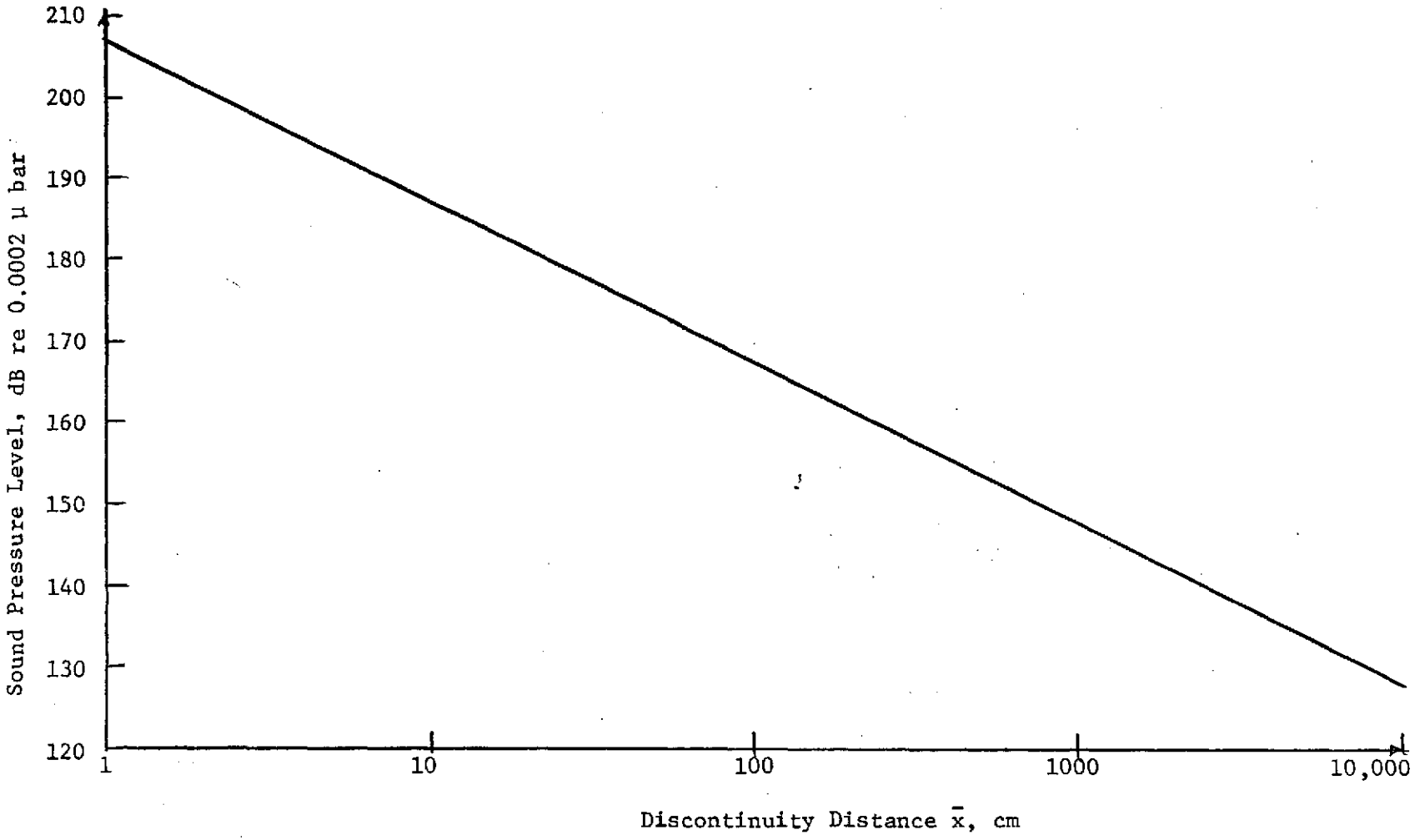

Figure 8 Sound Pressure Level Versus Discontinuity Distance for a 1 kHz Finite Amplitude Plane Wave

solution could be modified or utilized in some way to approximately predict the nonlinear behavior of waves other than plane waves.

This was done by the author in Reference 16 to determine the second and third harmonics for a one-dimensional spherically spreading wave (by one-dimensional,we mean in this case that there is only an r dependence on the wave's behavior). The method correctly predicts the second harmonic but is incorrect for the third and higher harmonics, even though a plausible mathematical proof was given (Reference 17) to justify the method. The results for the second harmonic are

$$\frac{P_2}{P_1} = \frac{(K+1)\ \omega\ P_o r_o}{2\sqrt{2}\ \rho_o\ c_o^3}\ \ln\ \left(\frac{r}{r_o}\right), \tag{3-32}$$

where r_o = radius of the source,

P_o = RMS sound pressure at r_o,

r = radial spacial coordinate,

and K = nonlinearity parameter = γ for a gas.

We use P_1 instead of P_o on the left-hand side of Equation (3-32) since P_1 in this case is approximately a spherically diverging quantity as a function of r. Most of the nonlinear behavior for spherical waves occurs close to the source since the amplitudes diminish rapidly with r due to spherical spreading.

The setup shown in Figure 9 was used to experimentally verify Equation (3-32). The medium in this case was water. A piezoceramic line projector was used as a source and fixed and movable hydrophones were used to measure the spherically diverging sound fields. Tone burst at 30 kHz, deliberately designed to be rich in second harmonic

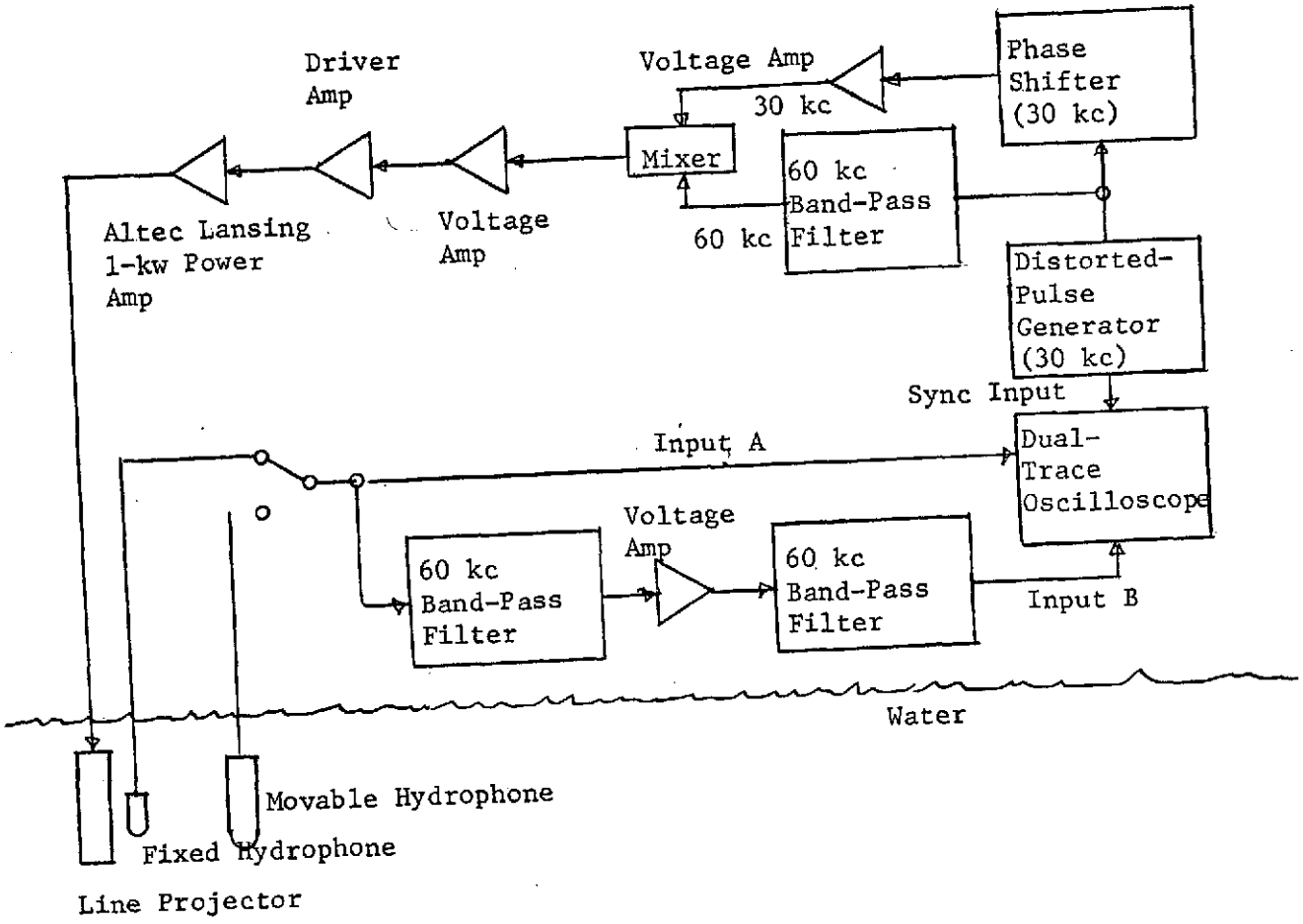

Figure 9 Experimental Setup for Spherical Wave Distortion

distortion, were produced by a distorted-pulse generator. These signals were passed through a phase shifter and amplified to drive the source. A separate 60 kHz second harmonic signal was obtained by filtering and was separately mixed with the original signal before final amplification to the source. In this manner, through phase and amplitude adjustments, complete control is obtained over the second harmonic content of the signal feeding the source. Initially, the controls were adjusted for minimum second harmonic distortion close to the source as measured by the fixed hydrophone. This is equivalent to an initially sinusoidal source and cancels the second harmonic distortion generated by the source itself. The progressive distortion was measured as a function of distance by the movable hydrophone and the results are shown in Figure 10. The solid line is computed from Equation (3-32) and the data substantially verify that this expression is correct at large distances. The controls were then adjusted such that a minimum in the second harmonic appeared in the far field with the results shown in Figure 11. This illustrates that, at least in this case, finite amplitude distortion can be minimized by control of the wave shape at the source. It should be pointed out that, due to the rapidly diminishing amplitude of the fundamental resulting from spherical spreading, no shock formation or wave steepening could be detected in this experiment. The waves were therefore very weakly nonlinear and the second harmonic cancellation of Figure 11 is not surprising, based on linear arguments where superposition of waveforms is allowed. In our recent experiments with plane waves in air at very high amplitudes, a scheme of this sort to control harmonics appears to be hopeless since the N shaped shock

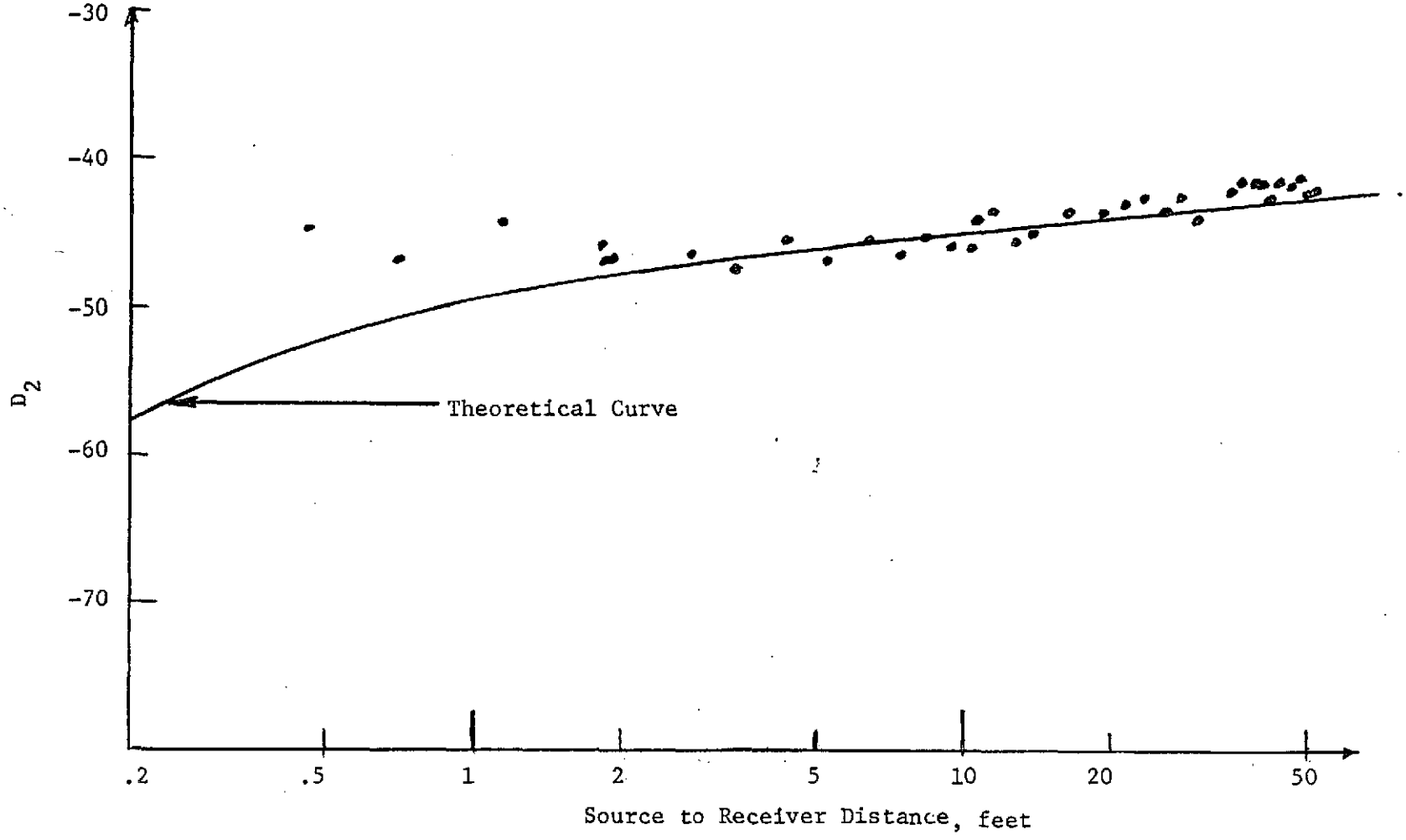

Figure 10 Second Harmonic Distortion Versus Distance from the Source

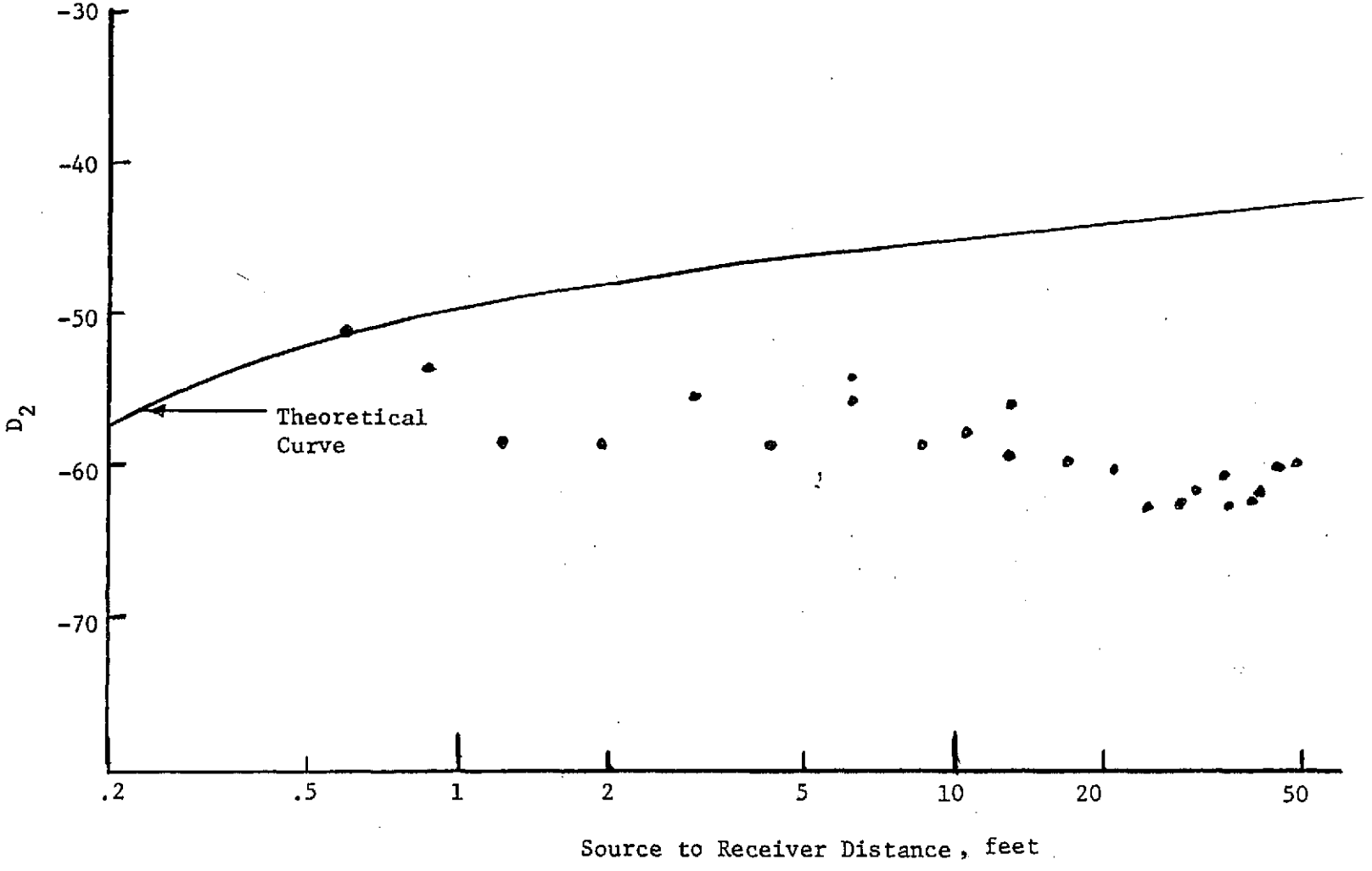

Figure 11 Second Harmonic Distortion After Cencellation

waves appear regardless of the initial waveform. The results of these experiments will be reported in a later chapter. In the above described spherical experiments in water, attempts to verify the third harmonic behavior failed since the third harmonic analysis is incorrect in Reference 16.

Solutions for one-dimensional spherical and cylindrical finite amplitude waves which are probably correct for higher order harmonics are given in Reference 18. Although the experiments would be difficult, it would be satisfying to see the results of Reference 18 verified for the third and higher order harmonics. The incorrect results obtained in Reference 16 through what appears to be a logical method points out one of the pitfalls of analyzing nonlinear problems. Many solutions can be generated, especially today with the aid of high speed computers, but the real task lies in identifying the correct ones. A theoretician can stay on the right path if he has access to at least some experimental results.

Our present problem, that of higher order modes at high amplitudes in a cylindrical duct, has been analyzed by Keller and Millman in Reference 19. Their analysis predicts that k_z and therefore the phase velocity is amplitude dependent. This would also indicate that the cut-off frequency is amplitude dependent. Our experiments show that this is not the case since no variations in phase velocity or cut-off frequency with amplitude were observed up to 175 dB. Their analysis does predict an absence of shock formation which was observed but the explanation for this can be argued on much simpler physical grounds.

In a private communication with Professor David Blackstock, it was mutually agreed upon that it may be possible to describe the z dependence of a finite amplitude higher order mode with a modified form of the Bessel-Fubini solution. The z dependence of higher order modes has a dependence

$$p(z) = A\, e^{-k_z z} \tag{3-33}$$

which is identical to that of a plane wave with the exception that k_z is frequency dependent. Equation (3-18) would therefore be modified as follows:

$$\sigma' = \frac{(\gamma+1)\, k_z\, P_o z}{\sqrt{2}\, P_o\, c_o^2} \tag{3-34}$$

and σ' would be used in place of σ to calculate the distortion. It will be seen later that Equation (3-34) exactly predicts the behavior at the cut-off frequency but has some problems at frequencies above cut-off.

There is one important difference between progressive distortion for a plane wave and for higher order modes which results from dispersion. If harmonics can be generated with a higher order mode the various harmonics will travel with different phase speeds and it is unlikely that a sawtooth or any stable non-sinusoidal waveshape will develop. It will be seen later, after the presentation of experimental results, that the dispersion has other more far reaching consequences.

CHAPTER IV

BASIC PROPERTIES OF SOUND ABSORBING MATERIALS

Sound absorbing materials, as the name implies, are used to absorb sound waves through conversion of a portion of the acoustic energy into heat. When a sound wave impinges upon the surface of a sound absorbing material, a part of its energy is dissipated within the material and the remaining portion is reflected. The fraction of the total energy absorbed represents the absorption coefficient of the material.

Absorbing materials are widely used to control the reverberant characteristics of rooms and enclosures, and as liners to attenuate sound propagating in ducts. In this study we are primarily interested in duct liner applications.

Absorbing materials are generally of a porous nature and the more common types are constructed from organic or inorganic fibers held together with a binder and from open cell plastic foams. Arrays of Helmholtz radiators are also used as sound absorbers and can be constructed using perforated sheet metal. Foamed glass and woven and sintered metals are also used for special applications. The woven and sintered materials are of great interest here since they can withstand the environment in gas turbine inlet and exhaust ducts.

The voids or pores of an absorbing material are filled with the fluid in which the sound wave is travelling and, in most applications, the fluid is air. The primary energy dissipation mechanism is hydrodynamic loss (viscosity, heat conduction, and molecular

relaxation) due to motion of the fluid filling the pores of the material. The mechanism is not well understood for most materials and attempts to theoretically predict absorption properties from physical characteristics of the materials has met with only limited success.

The absorption properties of a given material can be described by several different quantities which are:

1. The normal incidence absorption coefficient, α_N.
2. The statistical or random incidence absorption coefficient α_{ST}.
3. The normal surface impedance, Z_N.
4. The obliqud incidence impedance, Z_θ.
5. The complex bulk modulus, $\bar{\beta}$.

The definition of these quantities can be visualized with the aid of Figure 12.

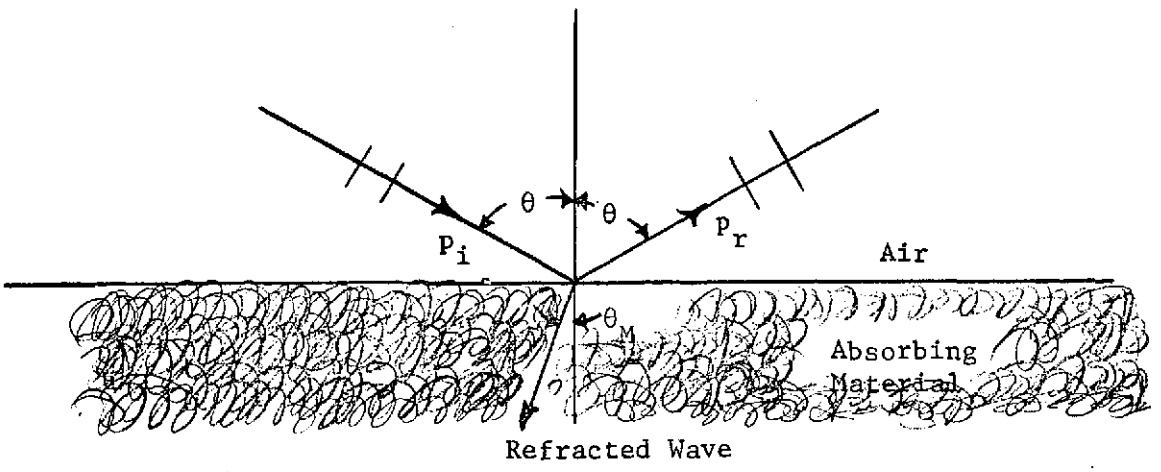

Figure 12 Reflection and Refraction from an Absorbing Surface

A plane sound wave, p_i, is impinging on the surface of a sound absorbing material at incident angle θ. A portion of the wave is absorbed by the material and the remainder is reflected as p_r. The sound absorption coefficient is defined as the fraction of the total energy of the wave absorbed by the material. Since the energy is proportional to the sound pressure squared, it can be easily shown (see Reference 20, page 5) that the absorption coefficient α is given by

$$\alpha = 1 - \left|\frac{p_r}{p_i}\right|^2 \quad . \tag{4-1}$$

It is always a real number between zero and unity. Its value is zero for perfect reflection and unity for complete absorption.

The normal incidence absorption coefficient, α_N, is obtained when θ=0, and is the easiest to measure experimentally. The statistical or random incidence coefficient, α_{ST}, obtained when the incident sound energy is impinging simultaneously from a large number of different incident angles; that is, the incident energy is uniformly distributed over all incident angles of θ=0 to $\theta = \pm 90°$. This quantity is of great importance in architectural acoustics and considerable research is currently being conducted into methods of measuring it. It is only of minor importance in the present study.

The normal surface impedance, Z_N, contains more information on the material's behavior than α_N or α_{ST} and is defined as the ratio of the total sound pressure to the total sound particle velocity with θ=0. It is given by the following equation:

$$Z_N = \frac{p}{v} = \frac{p_i + p_r}{v_i + v_r} \quad , \tag{4-2}$$

where v_i = incident particle velocity, and

v_r = reflected particle velocity.

The quantity Z_N is usually a complex number. It is, like α_N, a quantity which can be measured experimentally with little difficulty. It is shown in Reference 20 that α_N and Z_N are related by

$$\alpha_N = 1 - \left| \frac{Z_N - \rho_o c_o}{Z_N + \rho_o c_o} \right|^2 \qquad (4\text{-}3)$$

The oblique incidence impedance Z_θ is defined in an identical manner to that of Z_N except that $0° < \theta < 90°$. The difficulties of measuring Z_θ can be appreciated from the work of Wyerman reported in Reference 2.

Use of the concept of a complex bulk modulus, $\bar{\beta}$, to describe the wave propagation and losses in an absorbing material are restricted to the assumption that the material is homogeneous and isotropic, at least from a macroscopic point of view. Few materials used in air can be considered homogeneous and many are non-isotropic. In spite of this, these materials have been studied with some success using the bulk modulus concept (see, for example, Pyett's work in Reference 21). A complex wavenumber can be determined from $\bar{\beta}$ with the real part representing the ordinary wavenumber and the imaginary part accounting for the energy losses.

It should be emphasized at this point that $\bar{\beta}$ is a fundamental physical property of a material but that none of the other quantities α_N, α_{ST}, Z_N or Z_θ are fundamental properties. Take, for example, the two configurations shown in Figure 13.

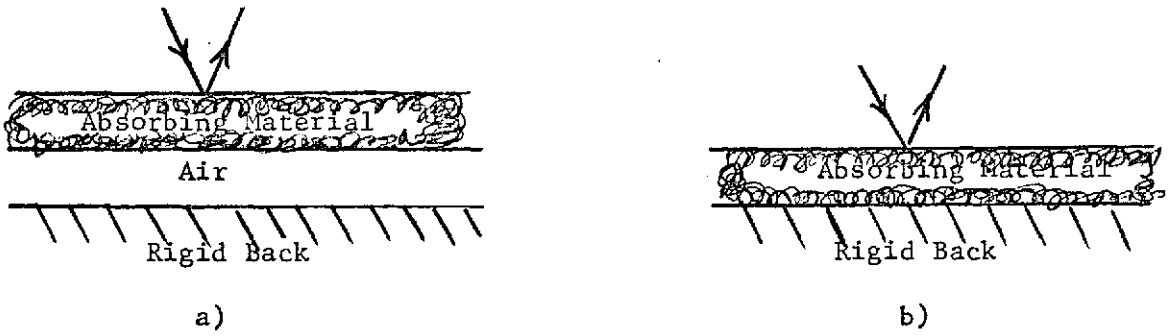

Figure 13 Two Absorber Configurations

Since the same material is used, $\bar{\beta}$ is the same in both cases. The other quantities are quite different between case a and case b due to the air space in case a. These quantities are also dependent upon the thickness of the material. If the material can be represented by a complex bulk modulus, then for any configuration such as a) or b) for example, α_N, α_{ST}, Z_N or Z_θ can be determined by solving a boundary value problem.

There are two important simplifying assumptions with regard to the behavior of plane sound waves at the boundary between air and an absorbing material. The first is that the reflection at the boundary is purely specular. This means that the waves can be represented in terms of ray paths as shown in Figure 12, that the angle of incidence equals the angle of reflection and that local reaction or Snell's law applies to the wave refracted into the material. It is obvious that this is an important assumption since our definitions of normal absorption coefficient, normal surface impedance, and oblique incidence impedance would be meaningless without it. Specular

reflection implies that there are no surface waves present which could radiate sound and that is no scattering of the reflected wave. Since most materials have surface irregularities, some scattering must occur; however, it is hopefully negligible. The second simplifying assumption, which sometimes cannot be made, is that the material is locally reacting. This means that the material's behavior can be described completely in terms of the normal component of the velocity at the surface. This is often justified on the basis of high damping in the material or on grounds that the velocity of sound c_M in the material is considerably less than in air. The first argument is plausible since, for sufficient damping, the motion at one point in the material does not greatly affect the motion at other points. The second argument can only be justified by examining the behavior of the wave refracted into the material. If this wave has a predominantly normal component, then local reaction can be assumed. For the case of specular reflection, the incident, reflected and refracted waves are described by Snell's law (see Reference 22, page 76) as follows:

$$\sin \theta_M = \frac{c_o}{c_M} \sin \theta \quad , \tag{4-4}$$

where θ is the angle of the incident and reflected waves and θ_M is the angle of the wave refracted into the material as previously shown in Figure 12. As θ is varied from normal incidence, it is apparent from Equation (4-4) that θ_M must vary more rapidly than θ if c_M is less than c_o and that the wave is even more oblique in the material than is the incident wave. This means that low sound velocity in the material does not justify local reaction and we are, at this point, contradicting the statements on page 166 of Reference 20 where this

argument is put forth. If we were to consider the absorbing material to have infinite depth with c_M less than c_o, the absorption coefficient would increase with increasing θ to an angle where there is complete penetration of the wave corresponding to an absorption coefficient of unity. Beyond this angle, called the angle of intromission, the absorption coefficient decreases and becomes zero at grazing incidence. It is apparent that under these circumstances local reaction can only be justified on the basis of high damping.

If we again consider a material of infinite depth in this case with c_M greater than c_o, the refracted wave is bent towards the normal. There is an angle, called the critical angle, at which the absorption coefficient becomes zero and remains zero from this angle to grazing incidence. The critical angle is given by

$$\theta_c = \sin \frac{c_o}{c_M} \quad . \tag{4-5}$$

For sufficiently large c_M, the critical angle is small and the only allowed wave motion in the material is at or near the normal direction. Under these circumstances with the sound velocity greater in the material than in air, local reaction could be justified. It is believed that an incorrect interpretation of Snell's law has led to justification of local reaction in the past for the opposite case where the sound velocity in the medium is less than in air. Officer shows in Reference 22 that local reaction is a violation of Snell's law and is equivalent to a boundary condition of continuity of acoustic impedance. The absorption coefficient obtained under this condition is completely different from that observed in experiments in optics and in underwater acoustics but, in these cases, the reflecting medium has very little

damping. Final resolution of the question of local reaction can be made only after a number of oblique incidence absorption measurements are available.

It is shown in Reference 20 that if local reaction can be assumed, then the relationship between Z_N and Z_θ is

$$Z_\theta = Z_N \cos \theta \quad , \tag{4-6}$$

and, from Equation (4-3),

$$\alpha_\theta = 1 - \left| \frac{Z_N \cos \theta - \rho_o c_o}{Z_N \cos \theta + \rho_o c_o} \right|^2 \quad . \tag{4-7}$$

It should also be noted that the assumption of local reaction is necessary when applying the boundary conditions in Equation (1-27) for a duct of finite wall impedance.

The majority of the work in the investigation of the properties of sound absorbing materials has been based on a phenomenological approach using several experimentally determined quantities (for example, see References 20 and 23). These macroscopic properties are the flow resistance, the porosity and the structure factor. The flow resistance can be readily measured (see Reference 1) by passing air through a sample of the material and measuring the flow rate and pressure drop across it. The porosity is easily determined since it is the ratio of the volume of the voids in the material to the total volume. The structure factor, however, must be determined by first measuring the acoustic impedance of the material and working backwards to obtain this quantity. In other words, with the phenomenological method, a theoretical model is developed with certain parameters which must be determined experimentally. This is not an ideal approach

since we are, in a sense, making the data fit the theory, but it has provided some insight in the past into the effects of varying various parameters in the construction of sound absorbing materials. There is one class of materials (see Kilmer, Reference 1, Chapters III and VIII), thin fiber metal with an air backing and rigid termination, where the acoustical behavior is determined from the flow resistance alone and the normal impedance and absorption coefficient can be determined theoretically with good accuracy from the flow resistance and depth of the air cavity.

Modern approaches to the problem, notably those of Pyett and Attenborough, (References 21, 24 and 25) are attempts to determine the complex bulk modulus discussed earlier. This quantity would give a complete description of the material including oblique incidence behavior for the cases where the locally reacting assumption may not be valid. Pyett measured the normal impedance of a material for different thicknesses and from these data deduced the complex bulk modulus. His measurements were based on the impedance tube method. He then developed a theory from which oblique incidence behavior could be obtained.

Attenborough's method is completely theoretical in nature and has the distinct advantage over all previous approaches in that the absorptive properties of a material, under proper conditions, can be completely determined from its microstructure. For most materials the microstructure is determined from easily measurable physical properties. For the case of the widely used glass fiber absorbing materials, the fiber radius and fiber concentration are the only required quantities in Attenborough's theory.

Attenborough's approach was to use scattering theory to predict the properties of fibrous absorbing materials. The fibers of the material are modelled as a three-dimensional array of scatterers. The degree of success of the method depends, of course, upon how close the theoretical model is to the actual model. Attenborough's first model consisted of an array of parallel rigid (or elastic) cylindrical fibers in air with equal diameters and equal spacing. His agreement of theory with measurements using a British product called Rocksil was poor and would appear at first to be discouraging. He does get better agreement using more complicated models with random scatterer diameter and orientation and this is an encouraging sign since Rocksil has a large variation in fiber diameter and orientation. Measurements in our laboratory using Owens Corning Type 705 Fiberglas are more encouraging. This material has relatively constant diameter fibers with fairly uniform spacing and generally parallel fiber arrangement. This indicates that this material is more representative of Attenborough's parallel freely suspended identical fibers, constant spacing prediction, his measurements of Rocksil and our measurements of Owens Corning 705 are shown in Figure 14. The reasonably good agreement of our measurements with theory lends considerably support to Attenborough's theoretical work. Additional experimental verification of his theory as applied to oblique incidence behavior of absorbing materials has been made by Sides and Mulholland (Reference 26).

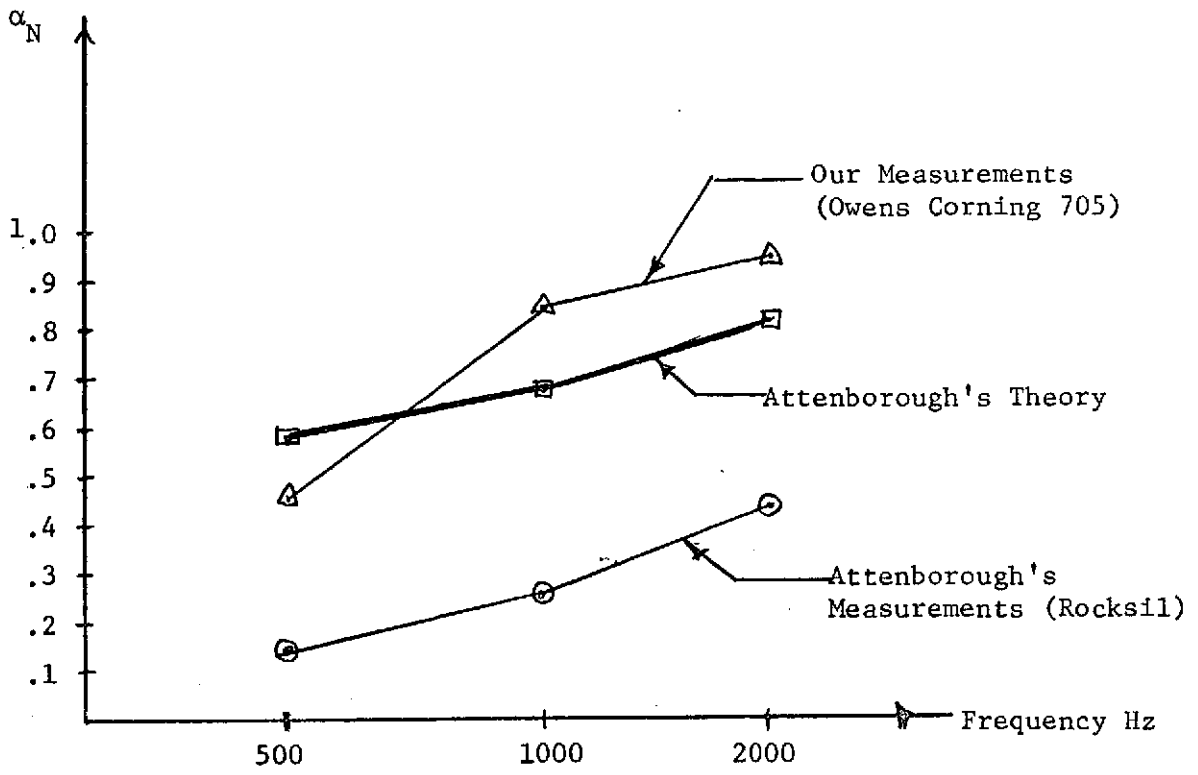

Figure 14 A Comparison of Measurements with Attenborough's Theory

Attenborough's postulate that the properties of absorbing materials can be explained in terms of scattering theory immediately brings to mind the possibility that the reflection of the wave at the surface of the material will be non-specular. This would result in the dire consequences mentioned earlier in this chapter; that is, that our definitions of normal absorption coefficient, etc., would be meaningless. Fortunately, this is not the case since one of the important assumptions in Attenborough's work is that only specular reflections occur. This is based on the argument that the dimensions

of the individual scatterers are small compared to a wavelength and this is clearly a valid assumption for common fibrous materials in the audio frequency range. This brings up the point of a criticism of Attenborough's work which is completely invalid. It has been argued that scattering can only be a significant problem when the dimensions of the scatterer are of the order of a wavelength or larger; therefore, since it is inherent in Attenborough's analysis that the scatterers be small compared to a wavelength that scattering cannot be an important mechanism. This erroneous conclusion can be reached by considering the scattered field from single rigid infinite cylinders with radii small and large compared to a wavelength. It is shown on page 99 of Reference 5 that the scattered power per unit length for the two cases is given approximately as follows:

$$W_S \simeq \frac{3}{4}\pi^2 a(ka)^3 I_o \quad , \tag{4-8}$$

for $ka << 1$ (radius <u>small</u> compared to a wavelength)

$$W_S \simeq 4a I_o \quad , \tag{4-9}$$

for $ka >> 1$ (radius <u>large</u> compared to a wavelength)

where W_S = scattered power per unit length of cylinder,

a = cylinder radius,

I_o = intensity of plane sound wave incident on cylinder,

k = ordinary wave number, and

$= \frac{\omega}{c} = \frac{2\pi}{\lambda}$,

where λ = wavelength.

It is obvious that the scattered power is extremely small when $ka << 1$ since it is a function of $(ka)^3$. Attenborough's work, however,

uses multiple scattering theory (based in large on earlier work by Twersky in Reference 27) in which the interaction of a large array of many scatterers is considered. We can visualize the scattering from an array of cylinders with the aid of Figure 15. One approach to this problem has been to assume that each scatterer sees only the incoming plane wave. The scattered field solution for a single cylinder is used for each element of the array and the total scattered field is a summation of the fields from all of the elements of the array. This is, however, still single scattering theory and does not adequately describe the problem since each scatterer also sees the scattered waves from all the other scatterers. Multiple scattering theory as used by Twersky and Attenborough take this factor into account and is formulated as follows: each scatterer sees the incoming plane wave minus the wave removed by previous scatterers plus the waves reflected back by forward scatterers. This formulation results in a complicated integral equation. Attenborough simplifies this equation by assuming specular reflection from the surface and that the far-field approximation for the scattered field from each fiber is approximately correct. This reduces the integral equation to the Helmholtz equation with the complex bulk modulus as one of the parameters. In this case, the complex bulk modulus is a function only of the microstructure of the material. The actual energy dissipation mechanism in the theoretical model results from thermal losses from the fluid motion around all of the scatterers.

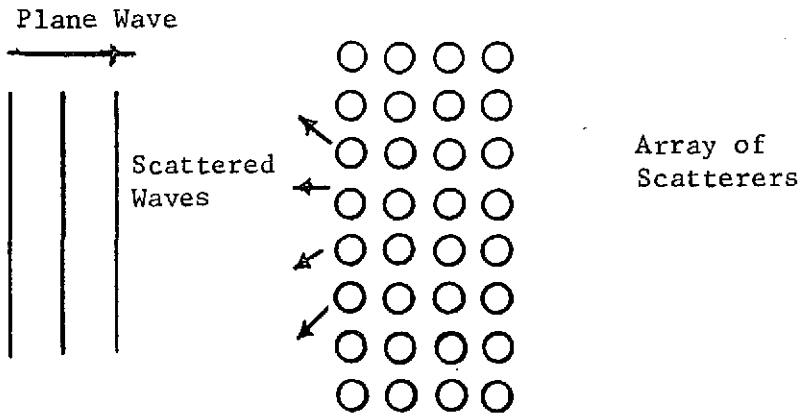

Figure 15 Array of Cylindrical Scatterers

The significance of Attenborough's work is that a plausible model based on a physical description of the microstructure of the material is used with a multiple scattering theory analysis to predict absorption characteristics which are in reasonable agreement with laboratory measurements. A remarkable feature of the outcome of this work is that scattering is the significant mechanism in explaining the absorptive properties of the material and at the same time a specular surface reflection can be assumed.

It is apparent at this point that any future theoretical work on the properties of fibrous absorbing materials should be based to a large extent on the theoretical foundation proposed by Attenborough even though some of his simplifying assumptions may have to be discarded. As we have stated earlier, the fiber metal materials can be treated in a simple manner as demonstrated by Kilmer in Reference 1.

For the case of open cell plastic foam materials it is not clear that any satisfactory scattering theory model could be devised and Pyett's approach may be the practical one. A number of foam materials are now commercially available and further research in this area is warranted.

The various methods for measuring the sound absorption characteristics of materials and the many problems associated with these measurements is not discussed here since the subject is treated in detail by Kilmer and Weyerman in References 1 and 2 with extensive references to previous work. It is sufficient here to recognize that there are many discrepancies between the various methods used to measure the impedance and absorption coefficient of sound absorbing materials and also that there is no completely satisfactory theory to describe their behavior. In the portions of this study concerned with lined ducts (that is, ducts with finite wall impedance), we will assume that our liners are made of approximately locally reacting materials and that we can measure their surface impedance with sufficient accuracy for our purpose. We have deliberately chosen liner materials where discrepancies between measurement methods is minimum and where local reaction is a reasonable approximation.

CHAPTER V

THE EVALUATION OF ABSORPTIVE LINERS AT LOW ACOUSTIC AMPLITUDES

The first experimental phase of this thesis project was to evaluate the performance of several absorptive duct liners constructed of a porous glass fiber material. The liners were commercially available pipe insulating material manufactured by Owens Corning Corporation and were identical except for length. They were hollow cylinders formed from the glass fiber material with an outside diameter of 12 inches and a one-inch wall thickness. The outside was wrapped with a thin vinyl protective coating and they could readily be inserted into a 12-inch inside diameter pipe to act as absorptive liners.

Most previous studies to evaluate liner performance have attempted to assign a single number to the characteristics of a liner in terms of so many decibels of attenuation per length of liner treatment. This number would, of course, be a function of frequency. Typical examples of this approach are given in References 28 and 29. The method assumes that only a single progressive plane wave exists in the duct. In most practical situations; however, both standing waves and higher order modes can be present. In fact, Morse has shown theoretically in Chapter VII of Reference 6 that a plane wave cannot exist in a duct with finite wall impedance. It is also obvious that, for a locally reacting wall, a plane wave would experience no attenuation since there would be no normal component of the particle velocity. Studies conducted in the aircraft industry

have side-stepped the problem by using the test setup shown in Figure 16 (see, for example, Reference 30). Reverberant chamber I is excited with a broad band noise source and sound pressure level measurements are made with lined and hard wall test sections. By filtering the microphone signals into various frequency bands, the insertion loss of the lined test section can be determined. The use of noise as a sound source and the reverberant terminations together obscure the effects of standing waves and of higher order modes. The method does, however, provide a means for crudely evaluating various liners on a comparative basis and was a sound solution to an urgent problem facing the aircraft industry, that is, reducing the radiated noise from jet aircraft.

The physical situation existing in general in a duct with a finite length liner is shown schematically in Figure 17.

An incident sound wave (Wave A) is produced by the sound source and propagates towards the liner. This is the wave which we want to attenuate by adding the liner. Since Wave A sees an impedance discontinuity as it enters the liner there will be a reflected wave at this point (Wave B). Wave C is the forward travelling wave within the liner and will be exponentially damped. This wave sees an impedance discontinuity at the end of the liner and there will be an additional reflection resulting in Wave D which will also be exponentially damped. Wave E represents the forward traveling wave leaving the liner and Wave F represents a reflection due to any impedance discontinuity at the downstream end of the duct. In all three regions (upstream, in the liner section, and downstream), the forward travelling and reflected waves will form interference patterns as

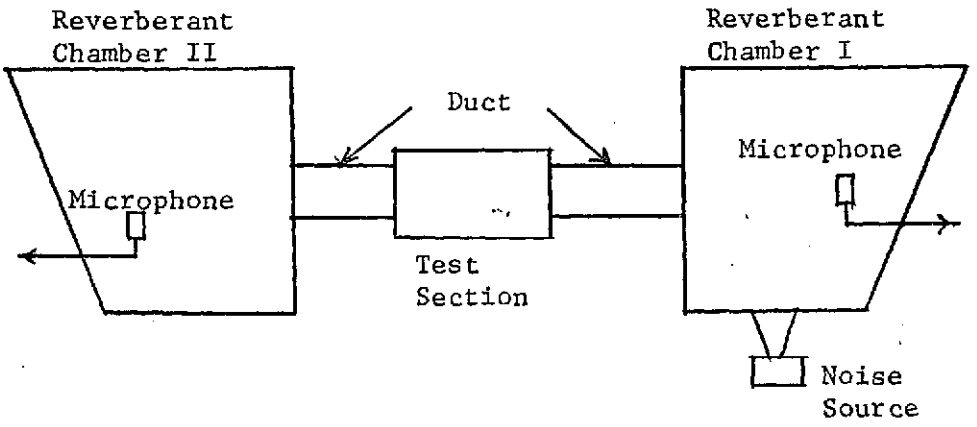

Figure 16 Test Setup Used Previously for Liner Evaluation

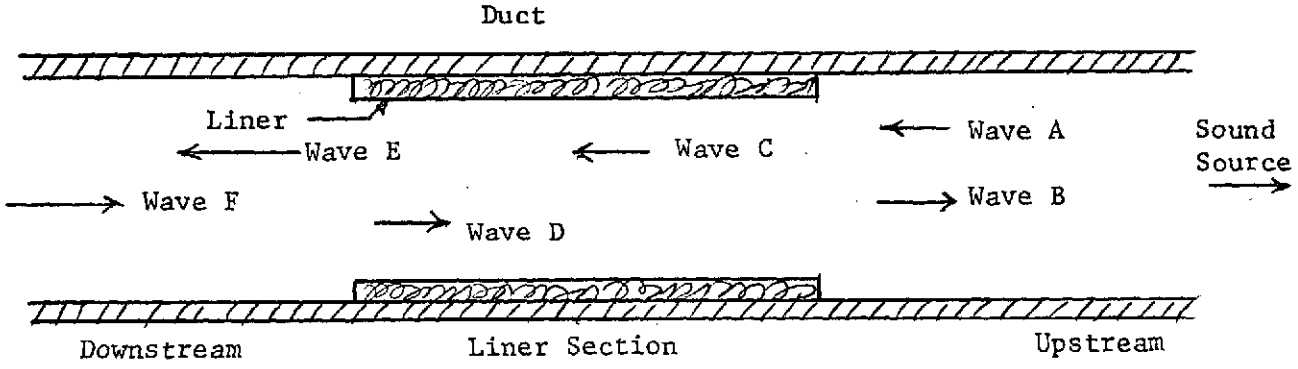

Figure 17 Various Waves in a Lined Duct

standing waves. In view of the situation shown in Figure 17, it is difficult to imagine that the test setup shown in Figure 16 could yield data that would reveal the true attenuation of a liner. In fact, it is difficult to even define the attenuation of a liner of finite length. In most practical duct noise control problems, we have a duct outlet which is radiating undesirable noise. We can measure the total sound power output from the outlet, install an absorbing liner in the duct, and measure the sound power output after this treatment. The insertion loss of the liner can then be defined as the difference in radiated sound power level in decibels between the untreated and treated case. It is obvious from the situation shown in Figure 17 that, for a given liner length, the insertion loss can be influenced by the length of the unlined upstream and downstream lengths of the duct and from the nature of the downstream termination. The insertion loss can therefore only be accurately determined for a specified test configuration and as stated earlier the reverberant chamber method shown in Figure 16 provides a method for comparing various liner configurations.

Liner attenuation can only be rigorously defined in terms of an infinite lined duct in the presence of a single progressive wave. The sound field inside of such a duct, in terms of a particular m, n mode is given by Equation (2-18) as

$$p_{mn} = P_{mn} J_m(\bar{k}_{mn} r) e^{j(\omega t - \bar{k}_z z + m\phi)}, \qquad (5\text{-}1)$$

where $\bar{k}_{mn}$ and $\bar{k}_z$ can be complex due to the presence of the liner. For a fixed ϕ and r, the z dependence of the sound field is

$$p(z) = \bar{A}\, e^{j(\omega t - k_z z)}, \qquad (5\text{-}2)$$

where $\bar{A}$ is a complex amplitude constant. This quantity is complex since the argument of $J_m(k_{mn} r)$ is complex.

Substituting Equation (2-32) into Equation (5-2),

$$p(z) = \bar{A}\, e^{j(\omega t - k_z z)}\, e^{-\alpha_z z}, \qquad (5\text{-}3)$$

and α_z as stated in Chapter II represents the liner attenuation for the m, n mode. There is a particular value of α_z for each mode for a given liner and α_z is also a function of frequency. The liner attenuation is the fundamental physical quantity which we wish to determine to describe the performance of a given liner. This quantity can in no way be deduced from the method shown in Figure 16.

Our experimental approach has been to devise the simplest possible test setup in order to gain insight into the nature of waves propagating in a duct with a finite length liner. The experimental procedure is shown in Figure 18.

It is consisted of a 12-inch inside diameter duct with one inch thick cement walls. The duct was a commercially available pipe known as "transite." Various sound sources were located at one end of the duct and the other end was anechoically terminated.

Preliminary measurements of plane waves using the standing wave method indicated that the termination was better than 90 percent absorptive down to 250 Hz. In subsequent measurements with plane waves and higher order modes, the uniformity of amplitudes and mode shapes at several locations downstream of the liner were indications of good anechoic termination. The termination consisted of a glass

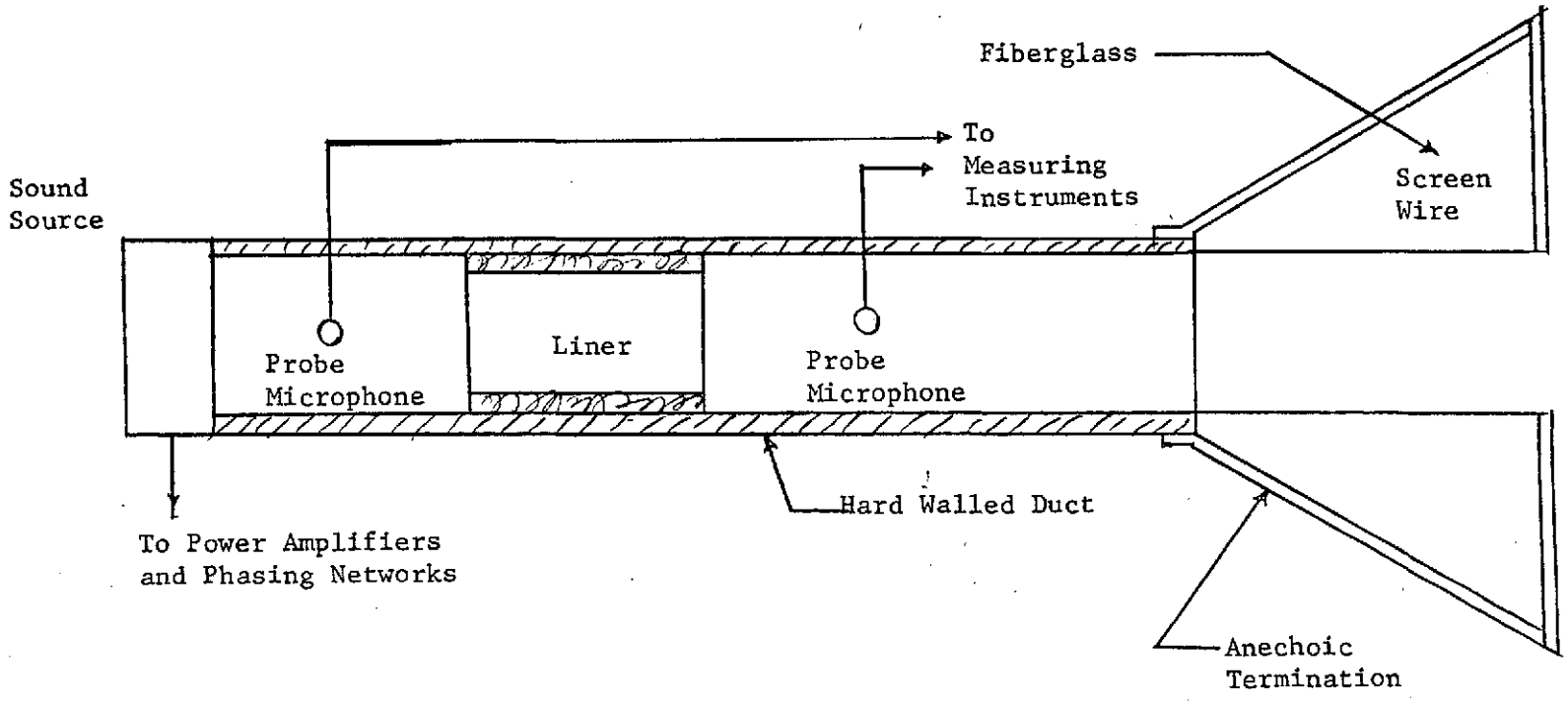

Figure 18 Test Setup for Low Amplitude Liner Evaluation

cloth reinforced polyester plastic conical shell filled with glass fiber absorbing material. The center portion of the termination was a hollow 12-inch diameter cylindrical section. This termination essentially eliminates reflections from the far end of the duct. In other words, Wave F in Figure 17 is not present. A view of the far end of the duct and termination are shown in Figure 19. Probe microphones were available to explore the internal sound field and could be placed at a number of measurement stations down the length of the duct. Several of the probe microphones were mechanized so that automatic plots of sound pressure level versus radial position could be obtained. Two planar arrays of loudspeakers were available as sound sources. The first consisted of eight one-inch diameter speakers located at 45° intervals near the duct wall. Separate phase and amplitude control was available for each speaker and plane waves and higher order modes could be generated using the method described by Seiner in Reference 31. The second array consisted of four loudspeakers located at 90° intervals near the wall of the duct all driven in phase with an additional loudspeaker at the axis of the duct driven out-of-phase by 180°. Using these arrays coupled to the duct in the absence of a liner, we could generate a number of modes individually with a high degree of modal "purity"; that is, with a very low content of other modes. The eight driven array was used to generate the "spinning" higher order modes (where $m=1, \ldots \infty$) and the five speaker array was used for the "non-spinning" higher order modes (where $m=0$).

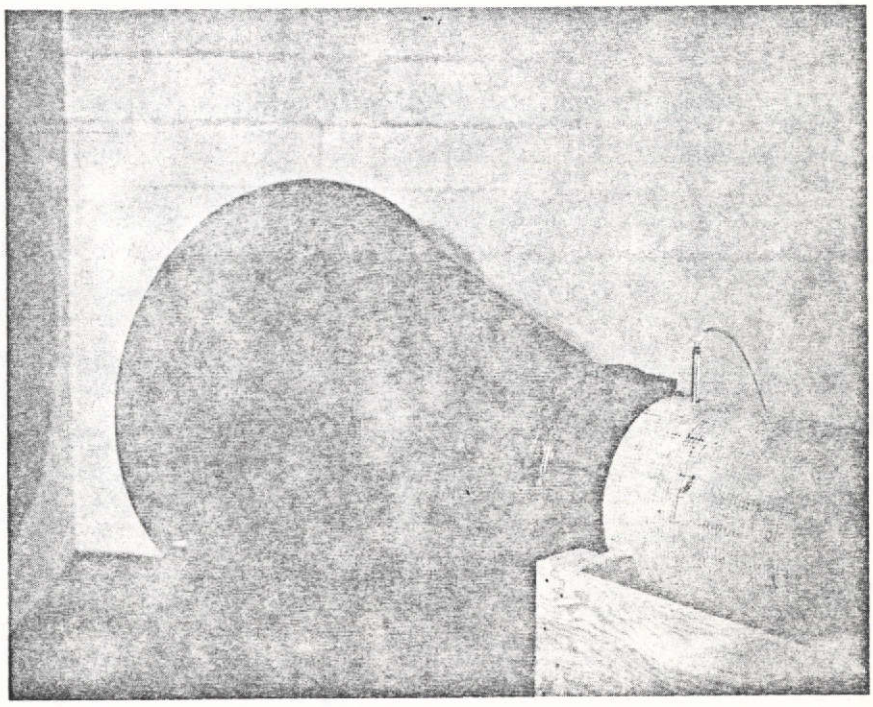

Figure 19 View of Duct and Anechoic Termination

The first phase of these experiments was to generate higher order modes without liners and measure the radial dependence of the sound pressure at fixed positions of ϕ and z to determine the degree of modal purity that could be obtained. The first requirement for generating higher order modes is that the frequency of the sound source be at or above the cutoff frequency of the desired mode. The second is that the radial amplitude dependence and circumferential phase dependence of the source be matched as close as possible to that of the mode itself. For example, for the m=0, n=1 mode the sound pressure has the form from Equation (5-1) of

$$p_{01} = P_{01} J_o(k_{01} r) e^{j(\omega t - k_z z)} . \qquad (5-4)$$

The sound pressure has a Bessel function radial dependence and no circumferential phase dependence. The cutoff frequency and wave numbers are found from the boundary condition of Equation (2-17) where

$$\frac{\partial}{\partial r} J_o(k_{01} r)\Big|_{r=r_o} = J_o'(k_{01} r)\Big|_{r=r_o} = 0 . \qquad (5-5)$$

In order to determine $k_{0,1}$, we need to know the argument of J_o' for the first instance of increasing argument from zero in which the value of J_o' is zero. The relationship between J_o and its first derivative is (for example, see Reference 5) as follows:

$$J_m'(x) = \frac{1}{2} [J_{m-1}(x) - J_{m+1}(x)] . \qquad (5-6)$$

It is also shown in Reference 5 that

$$J_{-m}(x) = (-1)^m J_m(x) \quad , \tag{5-7}$$

and from Equations (5-6) and (5-7),

$$J_o'(x) = - J_1(x) \quad , \tag{5-8}$$

and the boundary condition becomes

$$J_1(k_{01} r)\Big|_{r=r_o} = 0 \quad . \tag{5-9}$$

The first value for the argument at which $J_1(x)$ is zero is $x = 3.8$ and for the m=0, n=1 mode

$$k_{01} = \frac{3.8}{r_o} \tag{5-10}$$

and if r_0 is given in feet, $k_{0,1}$ is 7.6 for our 12-inch diameter duct. From Equation (5-10) the cutoff frequency for c_o = 1130 ft/sec is 1370 Hz. Cutoff frequencies for a 12-inch diameter duct for this and several other modes, as noted earlier, are indicated in Figure 5. The shape of this mode is illustrated in Figure 3. It has a maximum at r=0, a single node between r=0 and $r=r_o$ and another peak at $r=r_o$. There is a reversal in sign, indicating a 180° phase shift at the node point. It is clear that it would be extremely difficult to construct a sound source which exactly matches this mode shape, but it was found that the m=0, n=1 mode could be excited to a high degree of purity using the five speaker array with the center speaker driven 180° out of phase with the four outer speakers. A typical mode shape is shown in Figure 20. The array was operated at the mode cutoff frequency. Figure 20 is a plot of relative sound pressure level in decibels versus normalized radial distance r/r_o for a fixed ϕ and z.

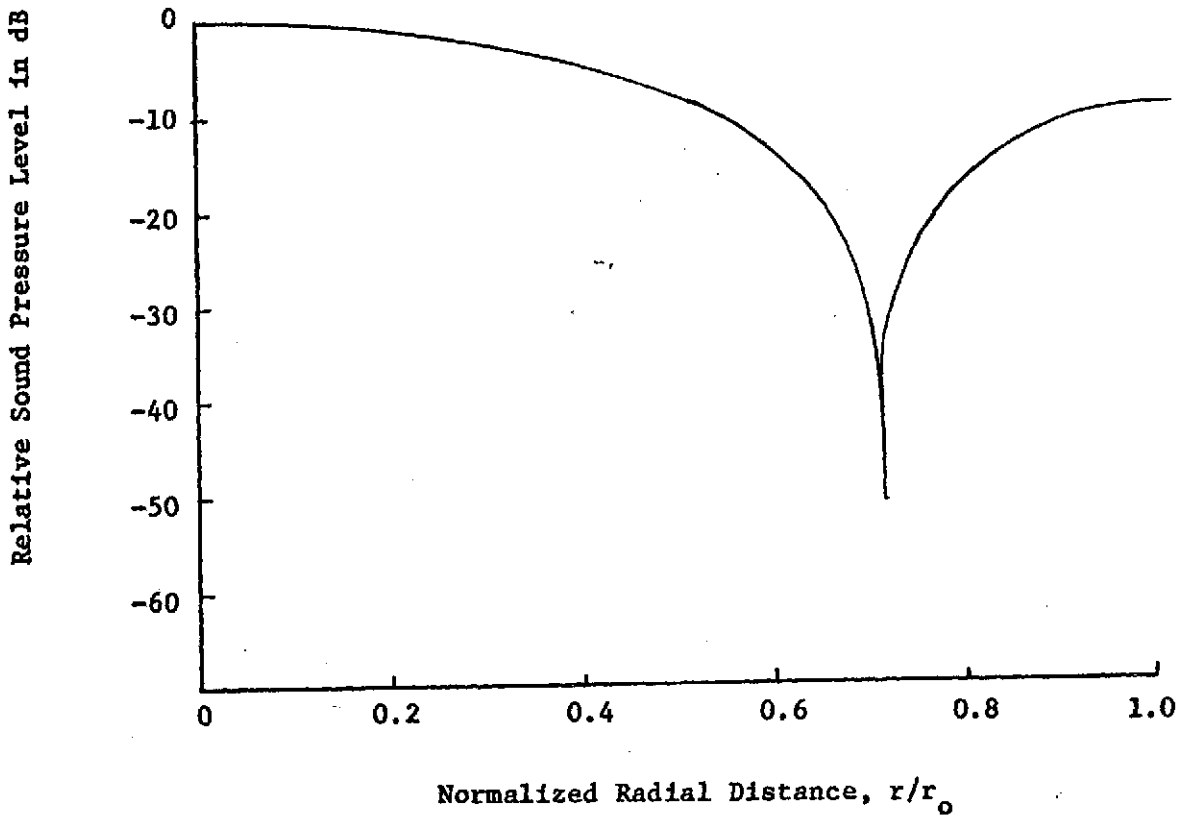

Figure 20 Measured Mode Shape for m=0, n=1 Mode

The equivalent theoretically predicted mode shape can be found from the expression

$$L_p = 20 \log_{10} J_o(3.8 \frac{r}{r_o}) \quad , \tag{5-11}$$

where L_p is the relative radial sound pressure level in decibels. Figure 21 is a theoretical mode shape calculated from Equation (5-11). The shape of the two curves agree closely, but the location of the measured node line (the null point in the curve of Figure 20) differs slightly from theory. This is attributed to dimensional irregularities in the duct and slight inaccuracies in the determination of the radial position of the probe.

The depth of the node point in Figure 20 is an indication of the degree of modal purity or lack of contamination from other modes. The node depth in this case is 50 dB below the maximum level at the center of the duct and is also approximately the dynamic range of the instrumentation. Figure 22 shows a mode shape with only the four outer speakers of the array in operation and the node depth in this case is only 30 dB. This illustrates that the out-of-phase center speaker greatly enhances the modal purity.

The reason for the enhancement of modal purity in this case can be seen from the mode shape shown in Figure 3 for m=0, n=1. The phase of the sound pressure undergoes a 180° phase shift in crossing the mode line and the presence of the center out-of-phase speaker provides a much better match to the actual mode shape than the outer speakers alone. This is analogous to the vibration of mechanical structures where the forcing function matches the mode

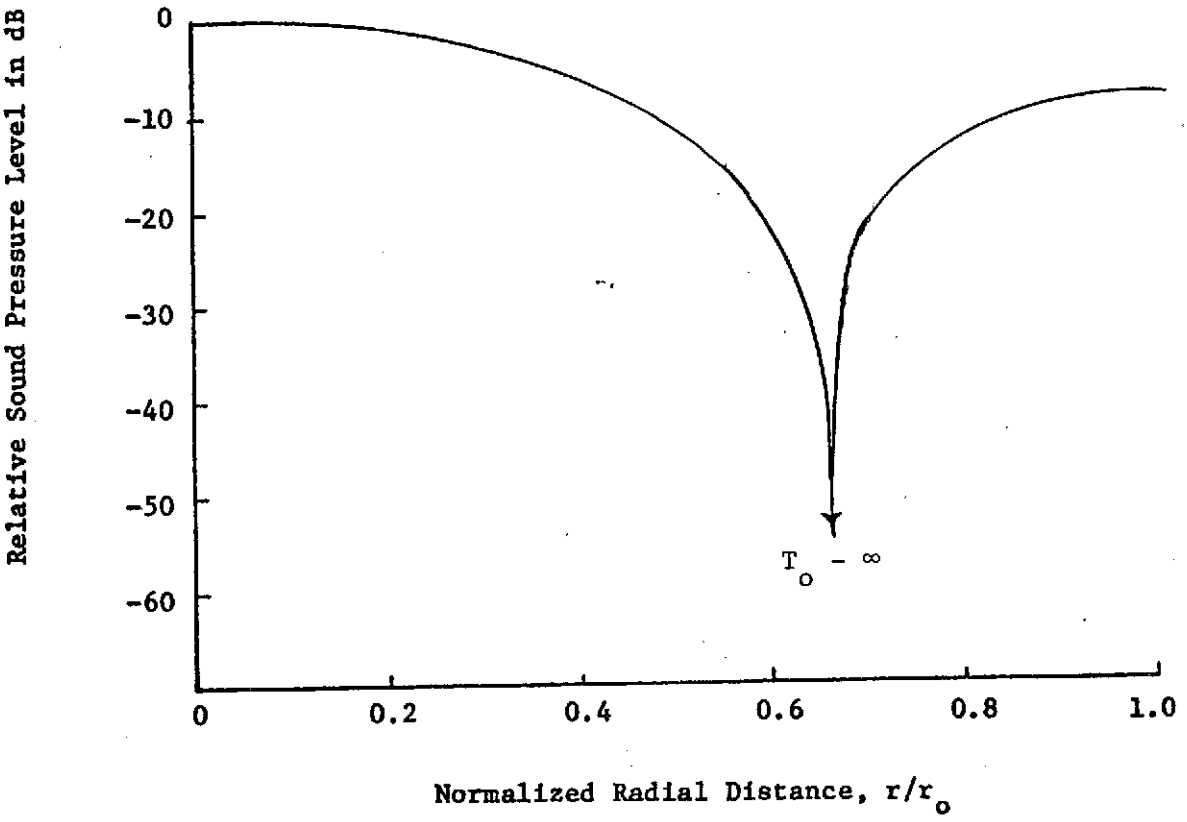

Figure 21 Theoretical Mode Shape for m=0, n=1 Mode

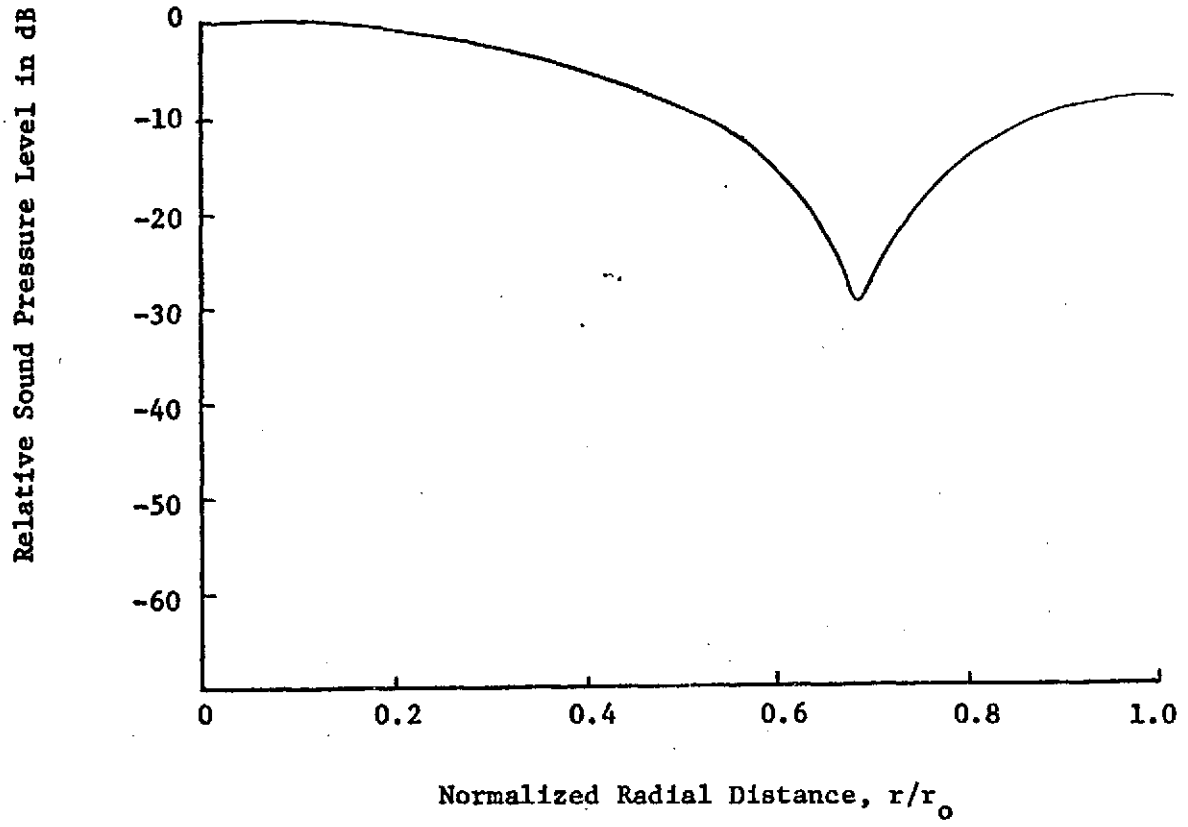

Figure 22 Measured Mode Shape for m=0, n=1 Mode Using Only Four Outer Speakers

shape. In this case also, the mode is strongly excited with an absence of other modes.

When the array is excited at the cutoff frequency of the second non-spinning higher order mode (m=0, n=2), the mode shape of Figure 23 is obtained. The cutoff frequency of this mode is 2520 Hz. The corresponding theoretical mode shape is shown in Figure 24. Our convention for specifying n discussed in Chapter II can be appreciated from the mode shapes presented in Figures 20-24 since n can be determined by counting the number of nodes. The nodal purity for n=2 is not as good as for n=1 and this is to be expected since the source is much less closely matched to mode shape for this case. For the case here of a circumferentially symmetric source, the primary modal contamination is a residual plane wave. Any non-symmetry circumferentially will allow contamination from the spinning higher order modes.

With the eight speaker array, the source is deliberately excited in a non-symmetrical manner in order to generate the spinning modes. The speakers are driven with identical amplitudes but are phased in a manner to match the circumferential phase dependence of the desired spinning mode. For example, the first spinning mode (where m=1, n=1) has the form from Equation (5-1) of

$$p_{11} = P_{11} J_1(k_{11} r) e^{j(\omega t - k_{zz} + \phi)} . \qquad (5\text{-}12)$$

For a 2π variation in ϕ, the phase of the sound pressure field for a fixed r and z must also go through a 2π variation. For an m=2 mode, this would be a 4π variation. The array is most closely matched to the m=1, n=1 mode when the eight speakers are sequentially phased in

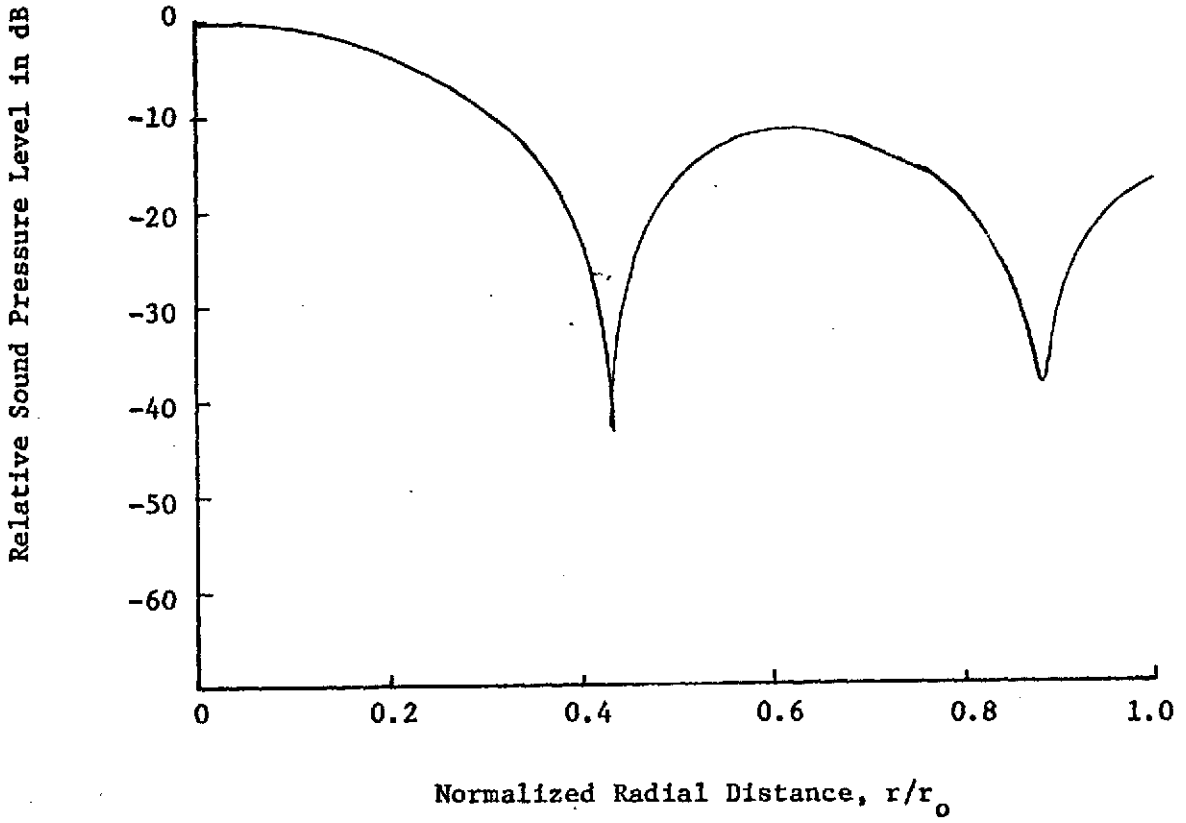

Figure 23 Measured Mode Shape for m=0, n=2 Mode

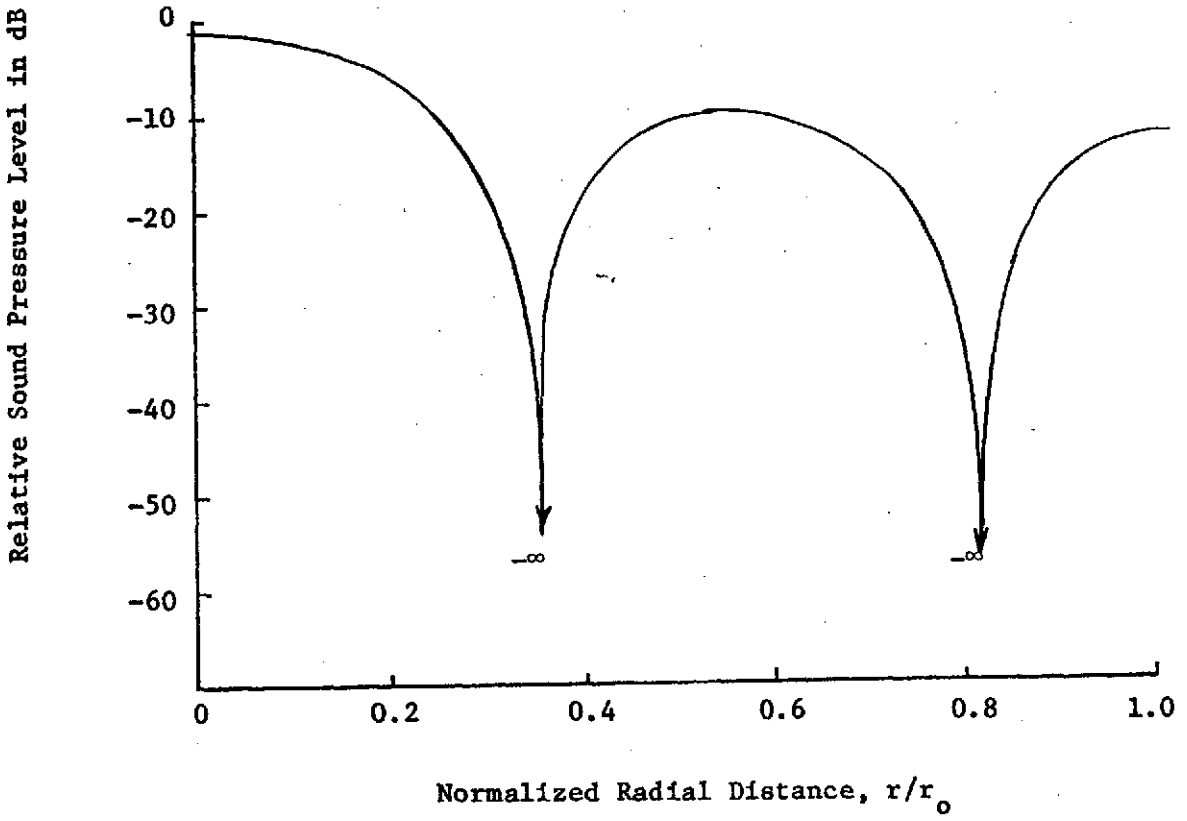

Figure 24 Theoretical Mode Shape for m=0, n=2 Mode

45° increments from 0° to 180°. Using this phasing scheme and exciting the source at the cutoff frequency of the m=1, n=1 mode (660 Hz), the mode shape of Figure 25 was obtained. The corresponding theoretical mode shape is shown in Figure 26. In this case, the agreement between theory and measurements is within the accuracy of the available instrumentation and is much better than for the case of the non-spinning mode shapes shown in Figures 20-24.

The close agreement between theory and measurements for the m=1, n=1 mode can be attributed to the nature of the sound source used to generate this mode. Each diagonally opposite pair of sound sources in the eight element array is operating in anti-phase and are spaced less than a wavelength apart. Each of the pairs can be considered as a dipole which is an inefficient radiator of plane waves or one could also consider that each member of each pair cancels the other member's sound field. As a result of the circumferential phase dependence of the sound source, little or no plane wave component can be generated. Also, at the cutoff frequency of the m=1, n=1 mode, none of the other higher order modes are allowed as can be seen From Figure 5. These factors provide a situation for generating a m=1, n=1 mode with a high degree of purity and therefore the resulting close agreement between theory and measurement. The dipole or cancellation effect can be readily observed by first operating the array below the cutoff frequency and then sweeping the frequency through cutoff. A 40 to 50 dB rise in sound pressure level in the duct can be observed as the frequency approaches and passes through cutoff. A good illustration of this is shown in Figure 69 of Chapter VI. At or above cutoff, the various elements of the array are no

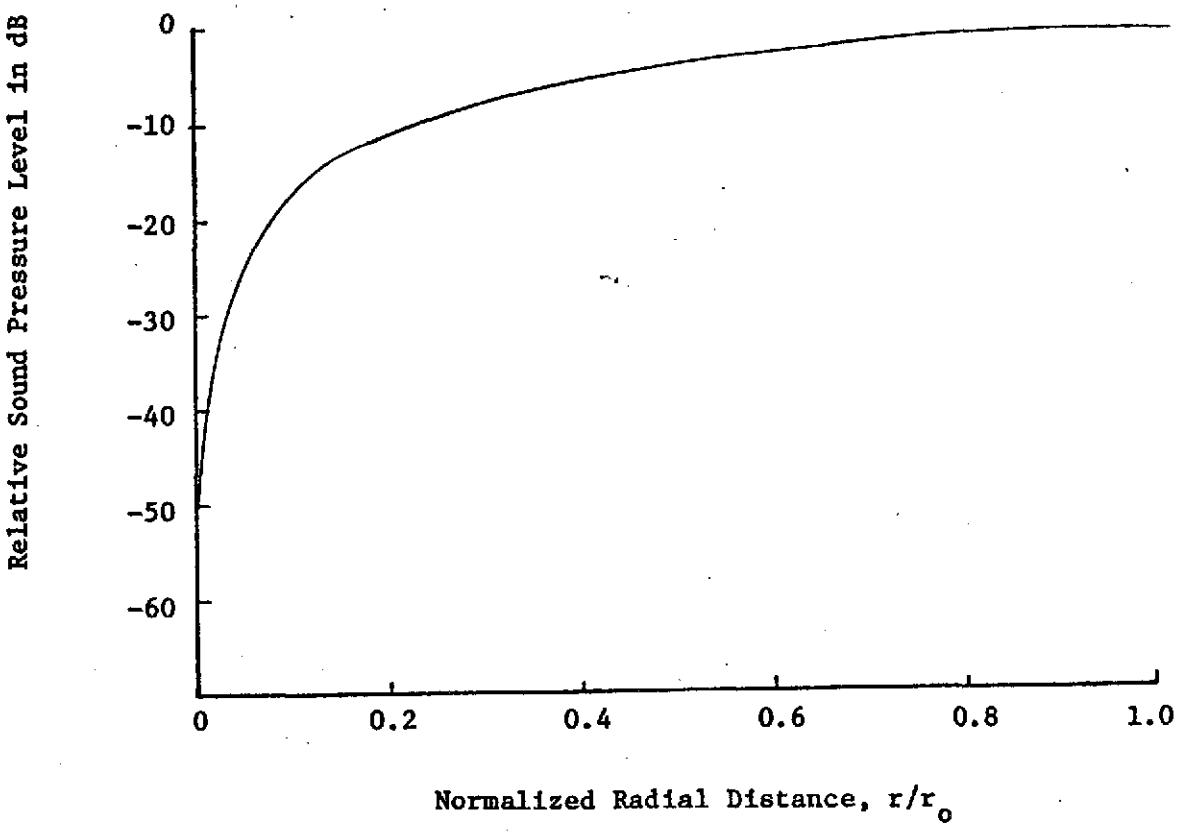

Figure 25 Measured Mode Shape for the First Spinning Mode (m=1, n=1)

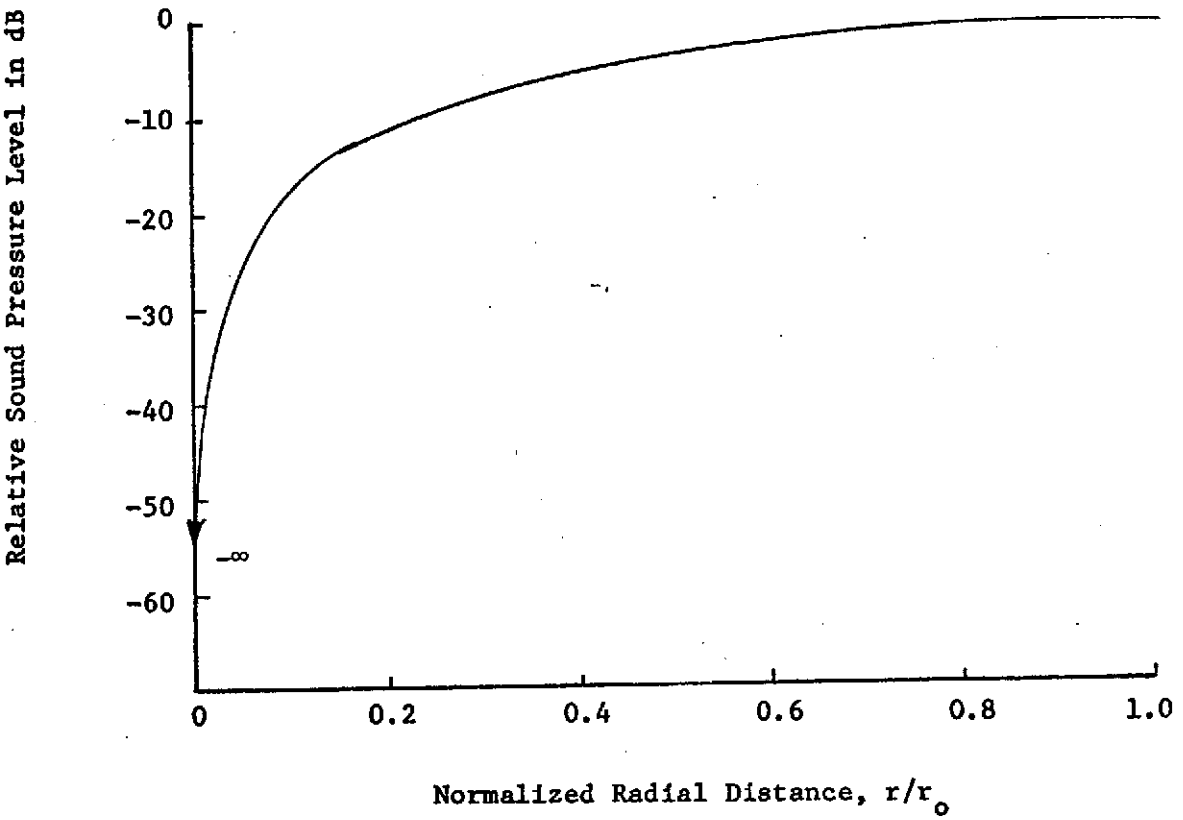

Figure 26 Theoretical Mode Shape for the First Spinning Mode (m=1, n=1)

longer cancelling one another but are circumferentially phase and amplitude matched to the m=1 and n=1 mode and a strong spinning wave is propagated. A multi-element array can usually be phased in such a manner as to "cancel" a particular mode. What is really happening, in effect, is that the array is phased for another mode at some higher cutoff frequency and, if the frequency is adjusted sufficiently upward, the cancellation effect will no longer be observed.

The next phase of the study was to investigate the sound field with use of absorptive liners installed in the duct. The setup shown in Figure 27 was used for the measurements with measurement stations (probe microphone locations) and liner location indicated. The signal processing system used to obtain the data and also the previous mode shapes presented is shown in Figure 28. The first series of tests were made using a two-foot length liner. Mode shapes were obtained at the four measurement stations indicated. Two upstream stations were used since any deviations between the mode shapes at these two positions would indicate the presence of standing waves in this region.

The plane wave case was investigated first using the eight element array with all speakers driven in phase. For a circumferentially symmetrical sound source, one could expect to generate reasonable plane waves up to the cutoff frequency of the first non-spinning higher order mode; that is, where m=0 and n=1 corresponding to a cutoff frequency of 1370 Hz. Any lack of circumferential symmetry would result in deviations from plane wave behavior above 660 Hz, the cutoff frequency of the first spinning mode (m=1, n=1). In this region, the results were uninteresting horizontal straight lines with

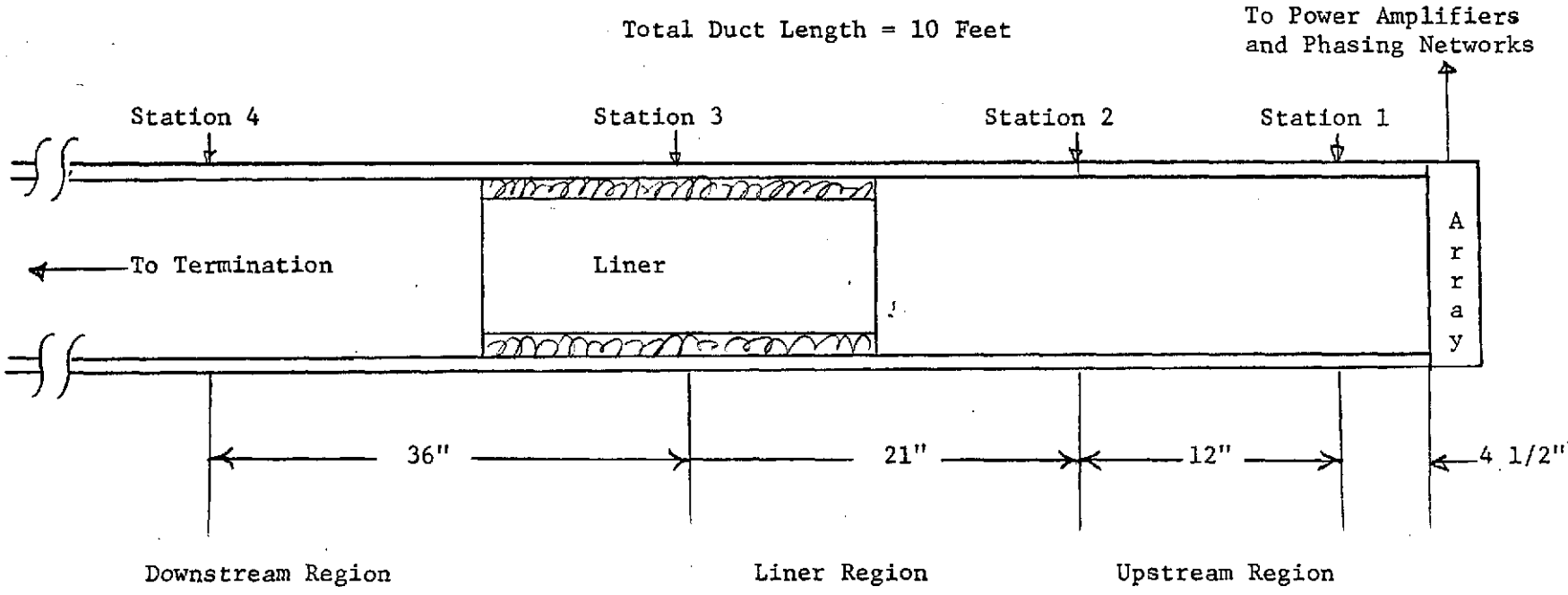

Figure 27 Details of Test Setup for Low Amplitude Liner Evaluation

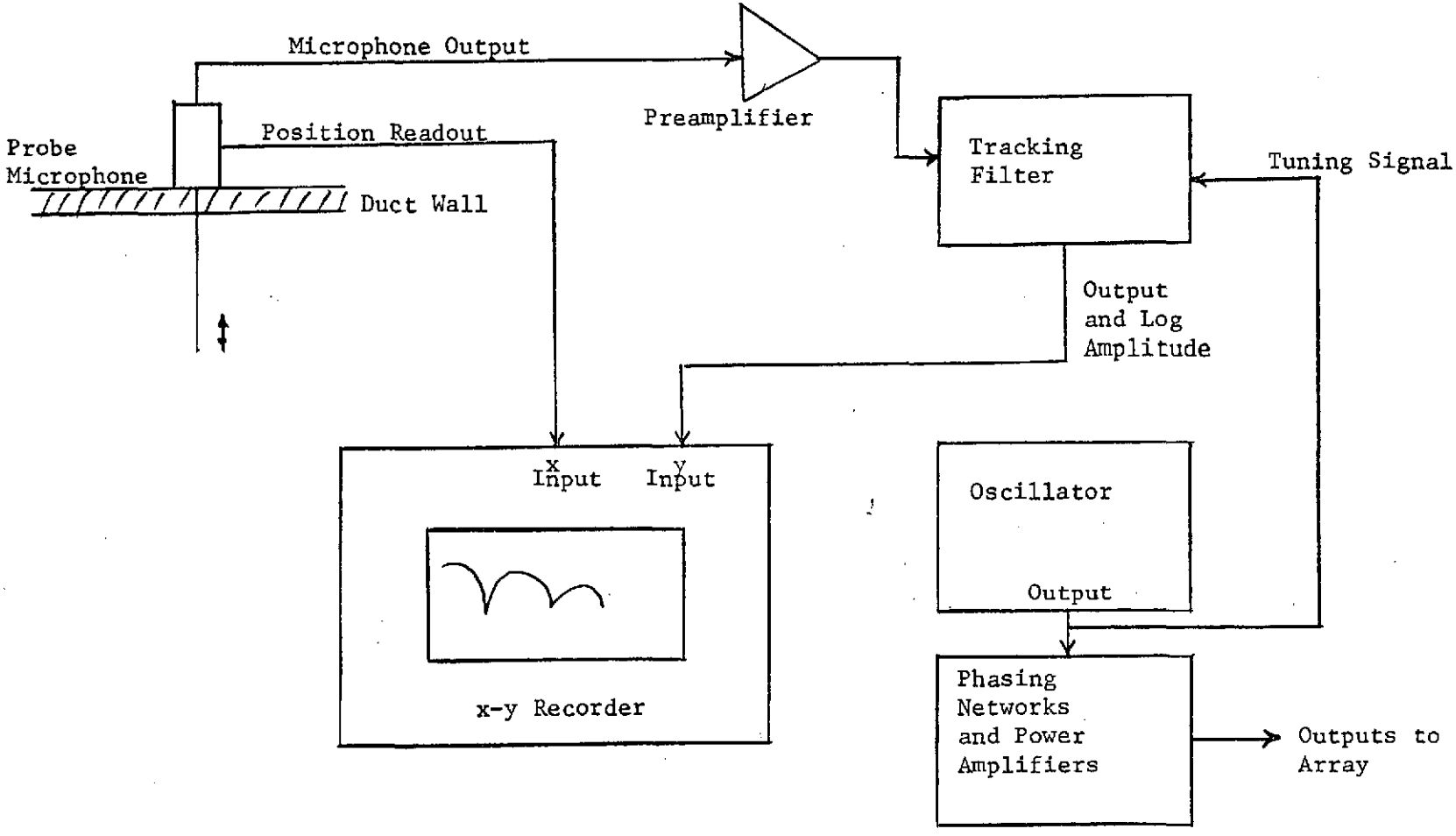

Figure 28 Test Setup Instrumentation

moderate attenuation increasing with frequency and reaching a maximum of about 6 dB. The levels at stations 1 and 2 were almost identical indicating no standing waves in that region. The results shown in Figure 29 were obtained at 670 Hz (slightly above m=1, n=1 cutoff). The results are very close to plane wave behavior indicating that the m=1, n=1 mode is considerably suppressed due to the source symmetry. At 900 Hz, the attenuation is still rising and has a value of 12 dB. Mode shapes at this frequency are shown in Figure 30. At this point, the mode shape inside the liner (station 3) is deviating slightly from plane wave behavior. This is to be expected since a strictly plane wave cannot exist when any appreciable absorption is taking place. A similar pattern exists up to 1100 Hz with the absorption still increasing.

Mode shapes at 1200 Hz are shown in Figure 31. The deviations between stations 1 and 2 indicate that there is now an appreciable standing wave in the upstream region but approximate liner attenuation can still be estimated. The mode shapes of Figure 32 were taken at 1300 Hz which is slightly below the 1370 Hz cutoff frequency of the non-spinning m=0, n=1 mode. The results at station 1 indicate that there is an m=0, n=1 modal component near the source (station 1 is only 4 1/2 inches from the source) but this component is rapidly damped and the plane wave indicated at station 2 is the only one entering the liner. It was found that it was impossible to generate plane waves above the m=0, n=1 mode cutoff frequency since this mode was strongly excited by the array. The plane wave case is not of great importance at high frequencies since higher order modes are usually predominant in most practical situations. A typical set of

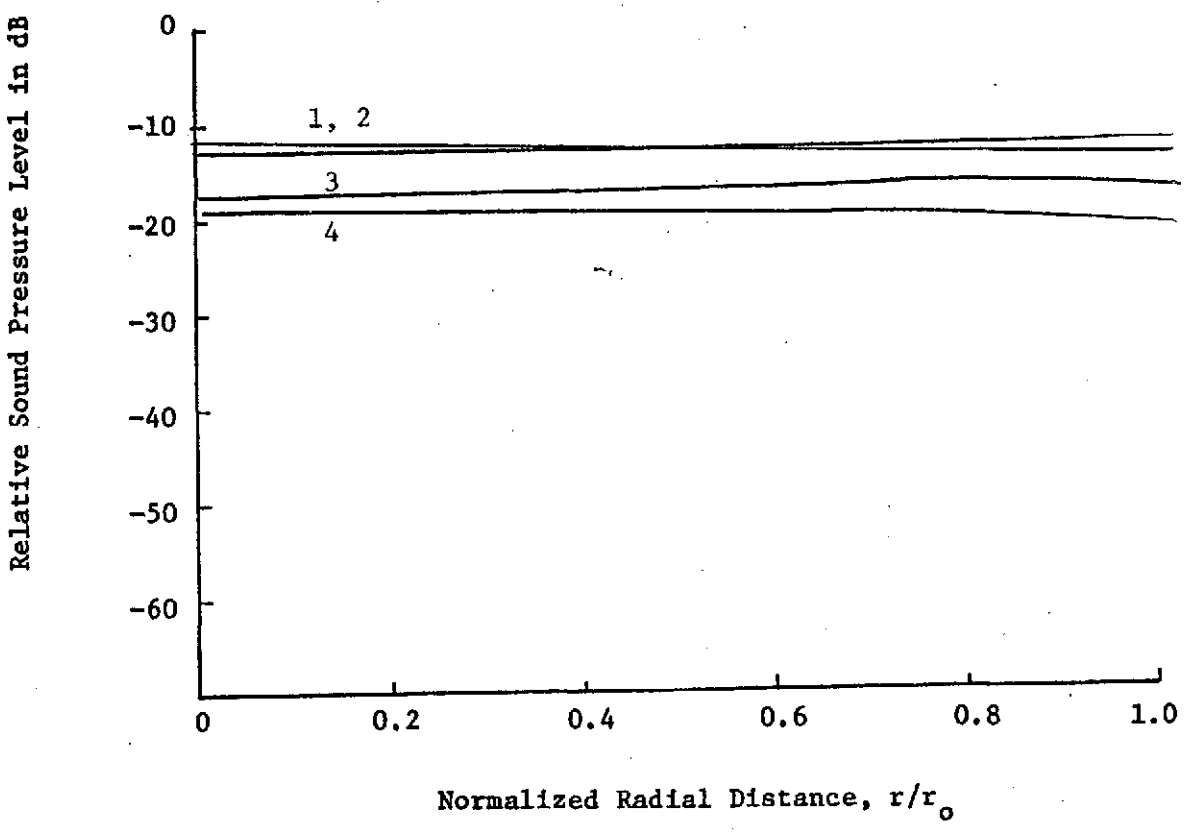

Figure 29 Mode Shapes for Two Foot Liner at 670 Hz

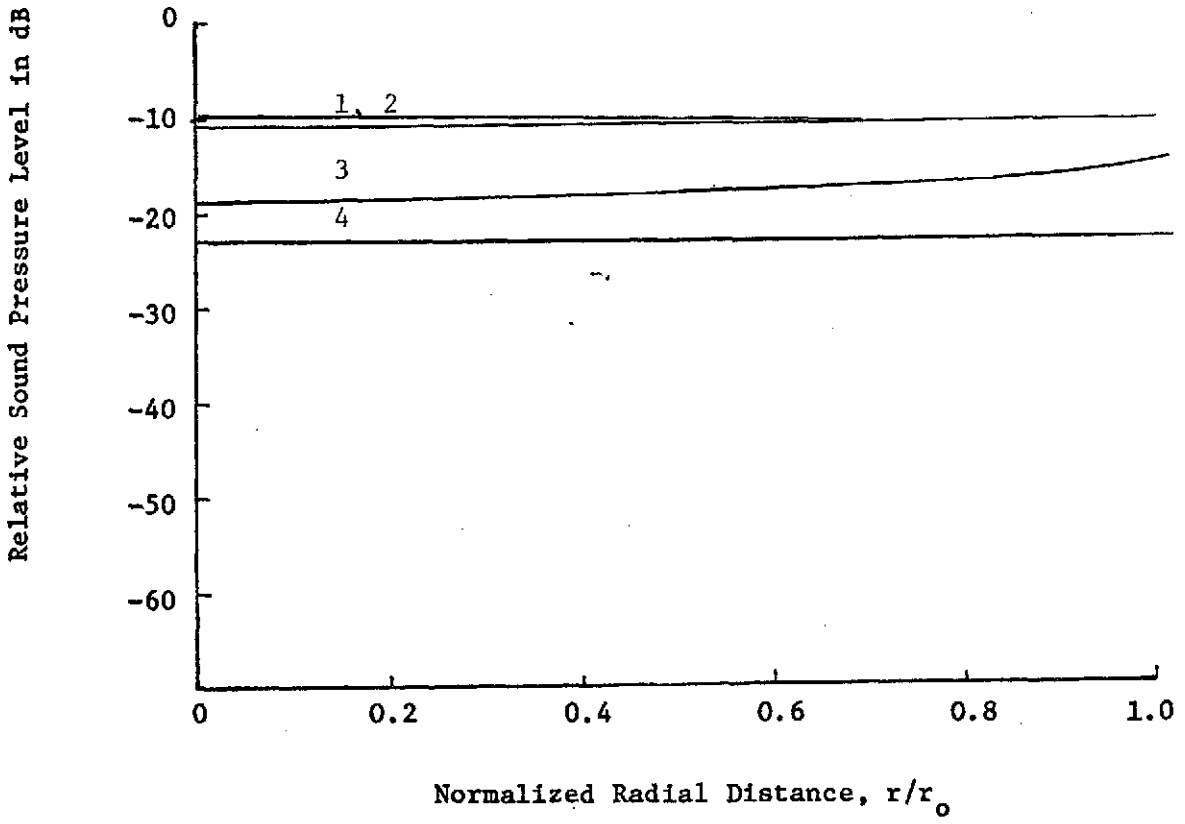

Figure 30 Mode Sahpes for Two Foot Liner at 900 Hz

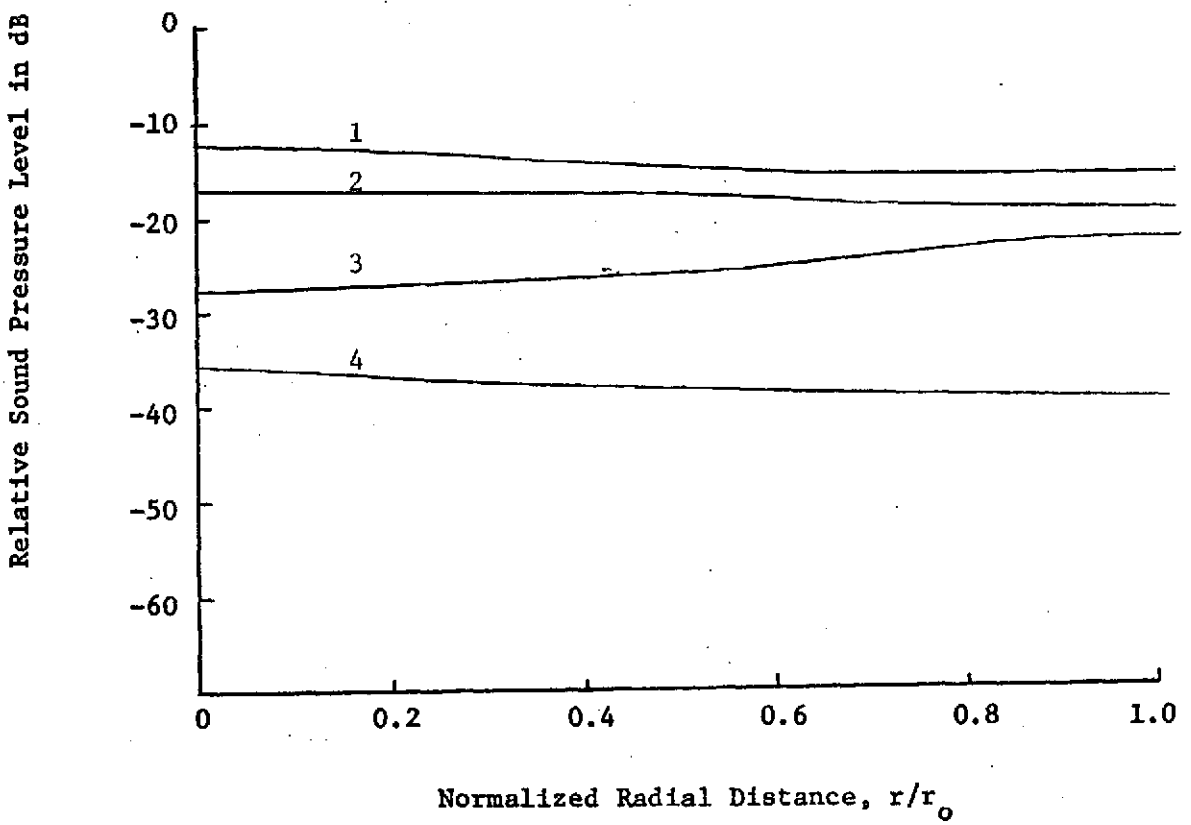

Figure 31 Mode Shapes for Two Foot Liner at 1200 Hz

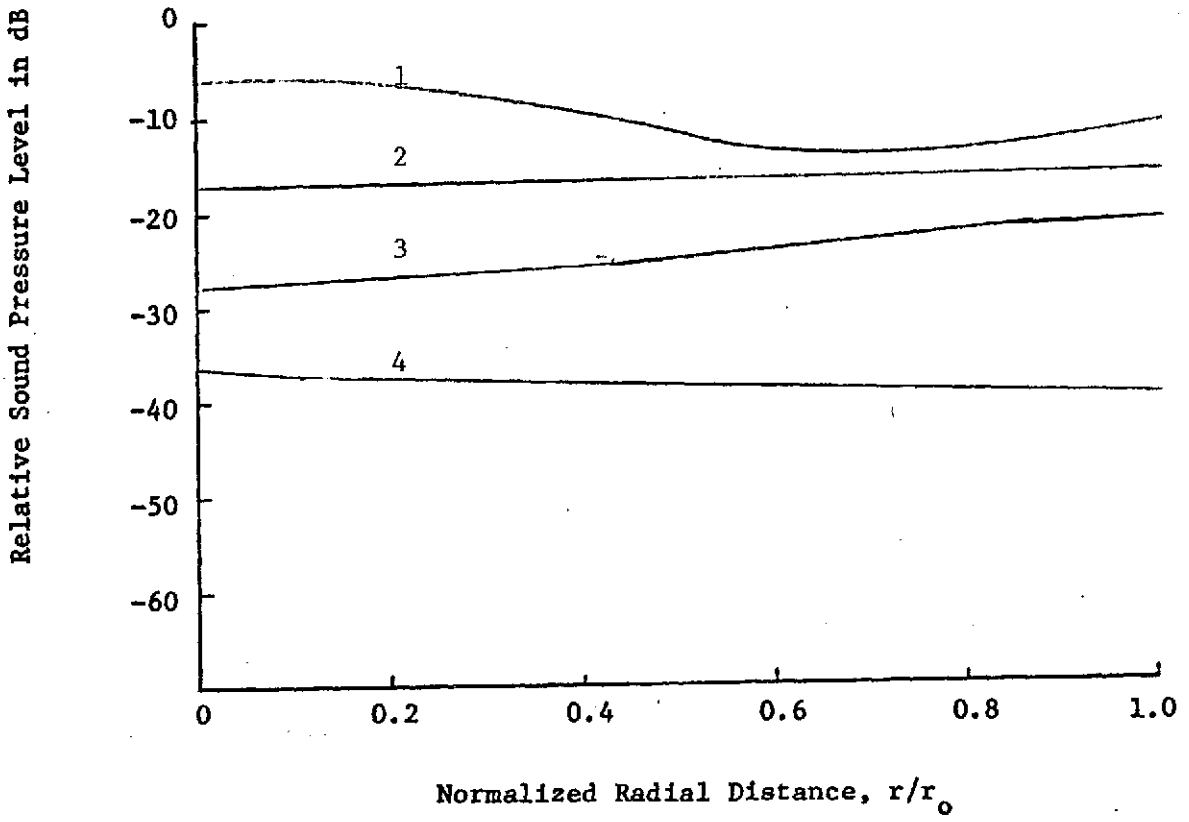

Figure 32 Mode Shapes for Two Foot Liner at 1300 Hz

mode shapes above m=0, n=1 cutoff are shown in Figure 33. There is appreciable non-uniformity in upstream mode shape in terms of amplitude and location of the node as indicated by measurements at stations 1 and 2. Essentially plane wave conditions exist downstream. In general, at a given frequency, liner attenuation for higher order modes is much greater than for plane waves and for the case shown in Figure 33 the m=0, n=1 mode has been attenuated by the liner to such a degree that only the plane waves component can be detected downstream. These data do suggest a method for generating plane waves at high frequencies. A supplementary liner could be placed in the upstream region to remove the higher order modes and the high frequency plane wave attenuation of the liner under study could then be measured. This is precisely the one practical situation where it would be desirable to know the high frequency plane wave attenuation of a liner. Suppose that in a given noise control problem a liner has been installed which sufficiently attenuates the higher order modes but that an objectionable plane wave exists in the duct. It would then be desirable to know the optimum additional liner configuration to install for maximum attenuation of the remaining plane wave.

It is obvious that the m=0, n=1 mode attenuation cannot be determined from Figure 33 since its downstream amplitude is obscured by the plane wave. It was found in later tests with shorter liners that this problem could in some cases be overcome since, in this case, the attenuation of the desired mode is considerably less. In addition, the irregularities in the upstream sound field are less with shorter liners. It was also found that the five element

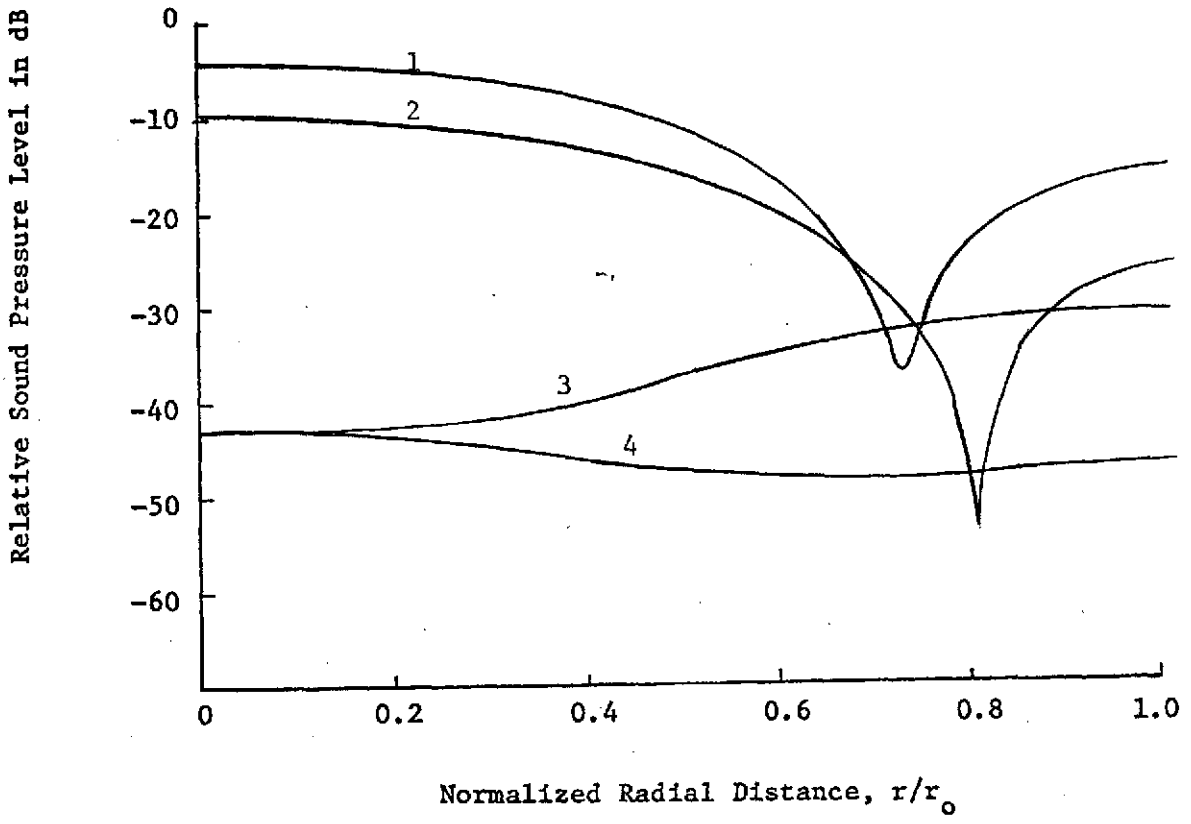

Figure 33 Mode Shapes for Two Foot Liner at 1380 Hz
(Above m=0, n=1 Cutoff Frequency)

array previously described produced better results for the case of non-spinning higher order modes.

The next step in the program was to examine the behavior of the two-foot liner for the first spinning mode (where m=1, n=1). The eight element array was used and phased as previously described for this mode. The identical test setup shown in Figures 27 and 28 was used. Mode shapes at the cutoff frequency for this mode (660 Hz) are shown in Figure 34. In this case, the mode shapes are all quite similar, the upstream field is reasonably uniform and this mode shape is preserved in the downstream section. At this frequency, the liner attenuation for this mode is low enough such that it does not become obscured by any residual plane wave present as was the case in Figure 33. The attenuation of the liner is, however, considerably higher than for the plane wave case at the same frequency as can be seen by comparing Figures 34 and 29 (17 dB versus 6 dB). The irregularities in the curves at small values r/r_o are unimportant in determining the liner attenuation since, based on cross-sectional area considerations, over 90 percent of the energy is propagated in the region between $r/r_o = 0.3$ and $r/r_o = 1.0$. A reasonable estimate can be made of the liner attenuation by first obtaining an average of curves 1 and 2 and then taking the difference between this average and value of curve 4. The resulting number will be approximately the same for any value of r/r_o above 0.30 for the data shown in Figure 34. Similar results were obtained up to 1300 Hz with the liner attenuation increasing with increasing frequency. Deviations from ideal mode shapes occurred at 1400 Hz and above and this would be expected since this frequency is above the 1370 cutoff frequency of the m=0, n=1

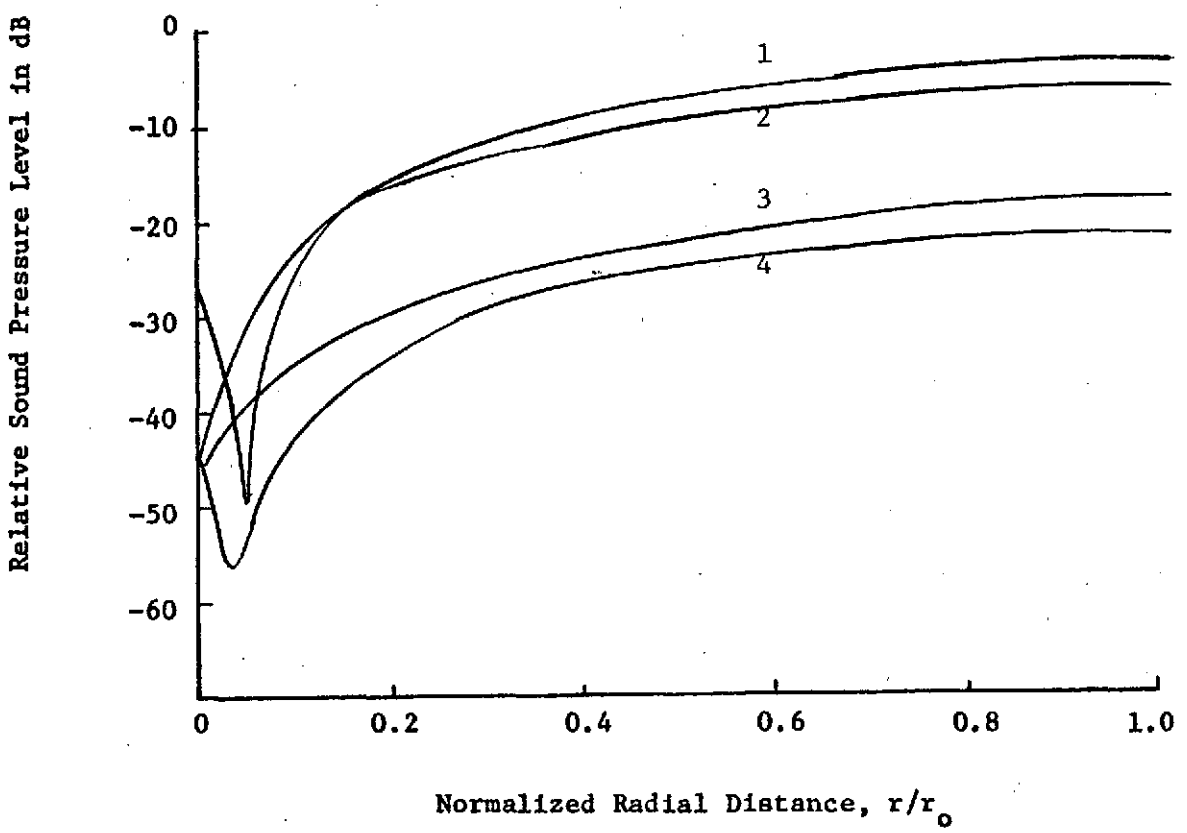

Figure 34 Mode Shapes for Two Foot Liner at 660 Hz
(Cutoff Frequency of m=1, n=1 Mode)

mode and we are in a region where two higher order modes are allowed. The mode shapes at 1400 Hz are shown in Figure 35. The station 1 data are omitted since they agree within better than $\pm$ 1 dB at all positions. The downstream curve indicates almost plane wave behavior giving rise to a situation like that of Figure 33. There is no indication at this point from Figure 35 that there is contamination from the m=0, n=1 mode. It should also be noted from the upstream mode shape that the modal purity is not particularly high. At 1500 Hz, contamination from the m=0, n=1 mode can be seen in the downstream mode shape as shown in Figure 36. Although precise attenuation figures cannot be obtained from Figures 35 and 36, an estimate of the minimum attenuation to be expected for the m=1, n=1 mode can be determined. Similar data are obtained up to 1800 Hz. The results shown in Figure 37 were obtained at 1930 Hz which is the cutoff frequency of the m=1, n=2 mode. Station 1 measurements are omitted for the reasons stated earlier. The upstream and downstream mode shapes show a similar pattern with the necessary 2 nodes for n=2 and the attenuation is high (approximately 30 dB). Station 3 has a mode shape which does not resemble any mode predicted by hard-walled theory but this is not surprising since this station is in the center of the liner and appreciable absorption is taking place. A solution to the boundary value problem with a finite wall impedance is necessary to predict the mode shape in the liner region. No attempt was made to extend these measurements beyond 1930 Hz since upstream mode shapes were not satisfactory above this frequency.

The chatacteristics of the shorter one-foot liner were investigated next. The results for the plane wave case at frequencies

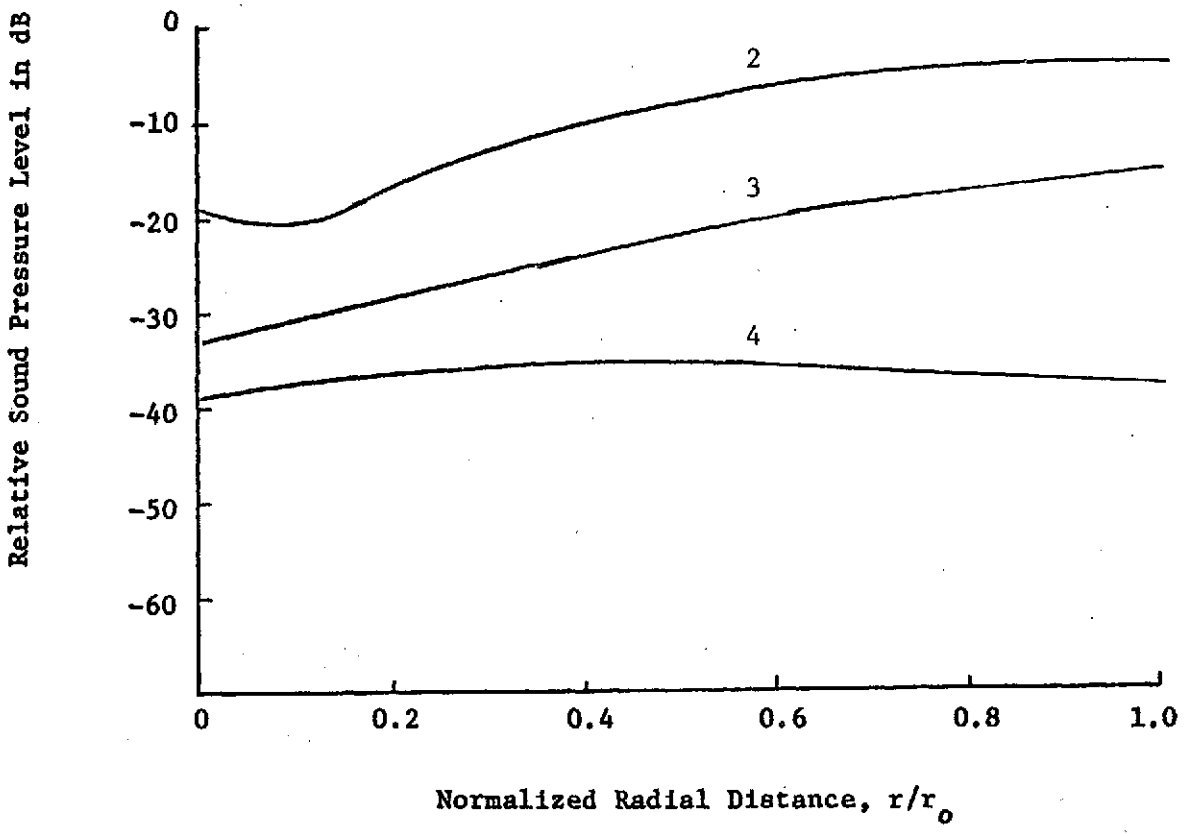

Figure 35 Mode Shapes for Two Foot Liner at 1400 Hz

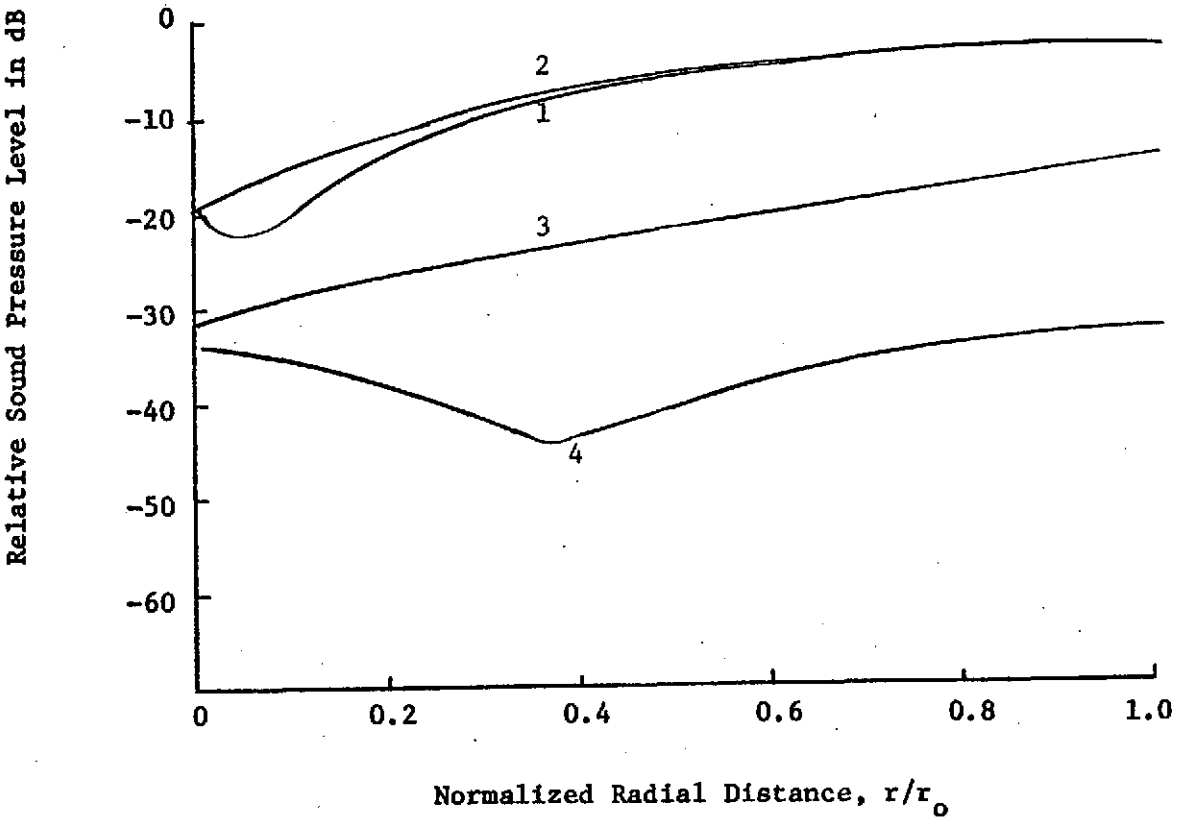

Figure 36 Mode Shapes for Two Foot Liner at 1500 Hz

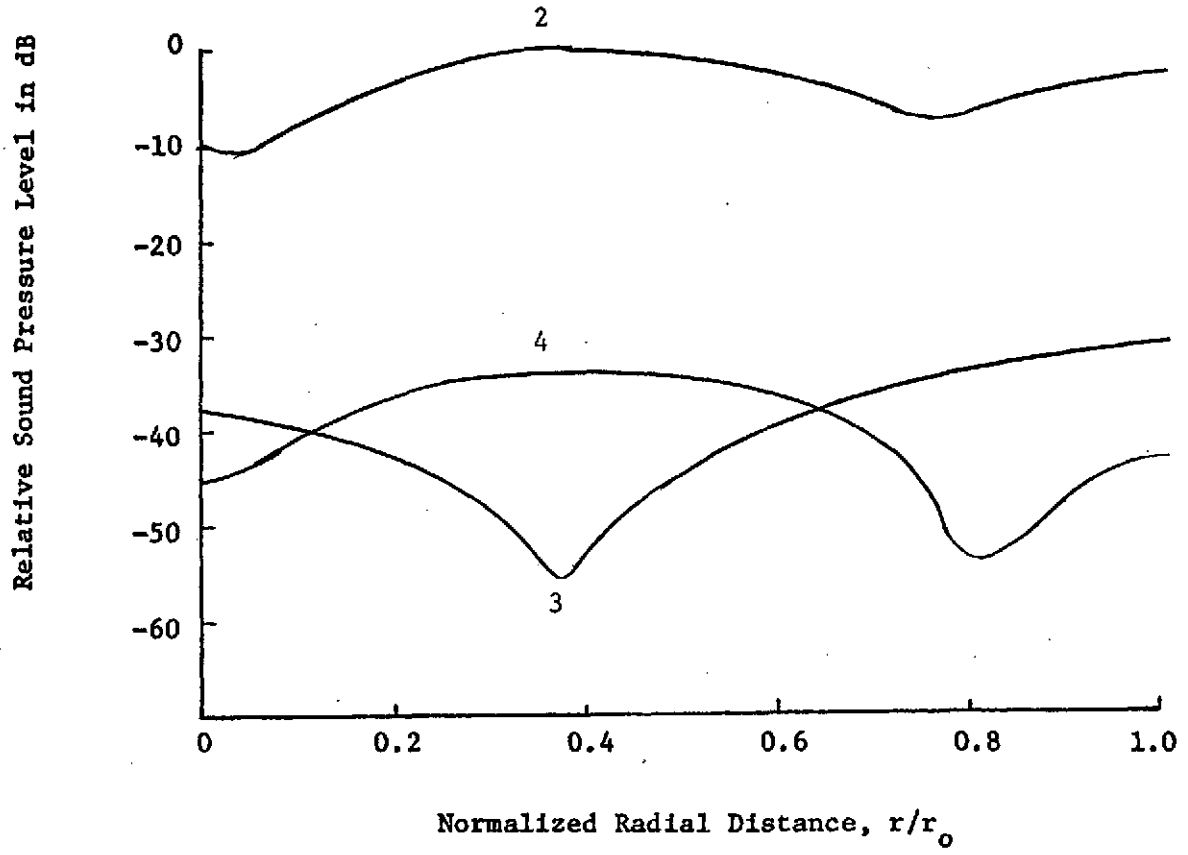

Figure 37 Mode Shapes for Two Foot Liner at 1930 Hz

below m=0, n=1 mode cutoff frequency (1370 Hz) were similar to those of the two-foot liner except for a correspondingly smaller attenuation. Mode shapes at 1370 were as shown in Figure 38. The upstream conditions are more uniform than the corresponding measurements for the two-foot liner shown in Figure 33 but again the actual attenuation of the liner is masked by an essentially plane wave downstream mode shape and only the minimum expected liner attenuation can be obtained for m=0, n=1 mode. At 1400 Hz, the mode shape is preserved downstream as shown in Figure 39 and the actual attenuation can be estimated. In this case, only the station 2 and 4 mode shapes are presented.

The next step was to study the one-foot liner for the spinning mode case. The results were similar to those described above for the two-foot liner except that the upstream mode shapes were more uniform and contamination from the m=0, n=1 mode did not occur until 1600 Hz. Mode shapes were measured above this frequency and the interesting results shown in Figure 40 were obtained at 1700 Hz. The m=1, n=1 mode is excited in the upstream region (admittedly with poor modal purity) and a mode shape appears in the center of the liner which is very similar to the m=0, n=1 mode for the hard-walled case except that it is a mirror image in terms of r/r_o and also the slope is not zero at $r/r_o = 0$. Plane wave conditions exist in the downstream region. The frequency and upstream conditions were such that a mode which would be predicted from the solution to the boundary conditions for a finite wall impedance was strongly excited. There is a similar but weaker indication of the same condition in Figure 37 although the position of the node is different. The

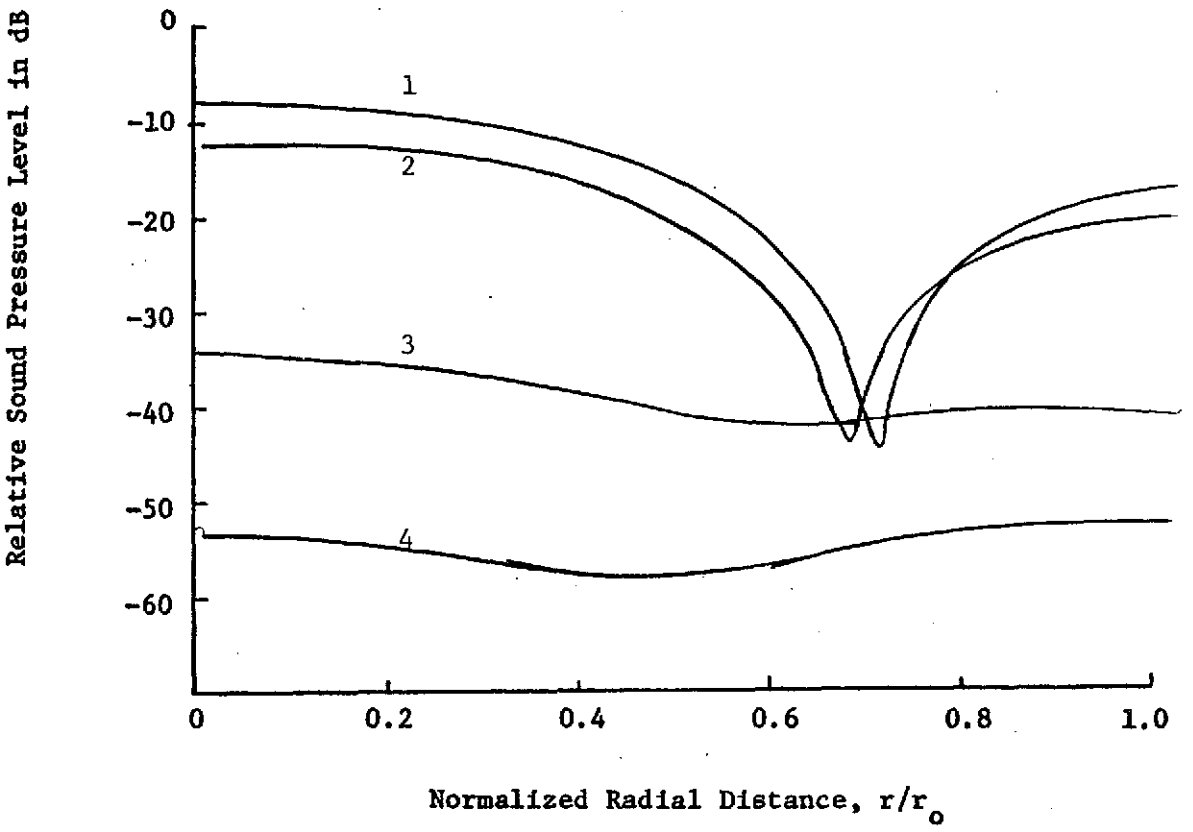

Figure 38 Mode Shapes for One Foot Liner at 1370 Hz

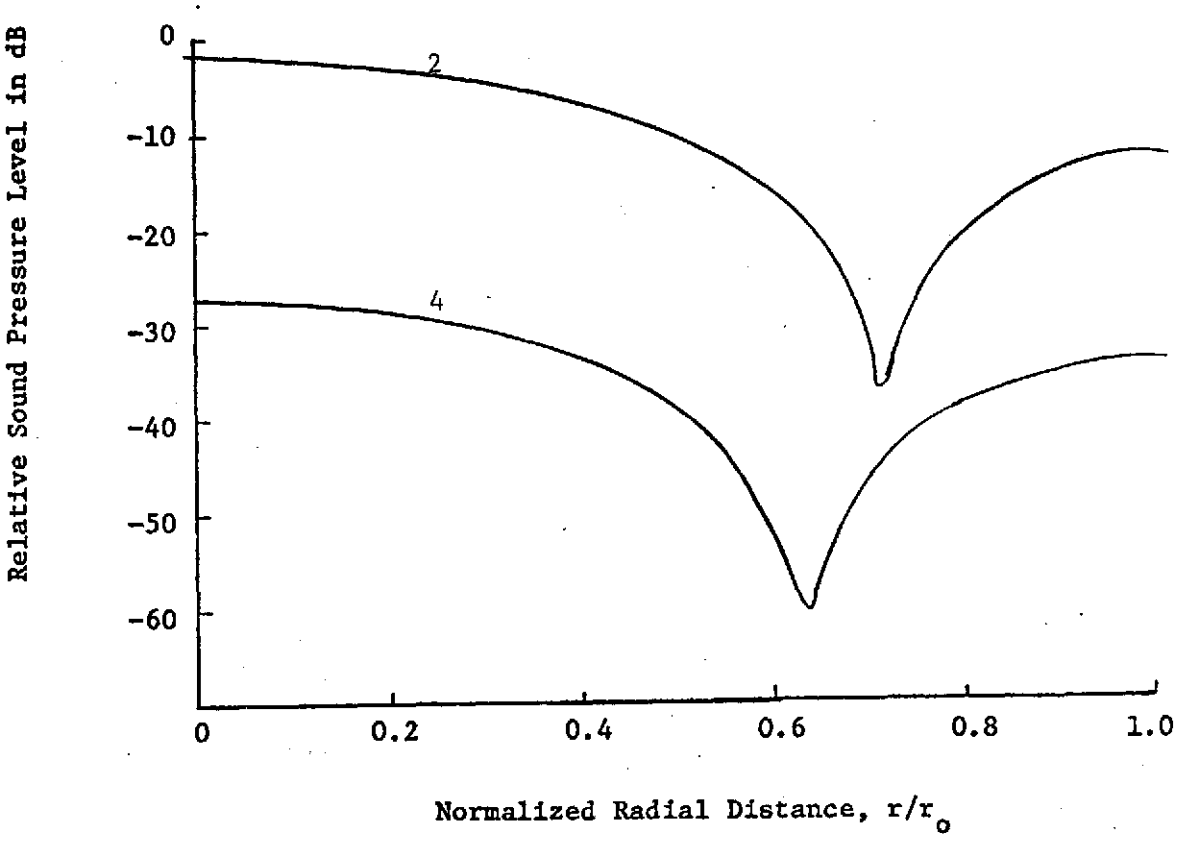

Figure 39 Mode Shapes for One Foot Liner at 1400 Hz

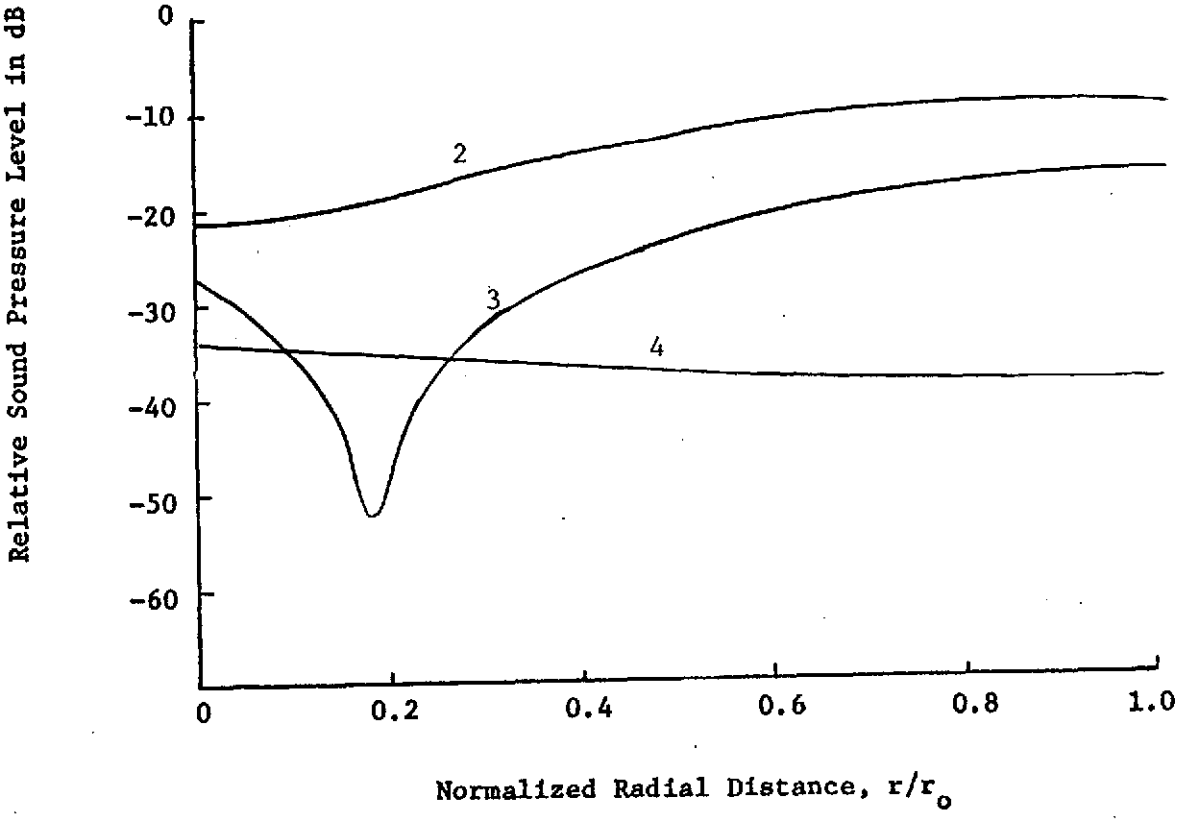

Figure 40 Mode Shapes for One Foot Liner at 1700 Hz

absence of this mode in the downstream region in Figure 40 is understandable since this mode is not an allowed solution for the hard-walled case.

The results of these liner tests are summarized by the attenuation curves shown in Figures 41-44. These curves were obtained by taking the difference between the average upstream sound pressure level and the downstream sound pressure level at $r/r_o = 1$ in the frequency range where the modes shapes in both regions were similar enough where such a method is reasonable. Figures 41 and 42 represent attenuation curves for the one-foot liner for the plane wave and spinning wave cases, respectively, and Figures 43 and 44 are similar data for the two-foot liner. For both liners, the attenuation is considerably higher for the spinning mode than for the plane wave. For the plane wave case, a doubling of length of treatment between the one-foot and two-foot liners resulted in an approximate doubling of attenuation as can be seen from a comparison of Figures 41 and 43. A comparison of Figures 42 and 44 indicate that the attenuation is less than doubled for spinning modes. This indicates that attenuation for spinning modes cannot be specified in terms of so many decibels per unit distance, at least for the case of finite liner length. The increased attenuation for spinning modes over plane waves for a given liner at the same frequency is not surprising since the group velocity for any higher mode is always less than c_o and the "dwell time" in the liner is always longer than for a plane wave. Attenuation curves for the first non-spinning higher order mode were not obtained due to the downstream plane wave contamination previously mentioned and the limited frequency range over which the mode could be generated.

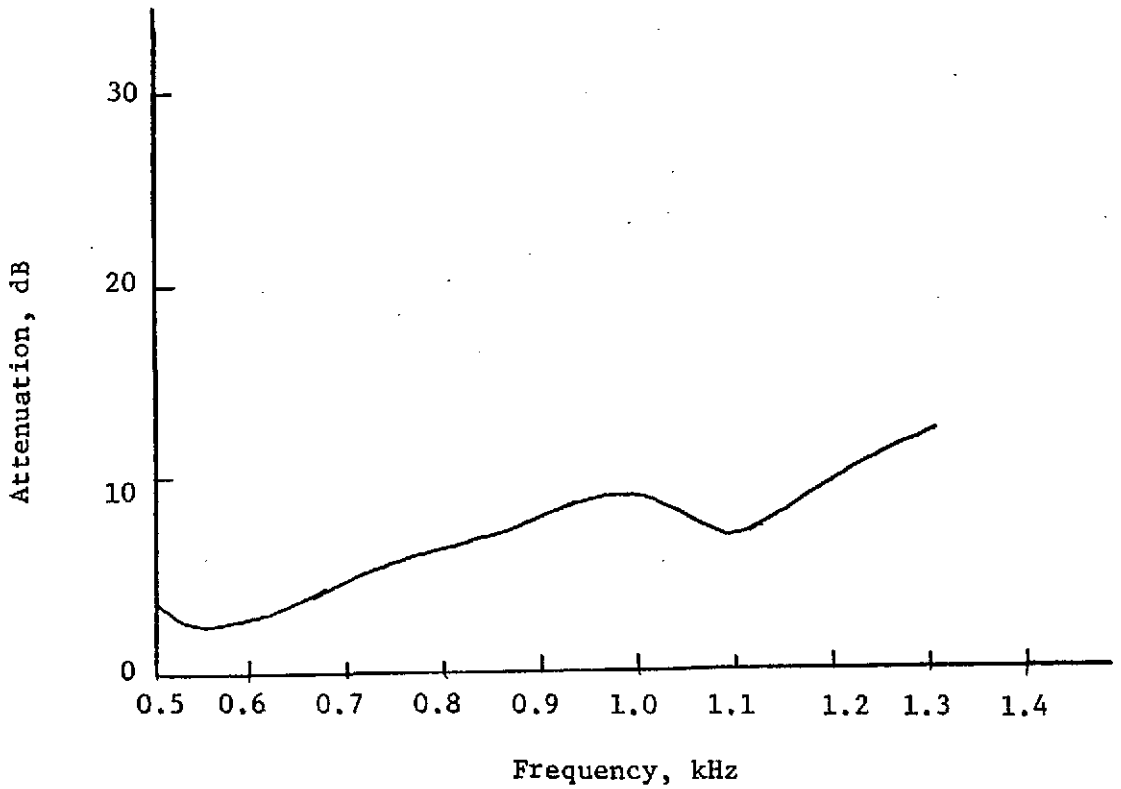

Figure 41 Attenuation Versus Frequency for the One Foot Liner with Plane Wave Propagation

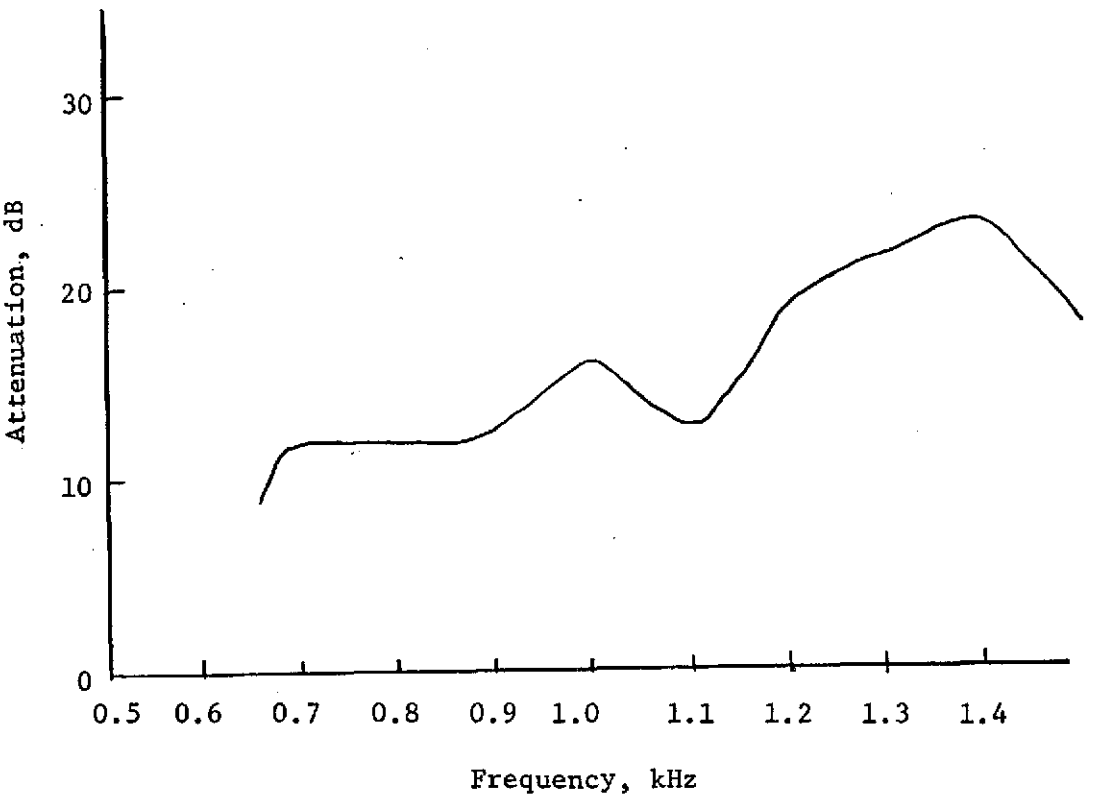

Figure 42 Attenuation Versus Frequency for the One Foot Liner with Spinning Wave Propagation

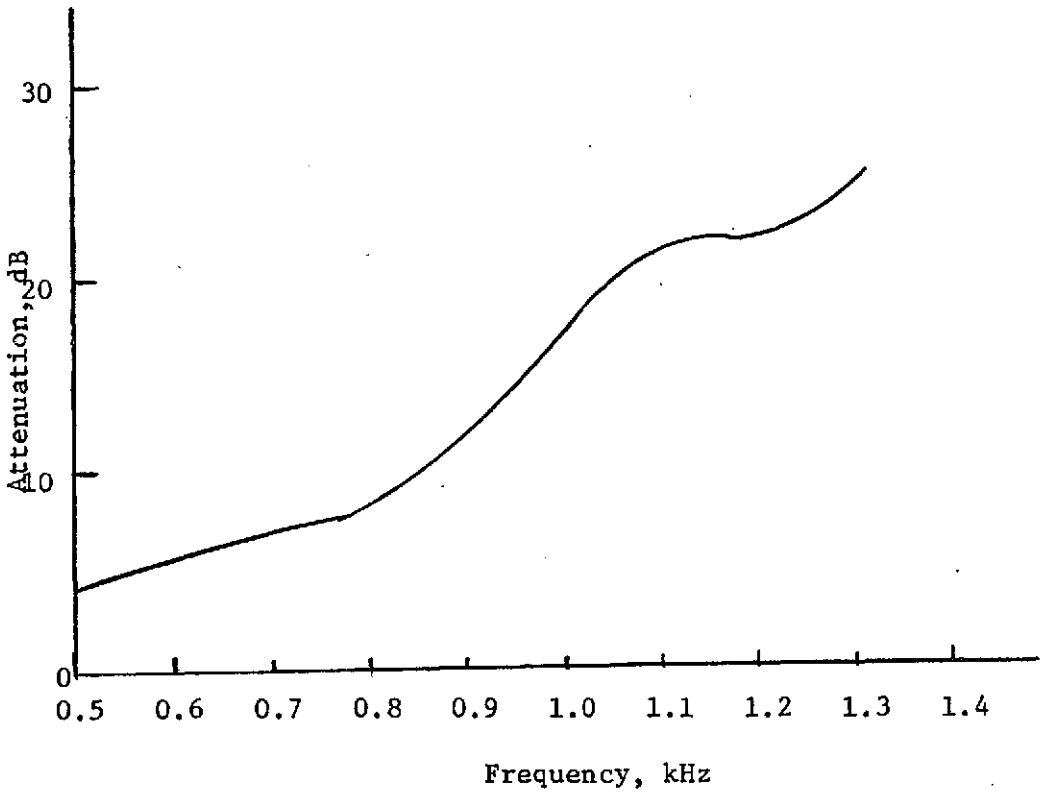

Figure 43 Attenuation Versus Frequency for the Two Foot Liner with Plane Wave Propagation

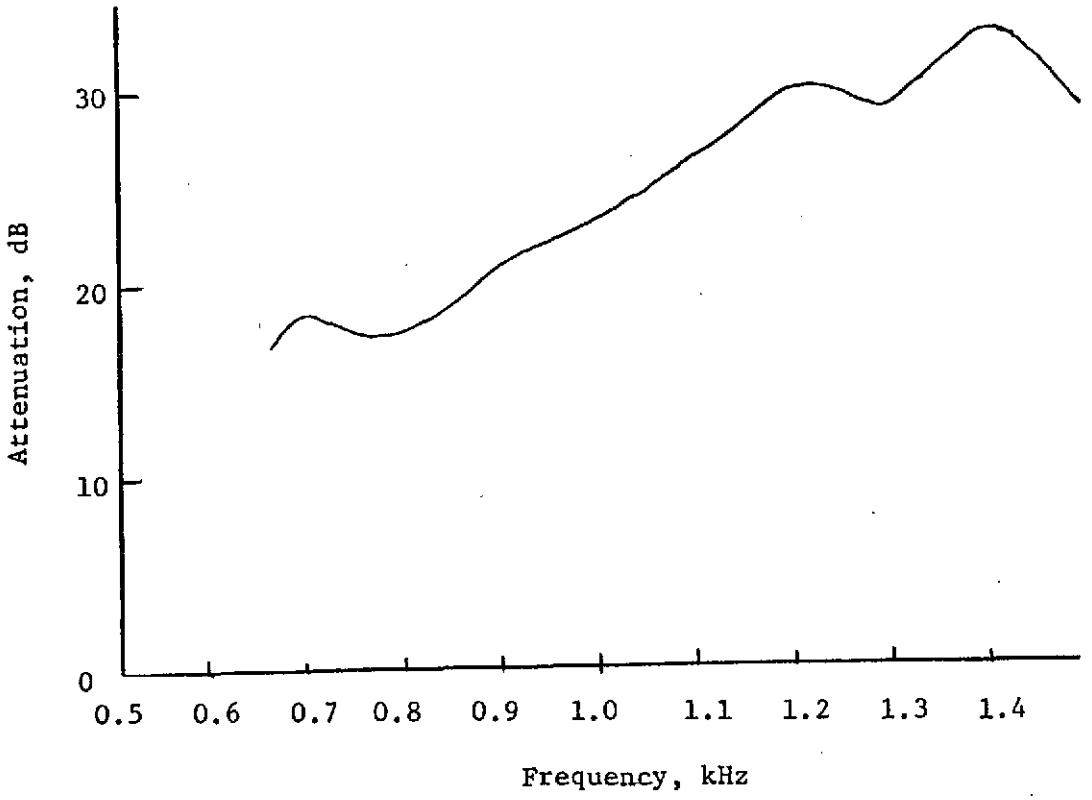

Figure 44 Attenuation Versus Frequency for the Two Foot Liner with Spinning Wave Propagation

The data obtained for this mode indicate that, in all cases, the attenuation is in excess of 30 dB.

CHAPTER VI

THE BEHAVIOR OF PLANE WAVES AND HIGHER ORDER DUCT MODES AT HIGH ACOUSTIC INTENSITIES

In this experimental phase of the project, we examined the behavior of finite amplitude waves for both a hard-walled and lined duct. Measurements were first made with plane waves and then extended to the case of higher order modes, an area which has not been previously explored experimentally. The basic objective of this series of experiments was to first verify that we could produce the wave steepening effect described in Chapter III and observed by others (see, for example, Reference 14) with plane waves, then to determine the behavior of higher order modes at high intensities, and finally to study the behavior of absorptive liners at high intensities for both the plane wave and higher order mode cases.

The transite duct previously described in Chapter V was used for all of the high intensity experiments with some modifications which will be described below.

Ling Model EPT 94 air modulator loudspeakers (electro-pneumatic transducers) were used as sound sources for all of the high intensity tests. This source consists of an electromagnetic valve which modulates an air stream in accordance with an electrical signal supplied to it. The device is capable of generating several thousand acoustic watts for a 50-watt electrical modulating signal when a sufficient amount of air is supplied to it from a compressed air source. The electro-pneumatic to acoustic conversion efficiency is in the order of ten percent so that for a 2000-watt acoustic output,

pneumatic power of about 20,000 watts must be available to operate the device. It was found that the compressed air supply available in the College of Engineering was capable of supplying one loudspeaker for continuous operation and could operate four sources for approximately ten minutes on a "blow-down" basis; that is, until a large storage tank was exhausted. The design and performance of the Ling EPT 94 loudspeaker are described in detail by Fiala and Hilliard in Reference 32. Maximum power output can be obtained up to 500-700 Hz and low frequency limiations are based on the method of coupling the drivers to the medium. For example, an exponential horn with a cutoff frequency of 100 Hz would provide constant acoustical output down to that frequency.

The initial plane wave studied were made using a single source coupled to the duct with an exponential horn. A diagram of the test setup is shown in Figure 45 with the location of measurement stations indicated. The anechoic termination shown previously in Figure 19 was used for these tests. The Ling source, exponential horn and upstream section of the duct are shown in Figure 46. Probe microphones can be seen at several measurement stations. The experiments were conducted in the anechoic chamber in order to take advantage of the chamber's high acoustic isolation which was necessary for safety and annoyance requirements. No one was permitted in the chamber when the sound source was in operation.

The hard-walled case was investigated first. Figures 47 through 51 show the sound pressure wave forms at various stations for an initial sound pressure level of 161 dB re 2×10^{-4} dynes/cm^2 at 450 Hz. The high frequency random noise present is due to the

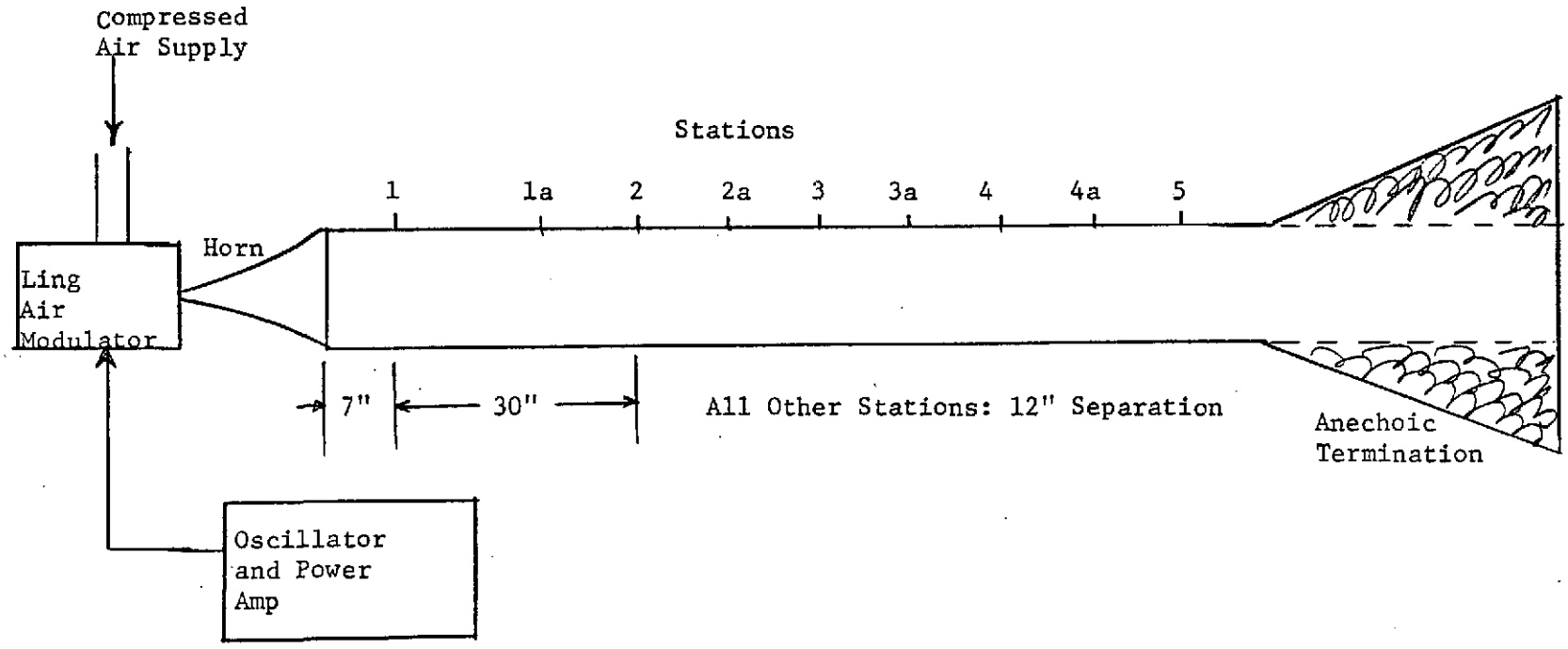

Figure 45 Test Setup for High Intensity Tests

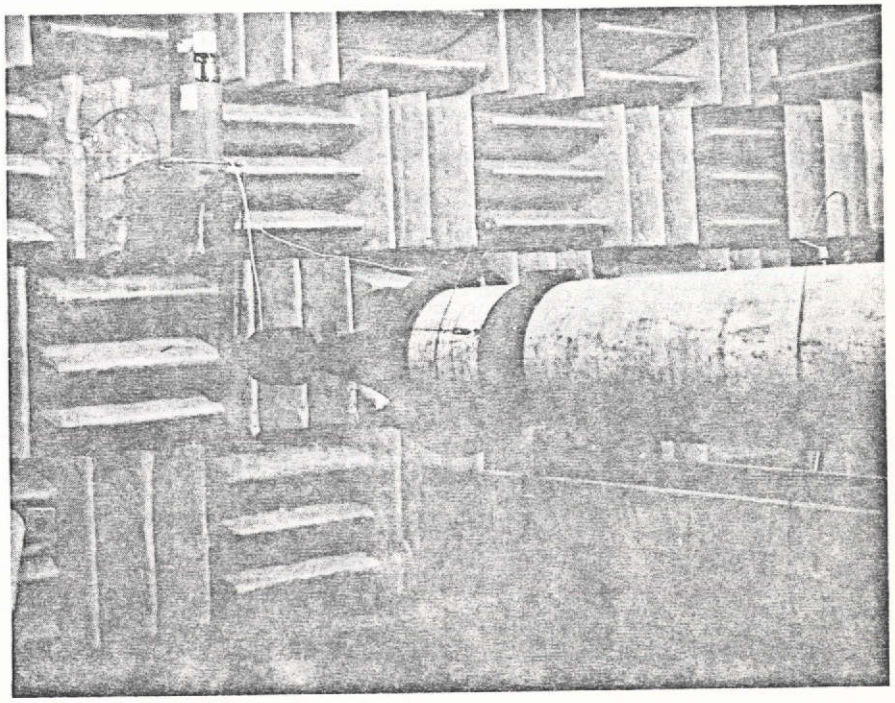

Figure 46 Source, Horn and Upstream Section of Duct

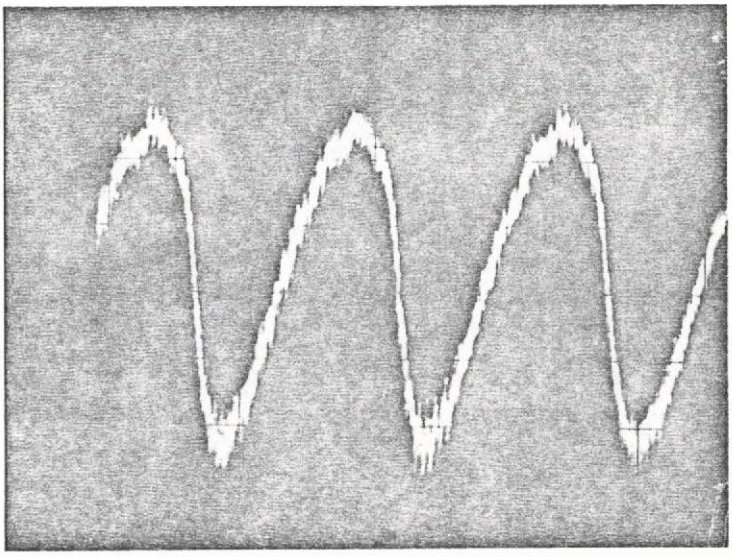

Figure 47 Sound Pressure Waveform at Station 1 Without Liner

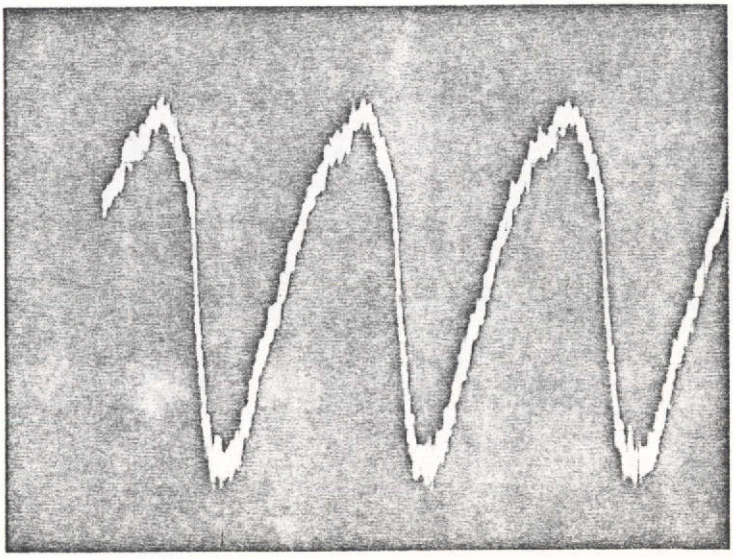

Figure 48 Sound Pressure Waveform at Station 2 Without Liner

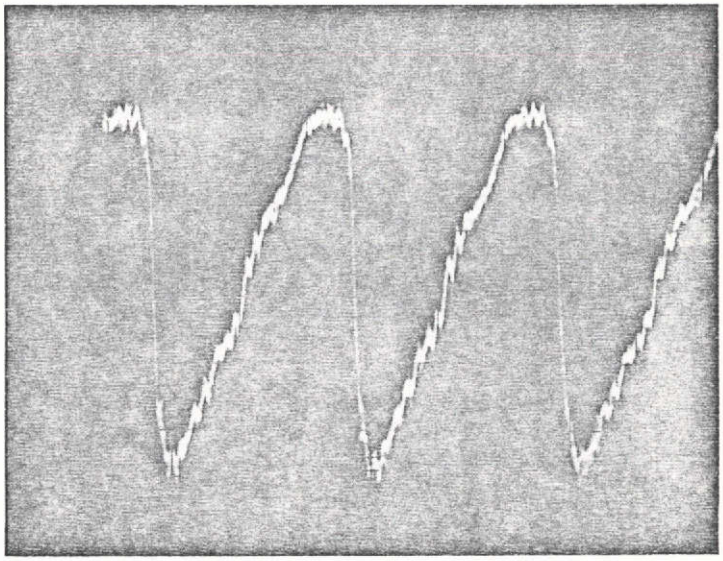

Figure 49 Sound Pressure Waveform at Station 3 Without Liner

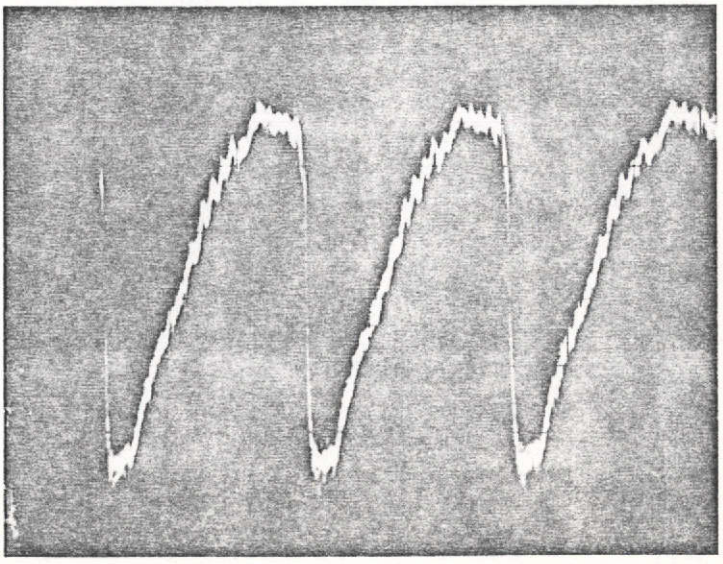

Figure 50 Sound Pressure Waveform at Station 4 Without Liner

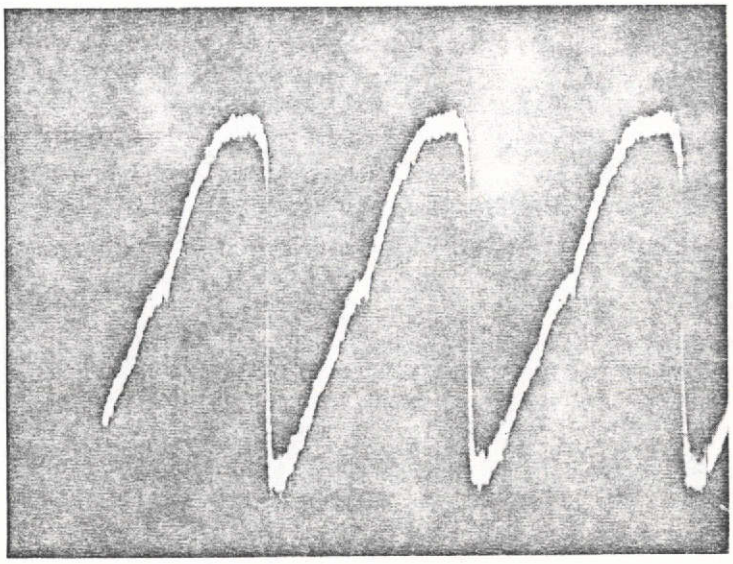

Figure 51 Sound Pressure Waveform at Station 5 Without Liner

aerodynamically-originated self noise of the acoustic source. The wavefront steepening and sawtooth shape, due to finite amplitude effects, are well-illustrated in these photographs. It was discovered after these data were obtained that a 180° phase shift existed in the microphone and preamplifier system and that the actual waveforms, for time increasing to the right on the horizontal axis, are the mirror image of those shown in Figures 47 through 51. This situation was corrected in the later series of measurements involving higher order modes so that the waveforms could be viewed in the more conventioned manner.

From Equation (2-30), the shock formation distance is 571 cm or 15.4 feet so that the measurements do not include the shock region even at station 5 (Figure 51) which is 9.5 feet from the source. The duct was later extended in length to include the x=x case.

Harmonic spectra for each station are shown in Figures 52 through 56, and the harmonic growth with distance is as would be expected from the Bessel-Fubini solution.

From Chapter III, the second and third harmonics are given approximately by Equations (3-27) and (3-28) as

$$\frac{P_2}{P_o} = \frac{(\gamma+1)\ \omega\ P_o x}{2\sqrt{2}\ \rho_o\ c_o^3} \tag{3-27}$$

and

$$\frac{P_3}{P_o} = \frac{3}{8}\left[\frac{(\gamma+1)\ \omega\ P_o x}{\sqrt{2}\ \rho\ c_o^3}\right] \tag{3-28}$$

so that the rate of growth of the second harmonic is proportional to the distance of propagation x and the growth of the third harmonic

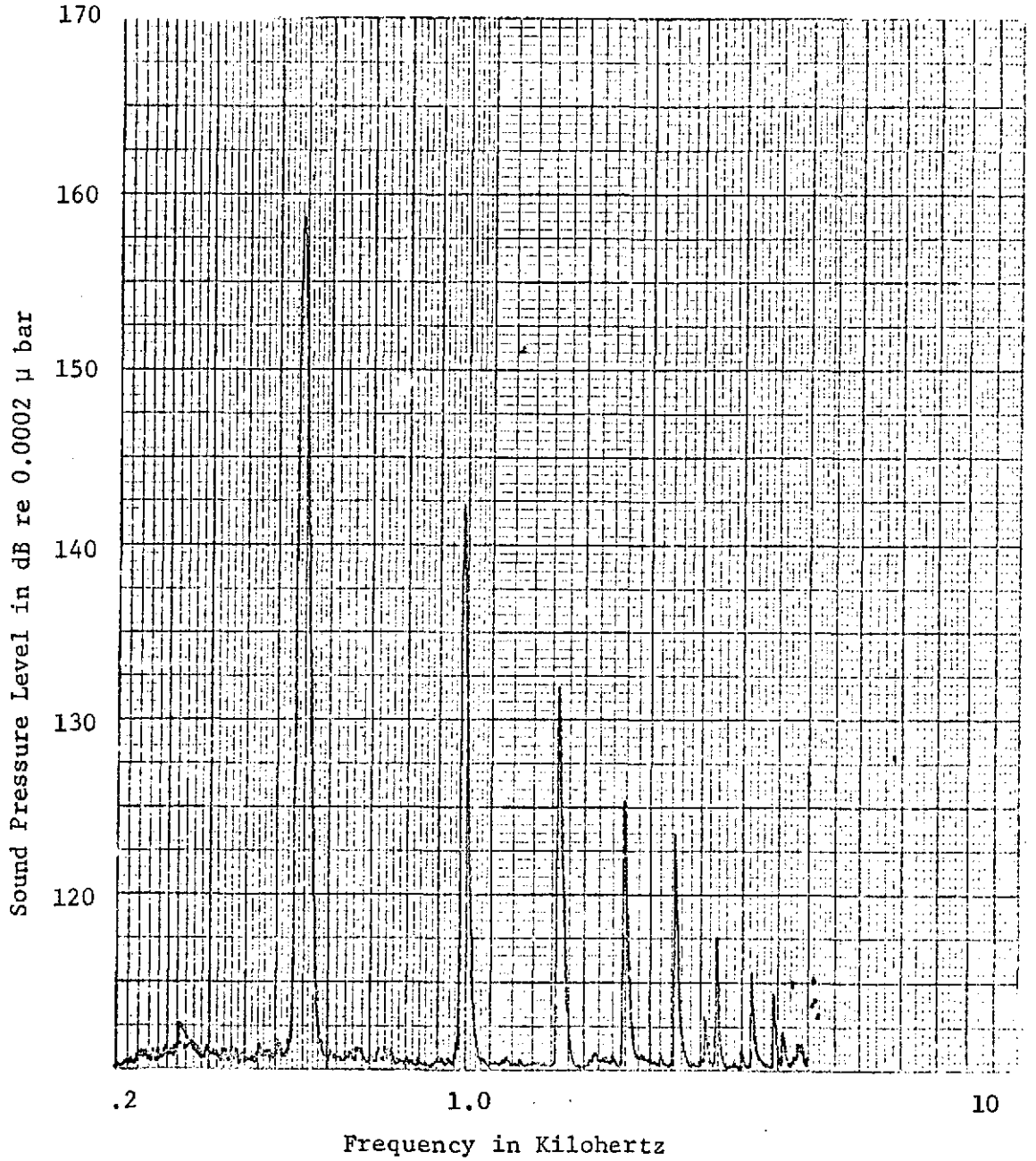

Figure 52 Spectrum at Station 1 Without Liner

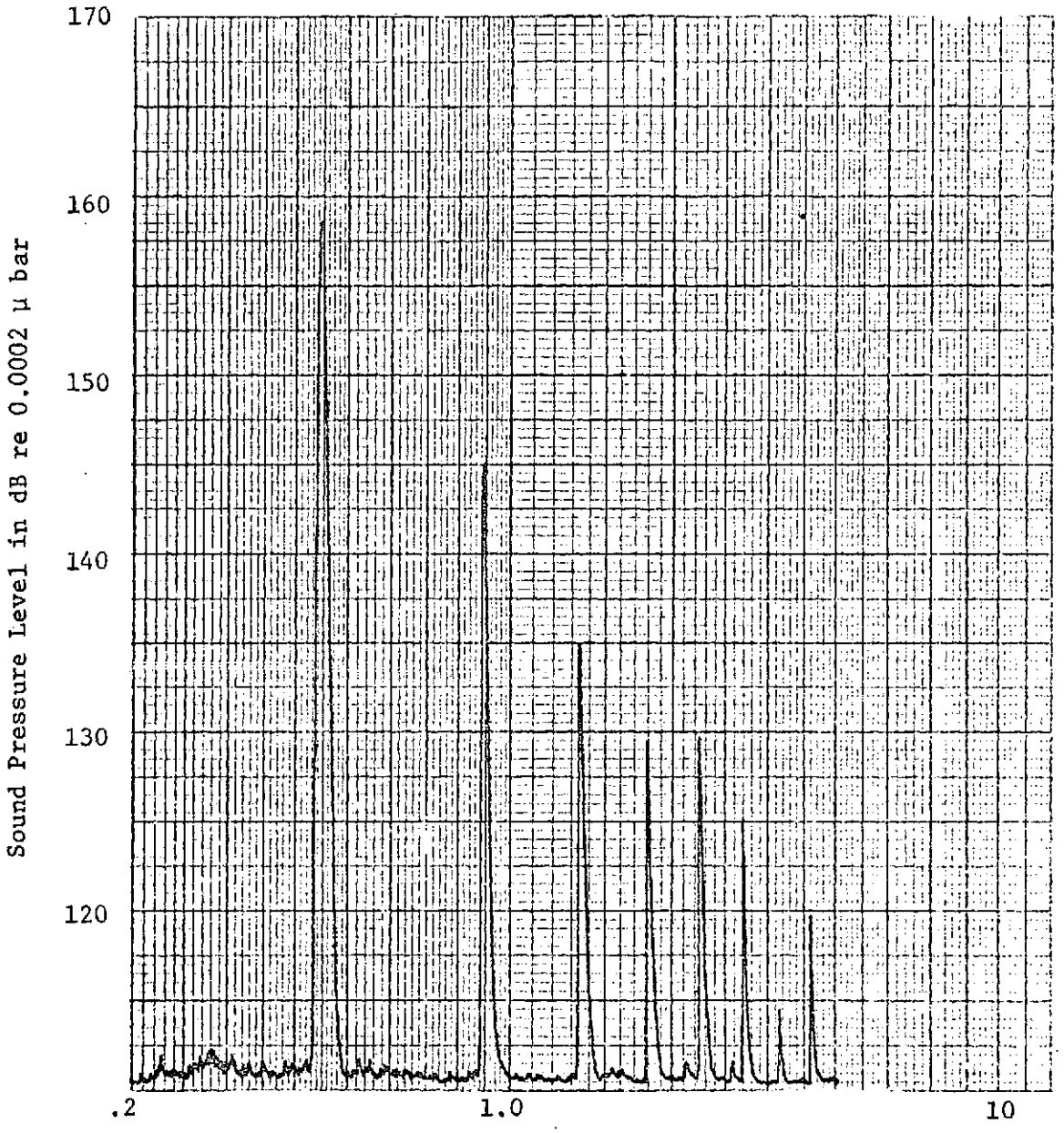

Figure 53 Spectrum at Station 2 Without Liner

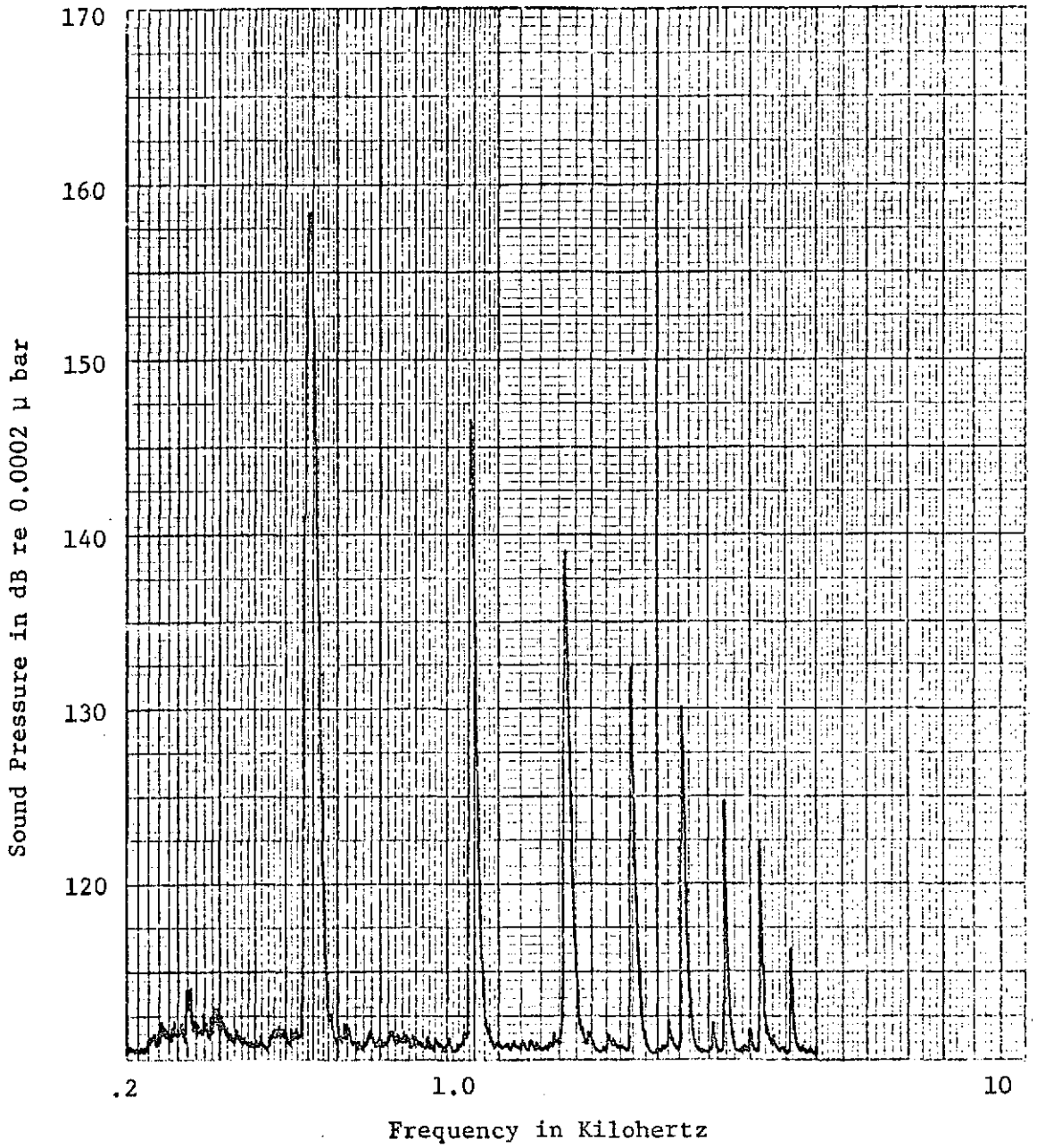

Figure 54 Spectrum at Station 3 Without Liner

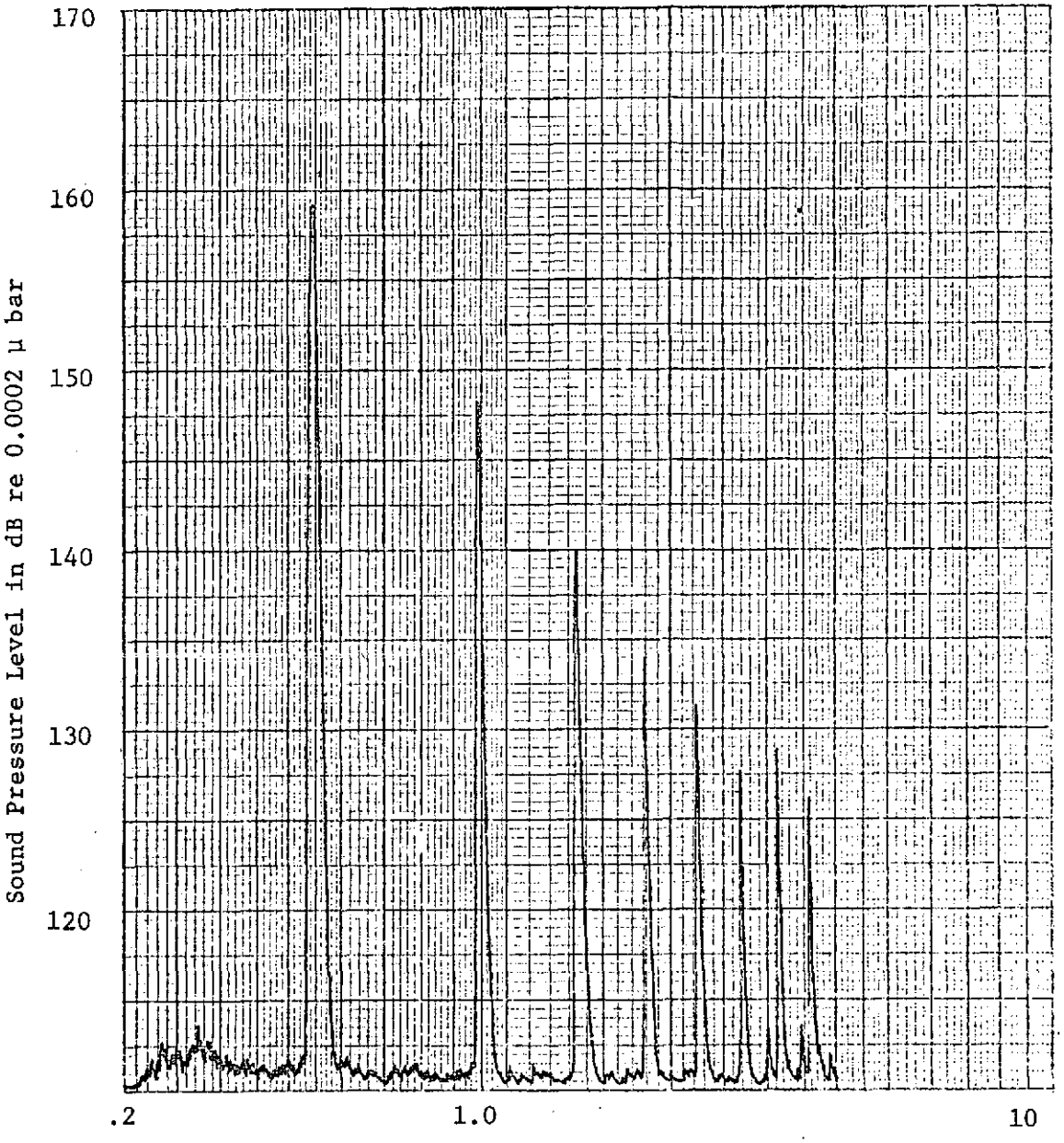

Figure 55 Spectrum at Station 4 Without Liner

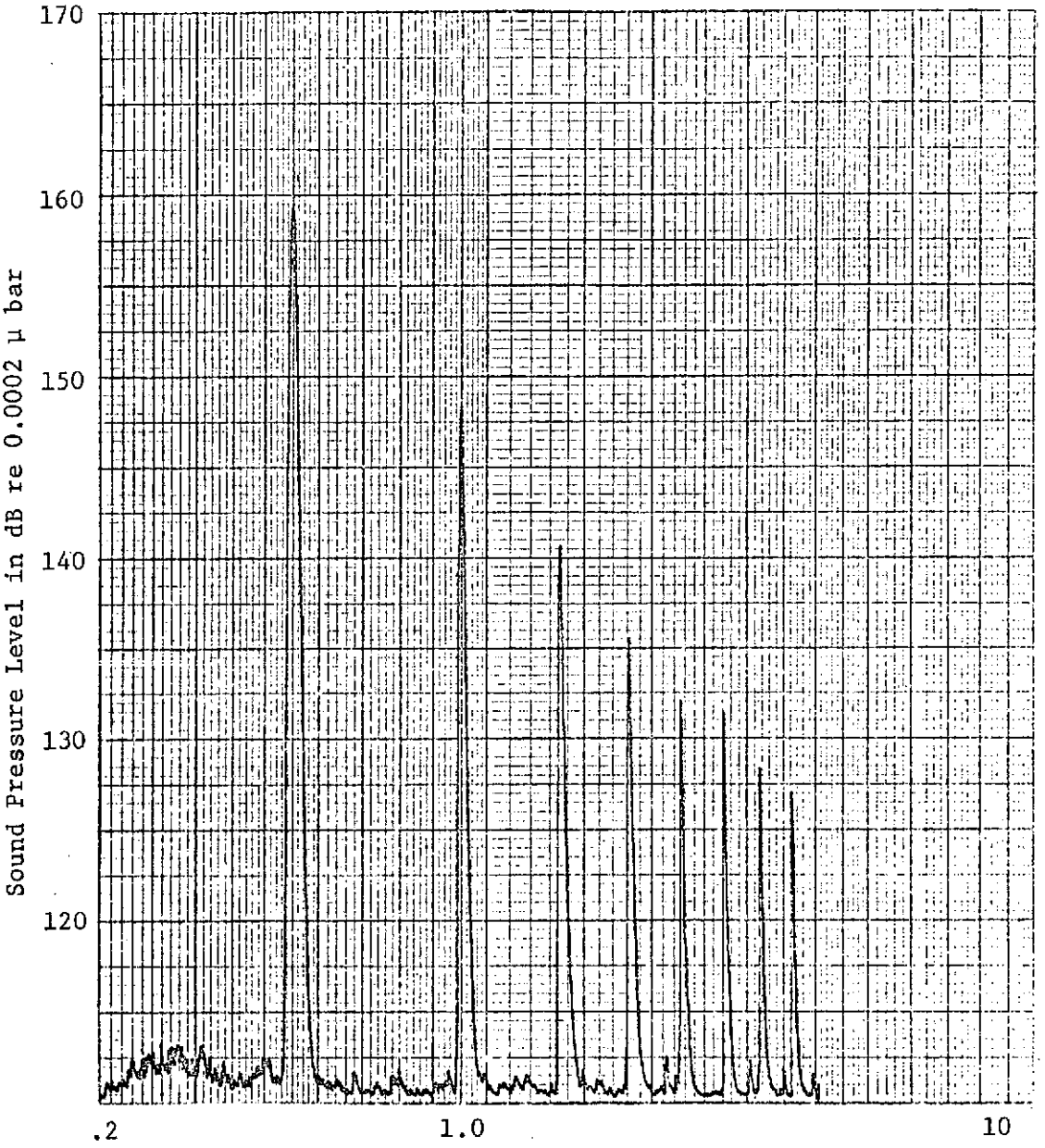

Figure 56 Spectrum at Station 5 Without Liner

is proportional to x^2. It can be shown in general that the rate of growth of the nth harmonic, Pn, is proportional to x^{n-1}. As stated earlier, a computer program has been utilized to determine the theoretical values of the second and third harmonic from the Bessel-Fubini solution. It uses the more exact form of the solution based on the first three terms of the power series expansion of Equations (3-25) and (3-26):

$$\frac{P_2}{P_o} = \frac{\sigma}{2} \quad 1 - \frac{5\sigma^2}{24} + \frac{\sigma^4}{96} \qquad (6.1)$$

and

$$\frac{P_3}{P_o} = \frac{3\sigma^2}{8} \quad 1 - \frac{7\sigma^2}{16} + \frac{\sigma^4}{15} \quad . \qquad (6\text{-}2)$$

The output of the program is in terms of

$$D_2 = 20 \log_{10} \frac{P_2}{P_o} \qquad (6\text{-}3)$$

and

$$D_3 = 20 \log_{10} \frac{P_3}{P_o} \quad , \qquad (6\text{-}4)$$

and D_2 and D_3 therefore represent how many decibels the second and third harmonics are below the fundamental. These quantities can be easily read from the harmonic spectra reported later in this chapter. The computer program can be run over any desired range of frequency, amplitude and propagation distance. A message "x exceeds shock formation distance" appears in the output when the range of validity of the Bessel Fubini solution is exceeded. In order to properly compare the measurements with theory, the distortion which occurs within

the exponential horn must be taken into account. The sound pressure level at the throat of the horn is extremely high and exponentially decreases to the constant value at the mouth and throughout the duct. As a result of the higher levels within the horn, the wave distorts more rapidly than in the plane wave in the duct as if it had traveled a much longer distance than the actual horn length. From a distortion measurement near the mouth of the horn (such as at station 1), a correction distance for propagation within the horn can be determined from Equations (3-27) or (3-28). This correction is then added to the measurement distances. A comparison between the Bessel-Fubini solution and the measurements of Figures 52-56 for the second and third harmonics is shown in Figure 57. The agreement between theory and measurements is within the experimental error inherent in acoustic measurements.

The next step was to install a one-inch thick fiberglass liner (Owens Corning Type 704) at the anechoically-terminated end of the duct. Stations 1 through 3 were in the hard-walled section of the duct, station 4 was at the beginning of the liner and station 5 was in the middle of the liner section. The frequency for these tests was 350 Hz, and the initial fundamental sound pressure level was 160 dB. Figures 58 through 62 show the waveforms observed during these tests. The waveform steepens as would be expected from station 1 to station 3; however, at station 4 (which is at the beginning of the liner), the waveform suddenly tends towards a triangular shape with a "ringing" effect present indicating the sudden appearance of a very high order harmonic. At station 5, the "ringing" has disappeared and the familiar sawtooth shape has re-appeared. The ringing effect

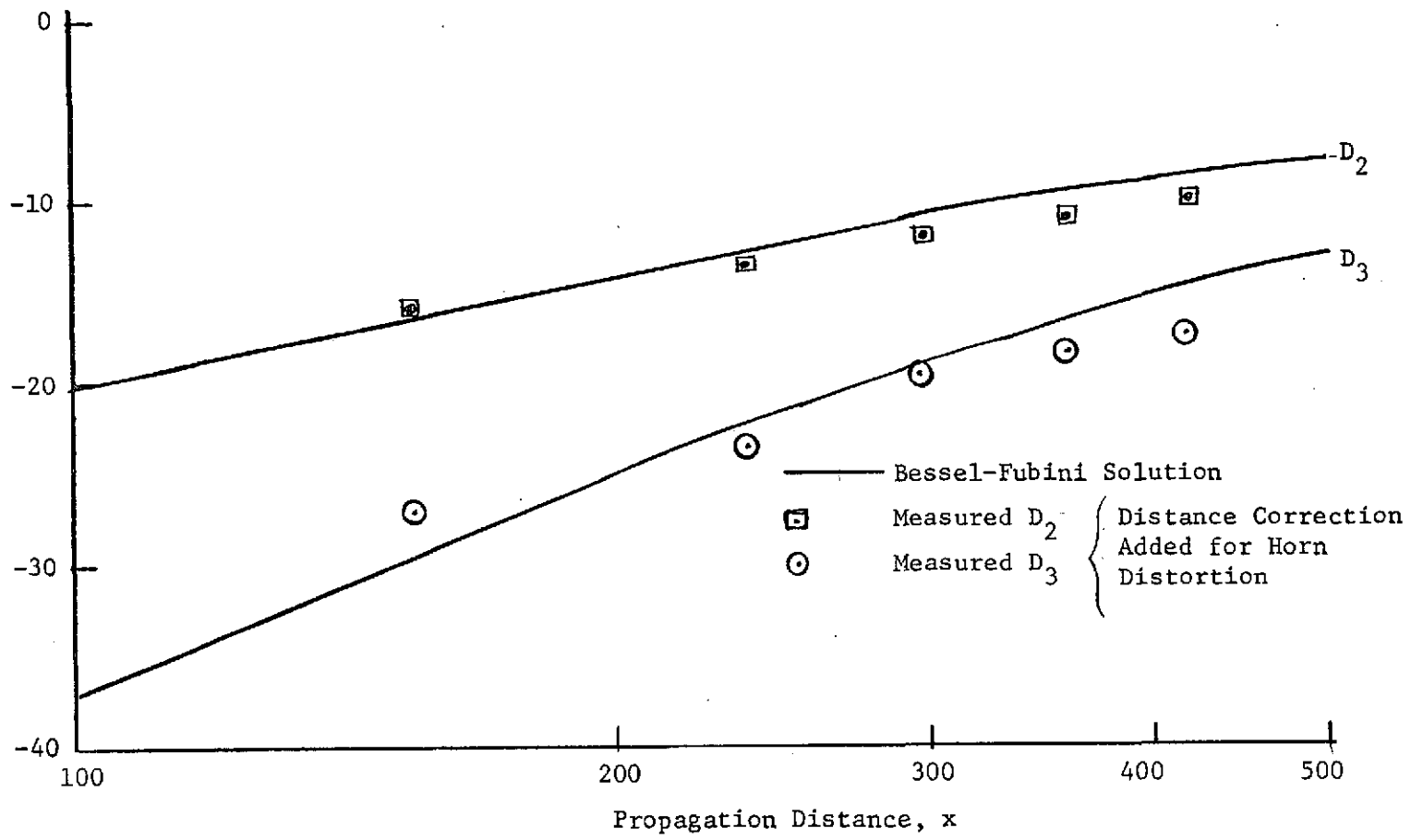

Figure 57 Distortion Level Versus Distance - 16 odB, 450 Hz

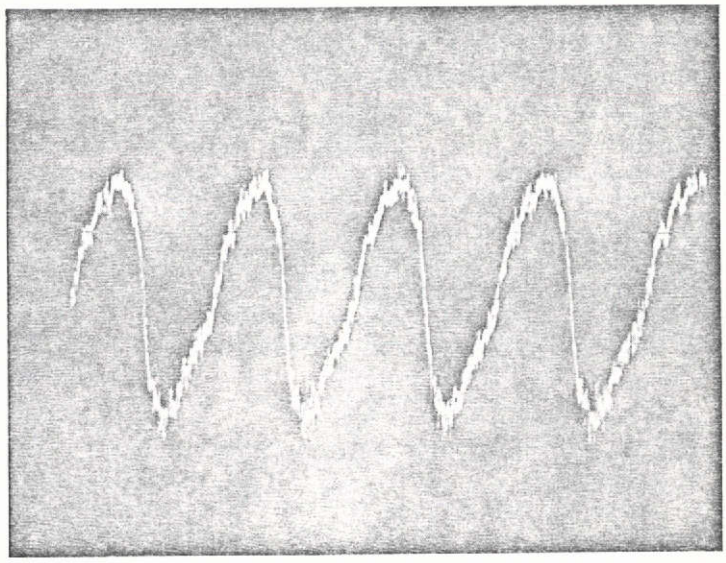

Figure 58 Sound Pressure Waveform at Station 1 With Liner

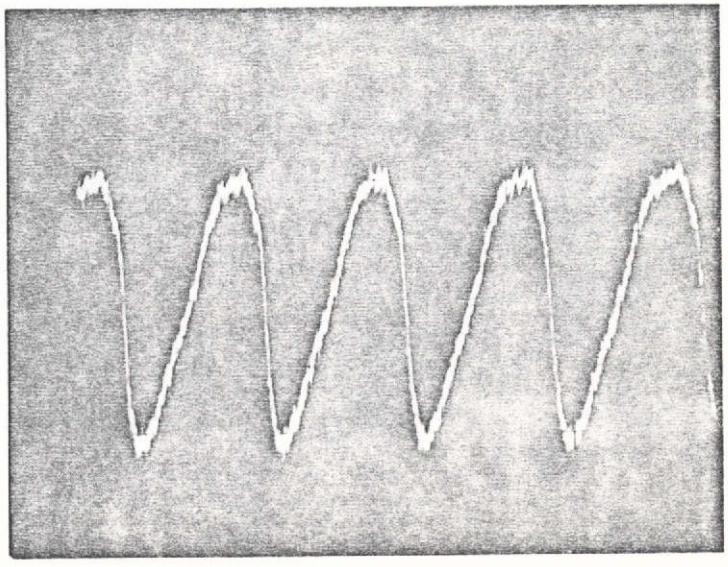

Figure 59 Sound Pressure Waveform at Station 2 With Liner

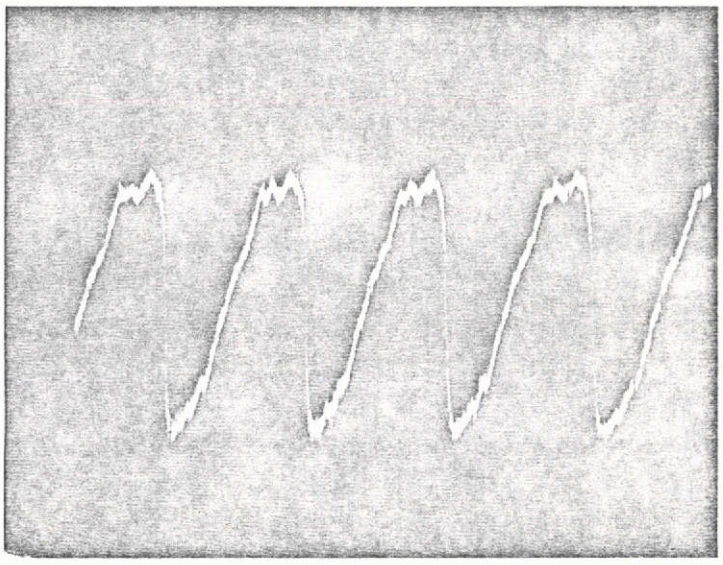

Figure 60 Sound Pressure Waveform at Staion 3 With Liner

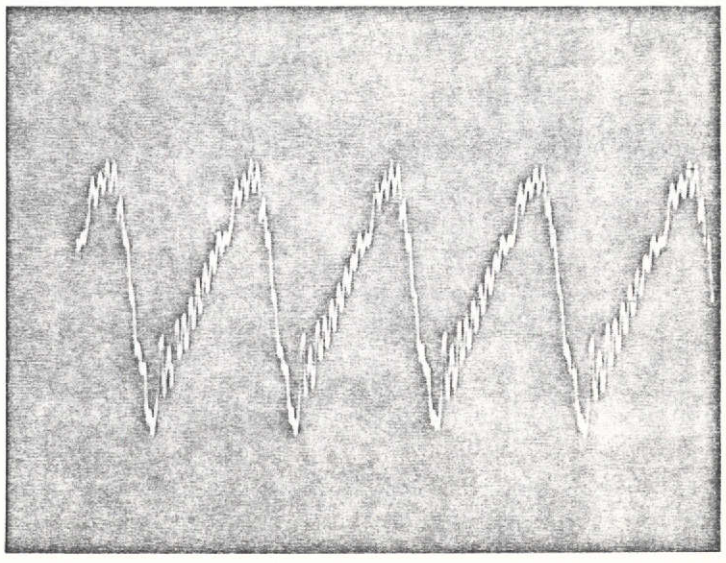

Figure 61 Sound Pressure Waveform at Station 4 With Liner

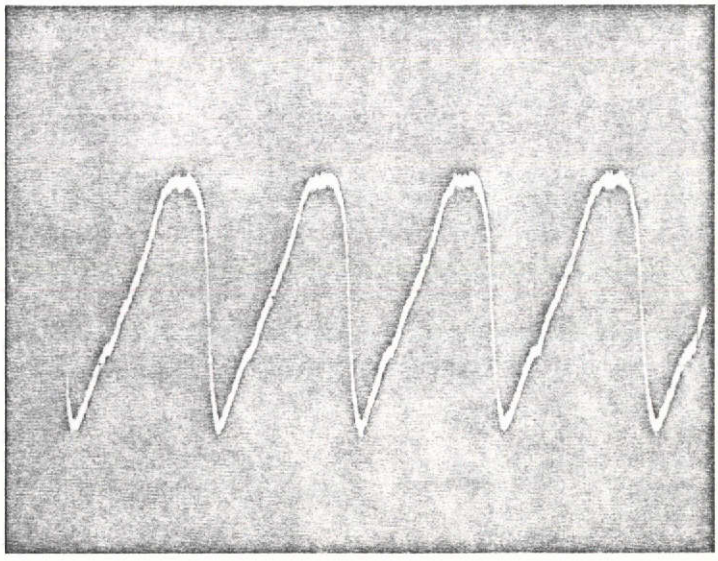

Figure 62 Sound Pressure Waveform at Station 5 With Liner

inspired a more detailed look at the high frequency end of the waveform spectra which are shown in Figures 63 through 66 for stations 1 through 4. The initial spectrum is not quite as uniform as for the unlined case, but the harmonic growth from stations 1 through 3 behaves nicely. The spectrum at station 4 is drastically altered as would be expected from the waveform observation. A strong band of frequencies appears around 7 to 8 KHz which corresponds to the "ringing" frequency. A comparison between the spectra of stations 3 and 4 reveal that some of the odd harmonics are suppressed. This would account for the tendency of the waveform to revert from a sawtooth to a triangular waveform (even functions lack odd harmonics). The ringing effect is probably due to a nonlinear interaction between the intense sound wave and the liner at the impedance discontinuity when the wave just enters the liner. The effect is more of a curiosity than anything else since it is completely absent downstream of the liner as can be seen from Figure 62.

In the final phase of the study, a four-element array of Ling EDT 94 high intensity sound sources were connected to the duct through short conical matching sections, and this installation is shown in Figures 67 and 68. The same previously-described transite duct was used for these tests, and an additional 6-foot section was installed between the downstream end of the duct and the termination. This 6-foot extension was added so that the shock formation region could be observed.

Separate phase and amplitude control of the four sound sources was available, and the sources could be operated in phase to produce a plane wave and in a 0°, 90°, 180°, 270° sequence to produce

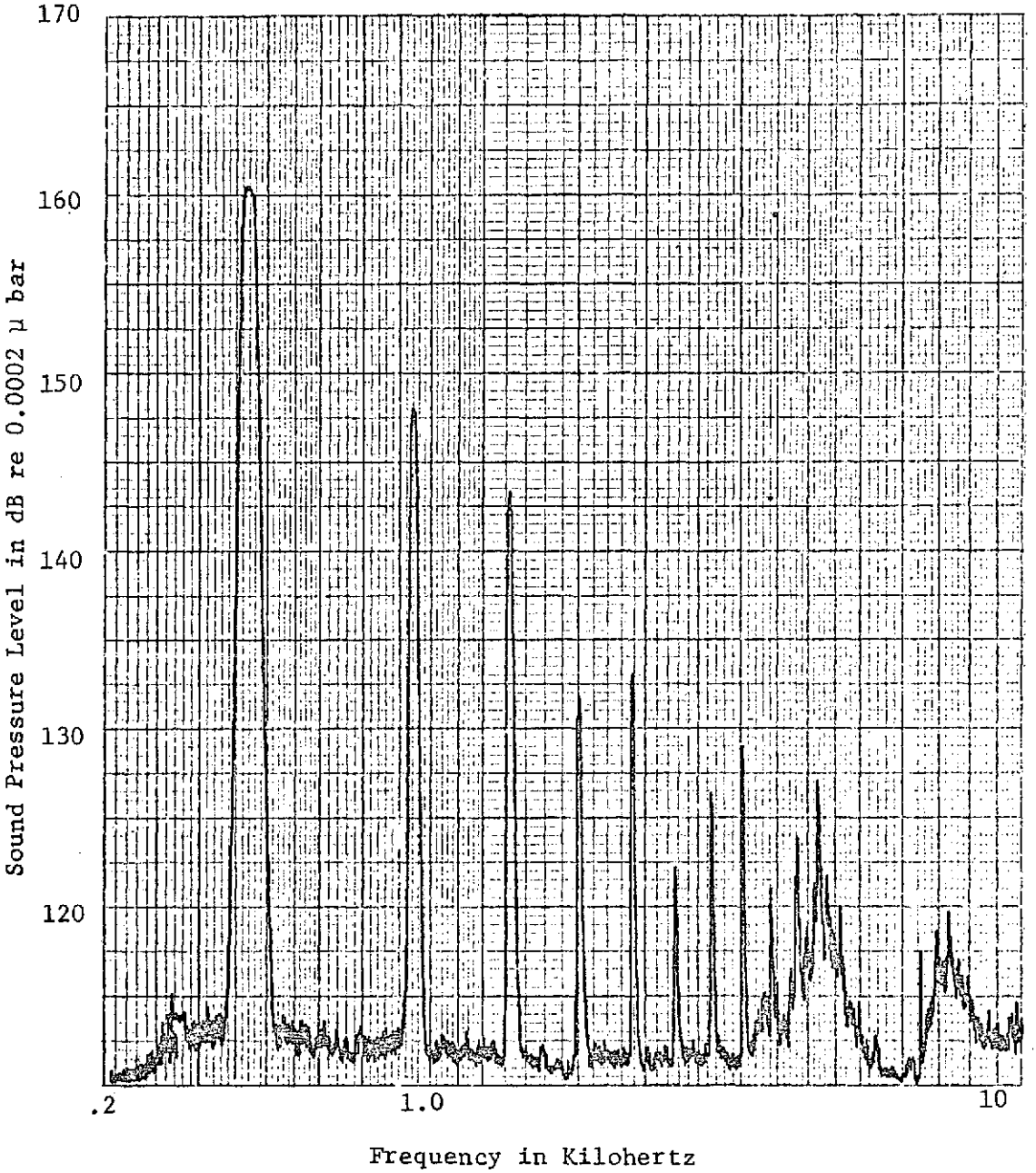

Figure 63 Spectrum at Station 1 With Liner

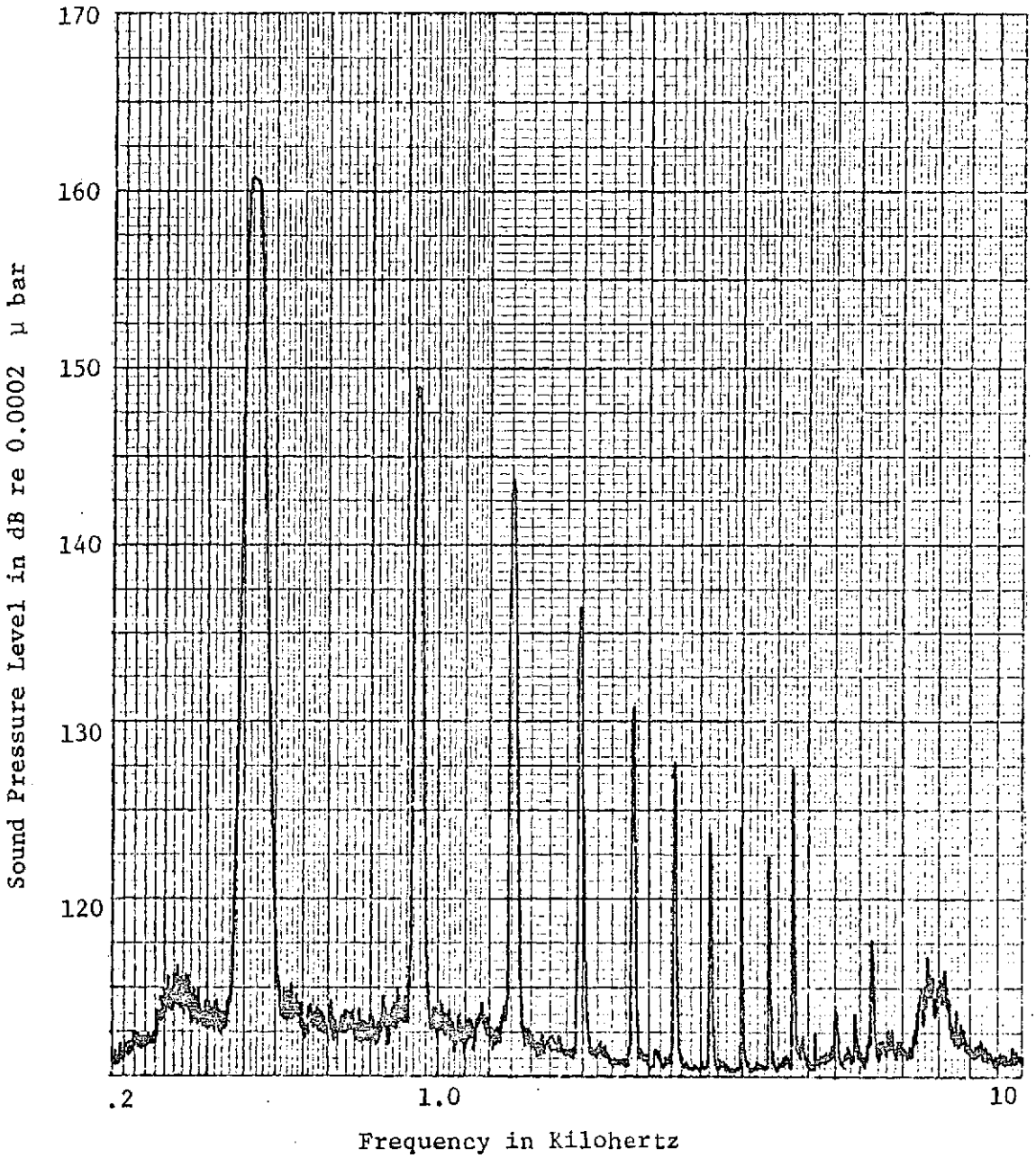

Figure 64 Spectrum at Station 2 With Liner

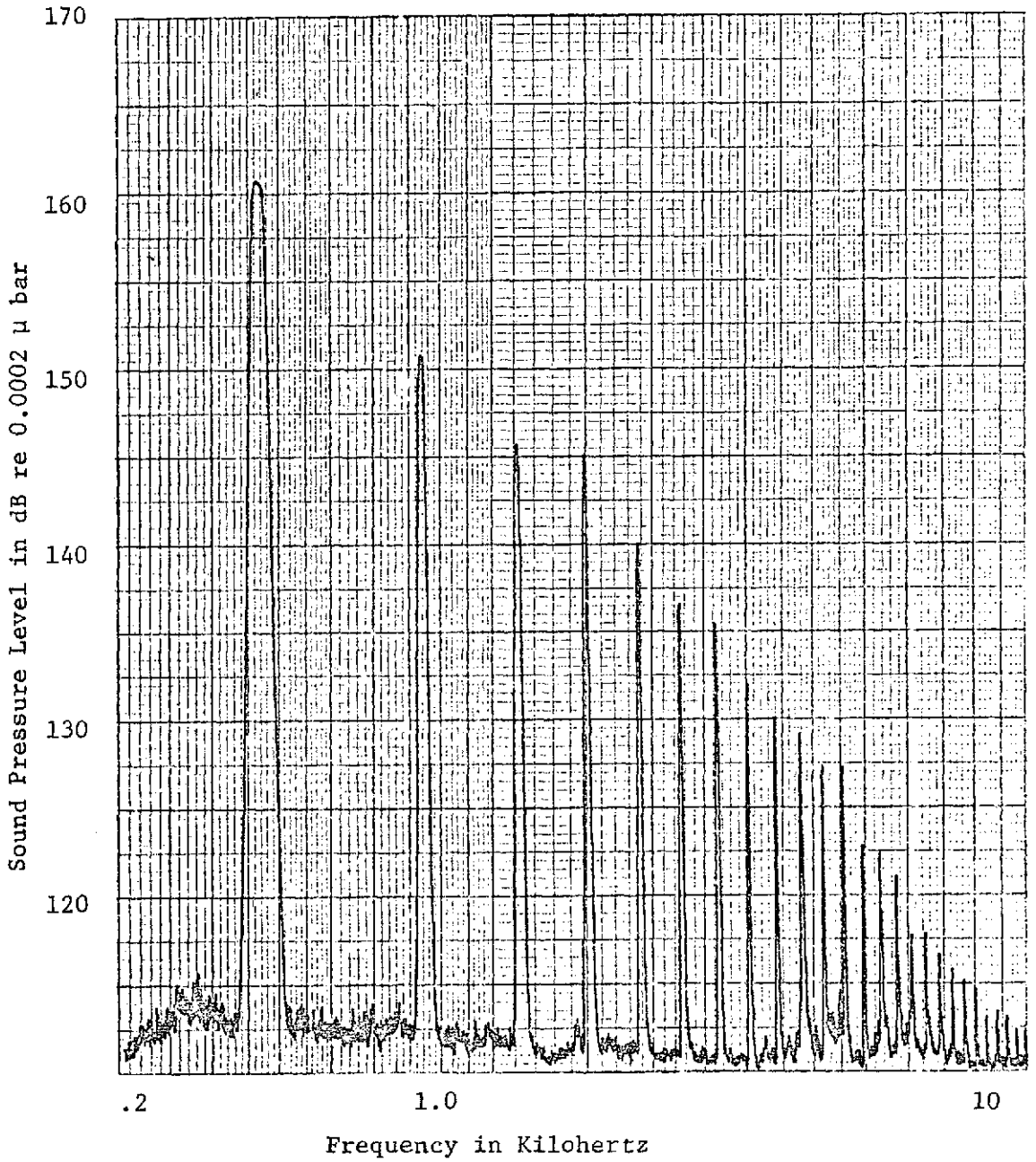

Figure 65 Spectrum at Station 3 With Liner

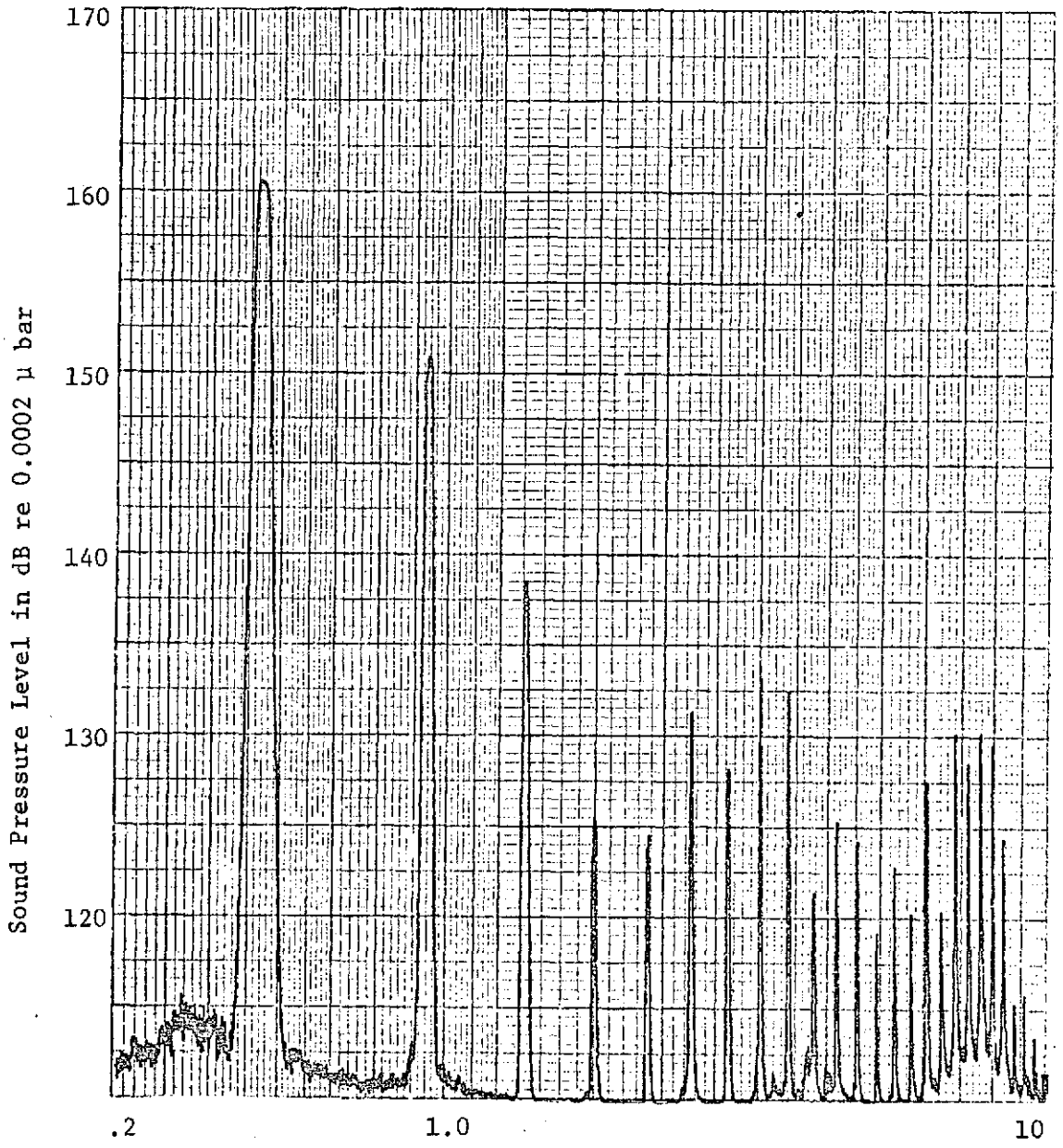

Figure 66 Spectrum at Station 4 With Liner

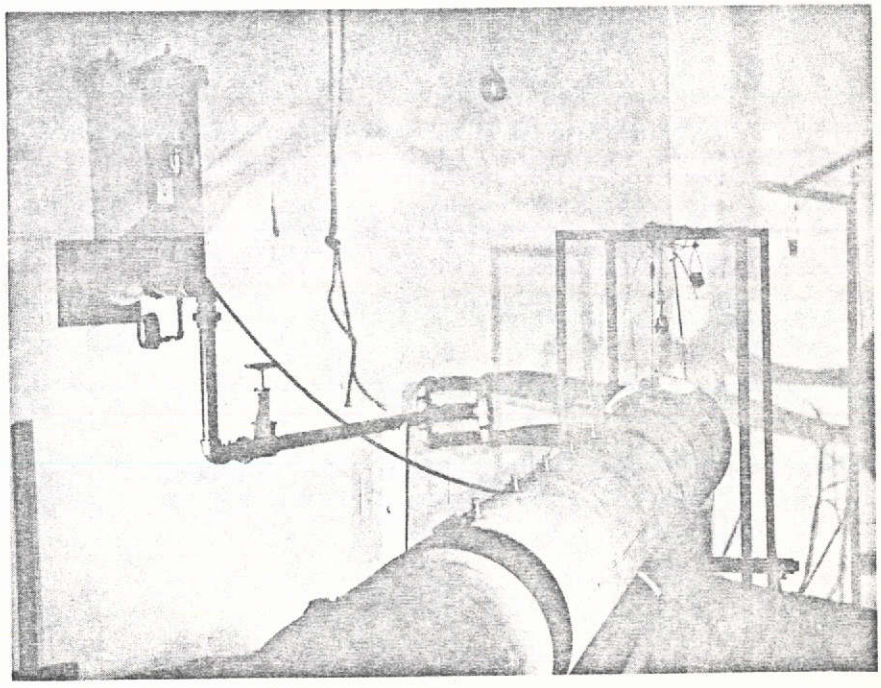

Figure 67 View of Duct, Array and Air Supply

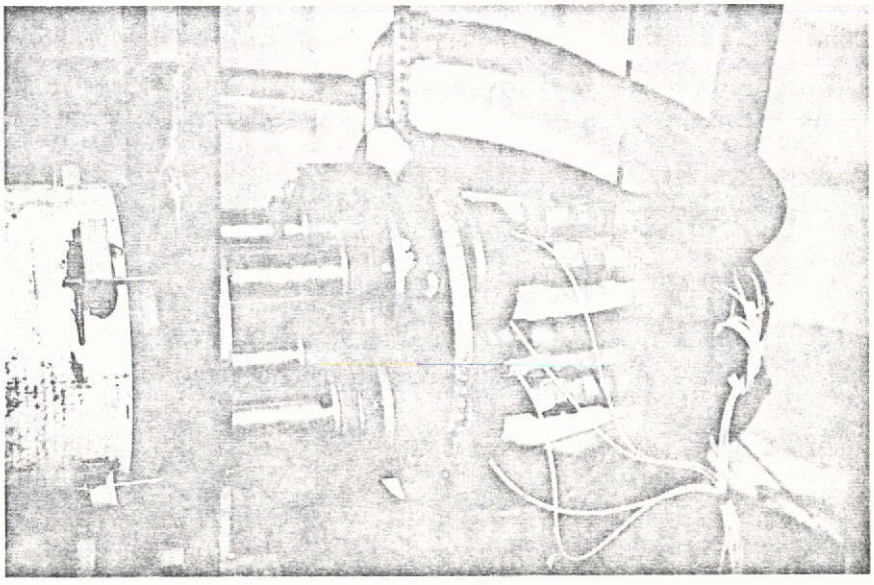

Figure 68 View of Four Element, High Intensity Array

the m=1, n=1 spinning mode. The high intensity higher order mode study was restricted almost entirely to this mode since maximum acoustic intensity could be obtained at and near the cut-off frequency of this mode. The frequency and amplitude limitations of the source for plane wave and m=1, n=1 phasing can be seen from the sweep frequency response curves shown in Figure 69. These curves were made without a liner with the microphone located halfway down the duct and 2 inches inside the duct wall. The sound sources were driven at about 4 dB below their maximum output power. The below cut-off cancellation effect can be seen in the spinning mode curve, and it is also evident that maximum intensity is obtained at 660 Hz, the cut-off frequency of this mode. It was also found that, with careful phasing, up to 160 dB could be obtained for the m=2, n=1 mode at its cut-off frequency of 1080 Hz.

The hard-walled plane wave case was investigated first, and the results were similar to those with a single driven and exponential horn described earlier, with the exception that initial wave forms near the source were more distorted and that steeper wavefronts were observed at the downstream end of the duct. The higher distortion results from less perfect acoustical matching of the sources to the duct and to less than optimum air pressure supplied to the sources. This lower pressure is due to pressure drop in the air filtering system. The higher distortion did have a beneficial effect in that we were able to observe that the sawtooth wave shape formed in almost all cases regardless of the initial wave shape. A typical illustration

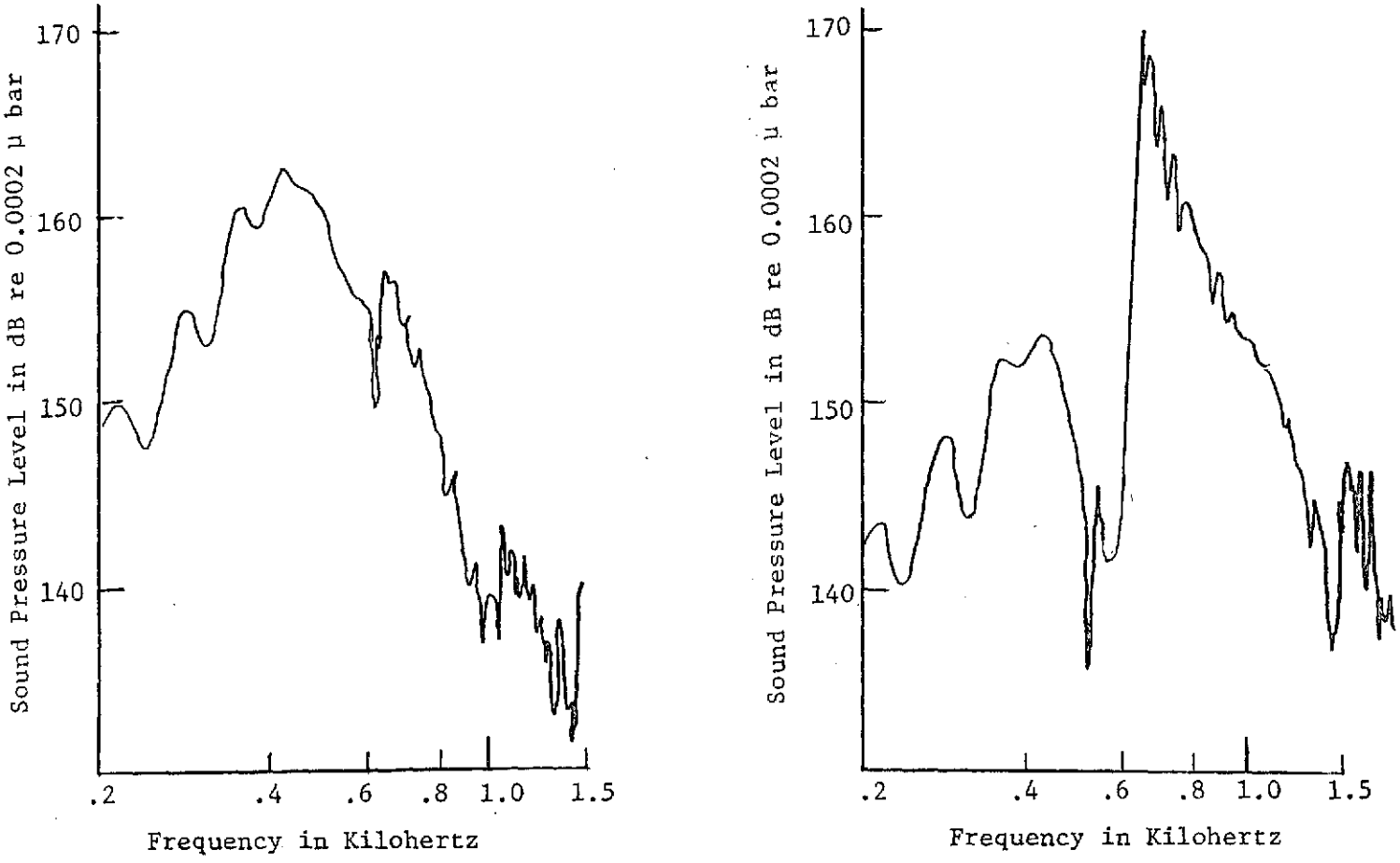

Figure 69 Frequency Response Curves of Array Phased for Plane Wave and Spinning Mode

of this is shown in Figure 70. The upper trace is the waveform one foot from the source, and the lower is measured one foot from the termination. The initial waveform varied considerably with frequency, amplitude and minor adjustments in phasing; but, in most cases, the sawtooth N-shaped wave appeared downstream. One exception to this was when the array was driven at very high amplitudes and adjusted such that the initial second harmonic distortion was comparable to that of the fundamental. In this case, a double shock forms downstream as shown in Figure 71.

The spectrum of this waveform is shown in Figure 72, and it can be seen that the second harmonic is actually higher than the fundamental. In this case, the frequency was 465 Hz, and the initial R.M.S. sound pressure level was 163 dB.

The steeper wavefronts observed in these tests as opposed to the single driver tests result from the extended length of the duct which allowed us to observe the waveform beyond the shock formation distance. A typical such measurement is shown in Figure 73 which was taken at 443 Hz at 162 dB one foot from the termination. The extremely steep slope is obvious in the photograph.

The next step was to investigate the behavior of higher order modes at high intensities for the hard-walled case. The array was phased for the m=1, n=1 mode and initially operated at the mode cut-off frequency of 660 Hz. The results were, at first, surprising to us in that no progressive distortion or wave steepening effect was observed. At 160 dB, the waveform at all measurement stations appeared sinusoidal from oscilloscope observations, and a typical spectrum is shown in Figure 74. There is some second and third

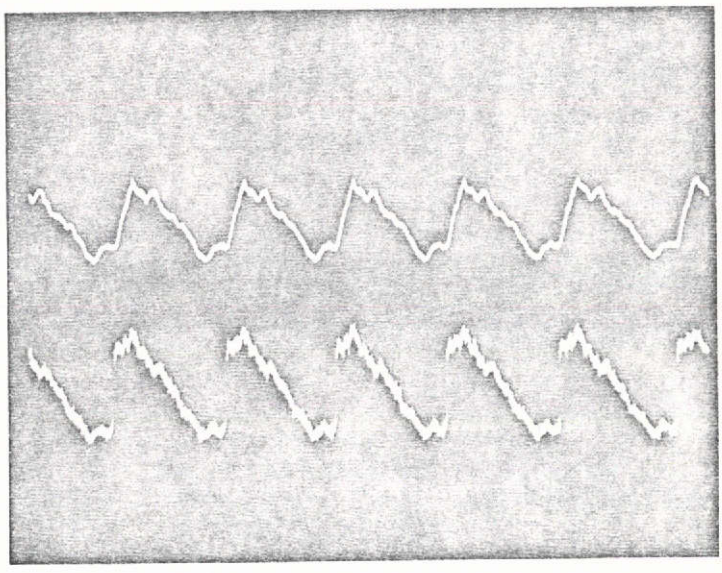

Figure 70 Typical Conversion to Sawtooth

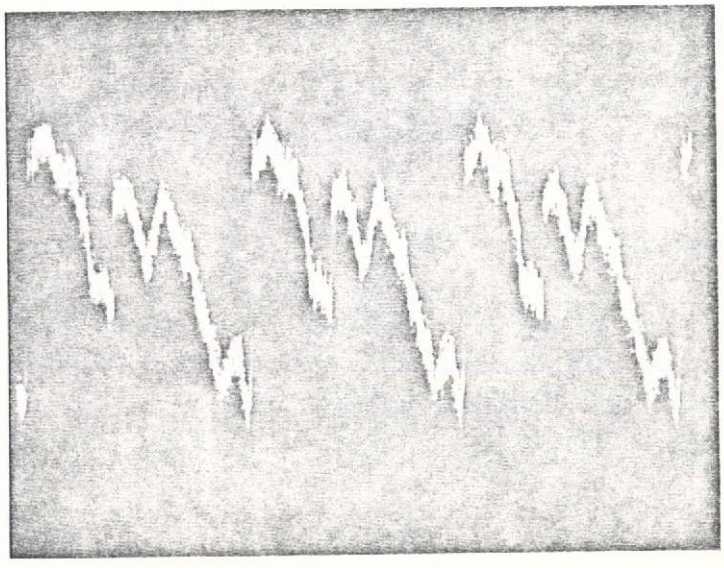

Figure 71 Double Shock Formation

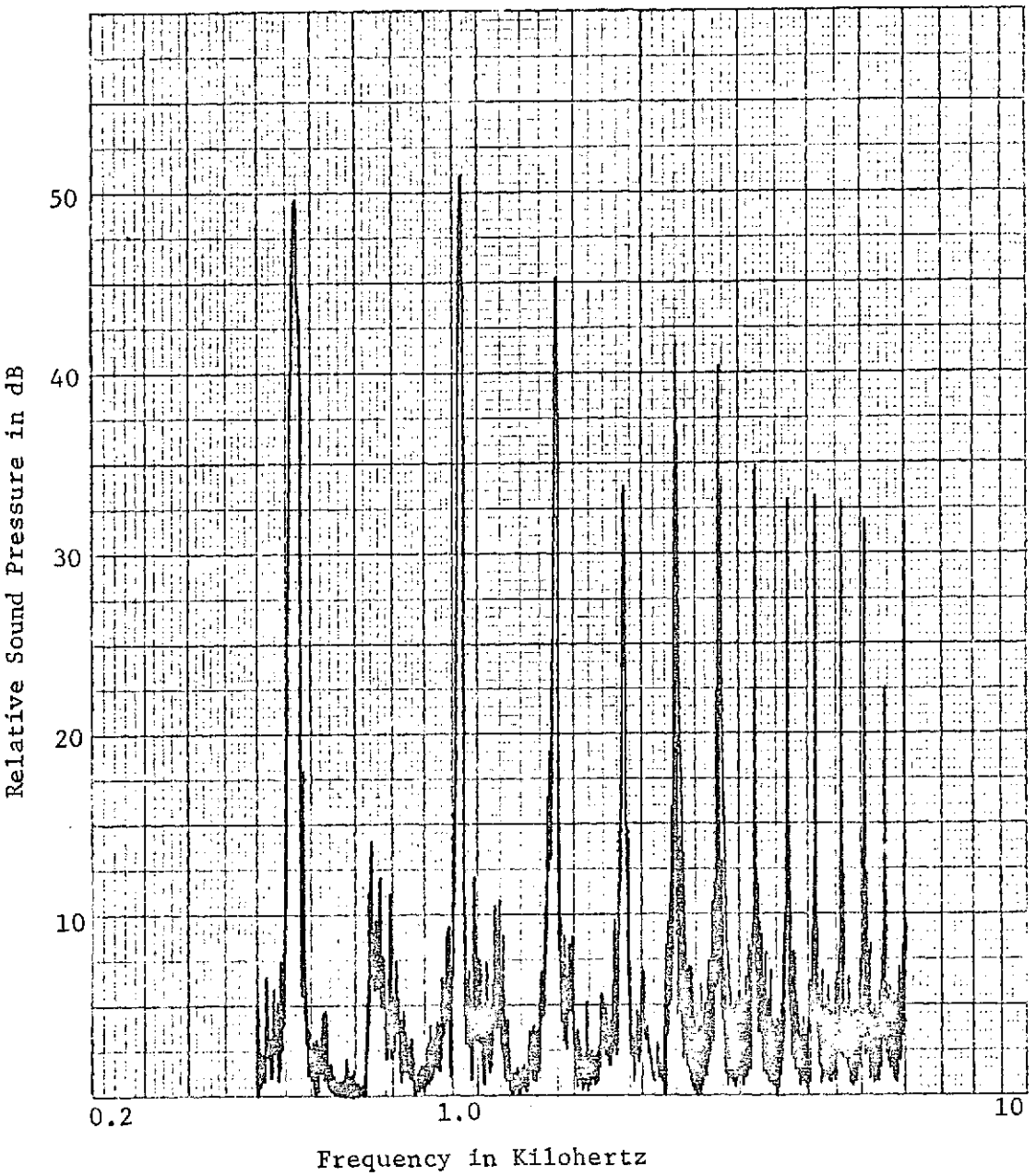

Figure 72 Spectrum of Double Shock Waveform of Figure 71

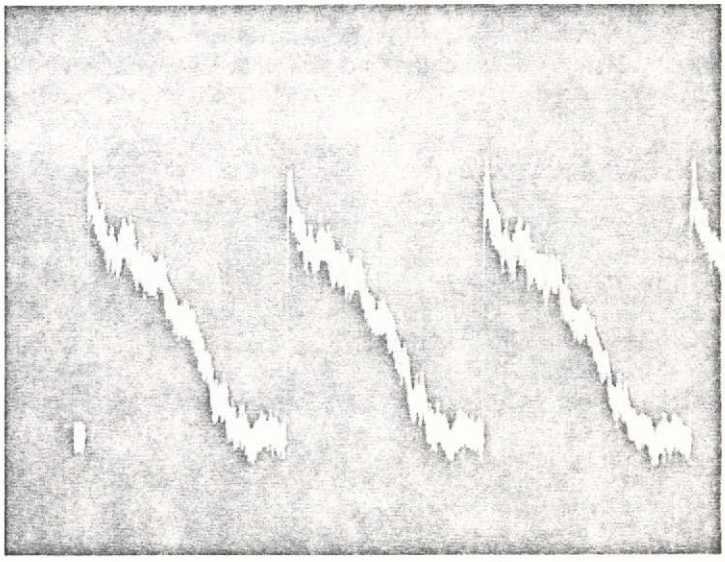

Figure 73 Typical Steep Shock at 162 dB One Foot from Termination

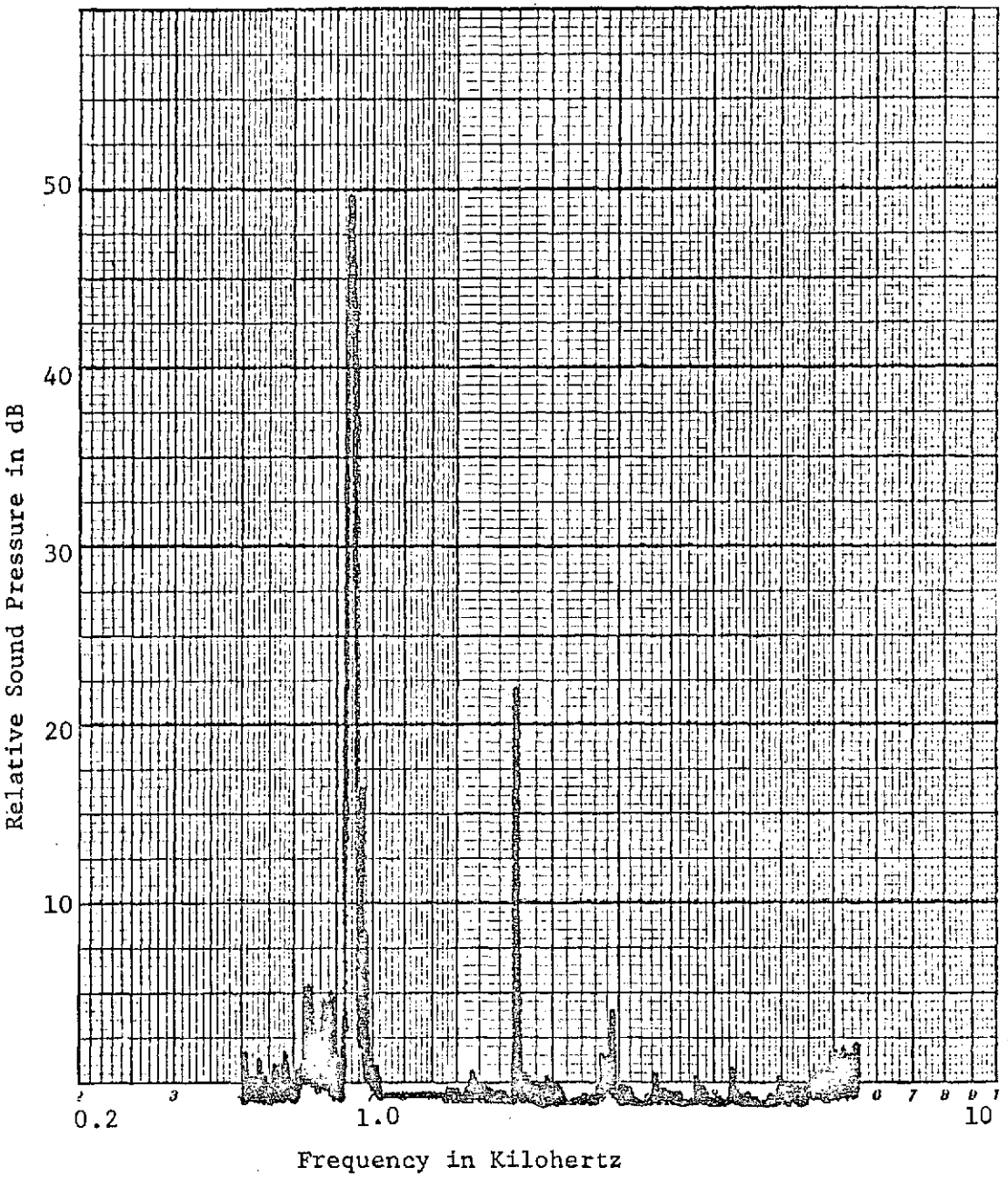

Figure 74 Typical Spinning Mode Spectrum Showing Low Harmonic Content

harmonic content, but this is a result of distortion inherent in the course. Spectra were obtained at 160 dB up to 805 Hz (22% above the cut-off frequency) with similar results. The harmonic levels were frequently even lower than shown in Figure 74. It was mentioned in Chapter III that a modified form of the Bessel-Fubini solution given by Equation (3-34) correctly predicts the behavior at cut-off; that is, that no harmonics are generated due to finite amplitude effects, and this is precisely what we have observed here. We also argued in Chapter III that the dispersive nature of higher order mode propagation would prevent the formation of a sawtooth or any stable waveshape. Our experiments have demonstrated that this is true and that, in addition, the dispersion prevents any progressive distortion in the frequency region of our observations.

The Bessel-Fubini Solution which is a Fourier series representation of the acoustic waveform can be written from Equation (3-16) as

$$p(x, t) = P_1 e^{j(\omega t - k_1 x)} + P_2 e^{2j(\omega - k_2 x)} + P_3 e^{3j(\omega t - k_3 x)} + \ldots \qquad (6\text{-}5)$$

and the Pn's are given by Equation (3-17). In the limit as $x \to \bar{x}$ the series represents a sawtooth wave. This can only be true if $k_1 = k_2 = k_3 = k = \omega/C$. We have shown that this is not the case for higher order modes since the wavenumbers of the harmonics have the form

$$k_z^2 = \frac{\omega^2}{C^2} - k_r^2 \qquad (6\text{-}6)$$

and are frequency dependent. The dispersion therefore prevents the formation of a sawtooth or any form of cumulative distortion. The distortion process described with the aid of Figure 6 in Chapter III cannot take place unless the wavenumber of each harmonic are proper integer multiples of the fundamental or very nearly so. It would be expected that at very high frequencies where the dispersion is small that finite amplitudes could again be observed, but there is a region where modal purity is difficult, if not impossible, to obtain and is beyond the frequency limitations of any available phase coherent high intensity sound sources.

A non-progressive type of distortion was observed for the m=1, n=1 mode at extremely high amplitudes, and this is illustrated by the waveforms shown in Figures 75 and 76 with corresponding spectra in Figures 77 and 78. The sound pressure levels are 170 and 175 dB, respectively. This distortion is attributed to inherent distortion in the source and to the fact that at 175 dB, we were modulating the air at an amplitude of ± 0.1 atmosphere where the nonlinearity of the pressure-density relationship is quite pronounced.

An additional nonlinear effect was observed for the m=1, n=1 mode at 680 Hz which is about 3% above the cut-off frequency. The waveform had an amplitude-modulated appearance with a spectrum shown in Figure 79. The sound pressure level was 166 dB (the maximum obtainable at that frequency) and a one-half order subharmonic can be seen in the spectrum. Fractional harmonics of order 2-1/2 and 4-1/2 are also visible. Subharmonics and fractional harmonics have previously been observed at high intensities in the ultrasonic region in liquids (see, for example, References 33 and 34).

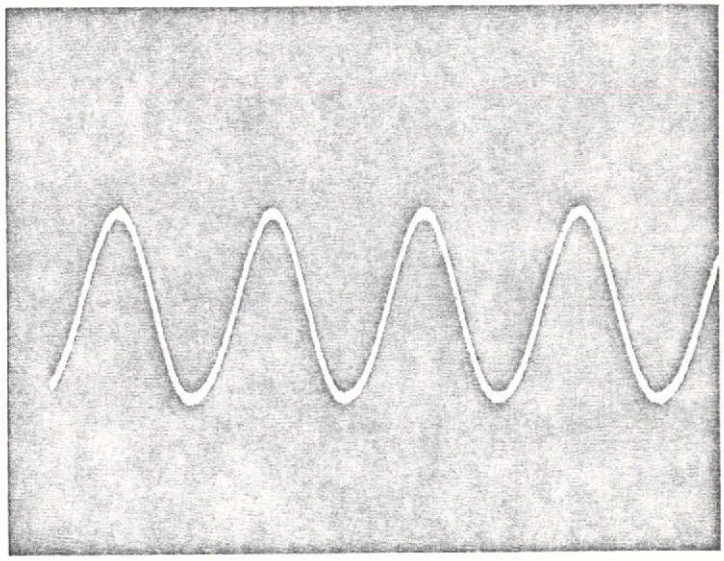

Figure 75 Sound Pressure Waveform at 170 dB

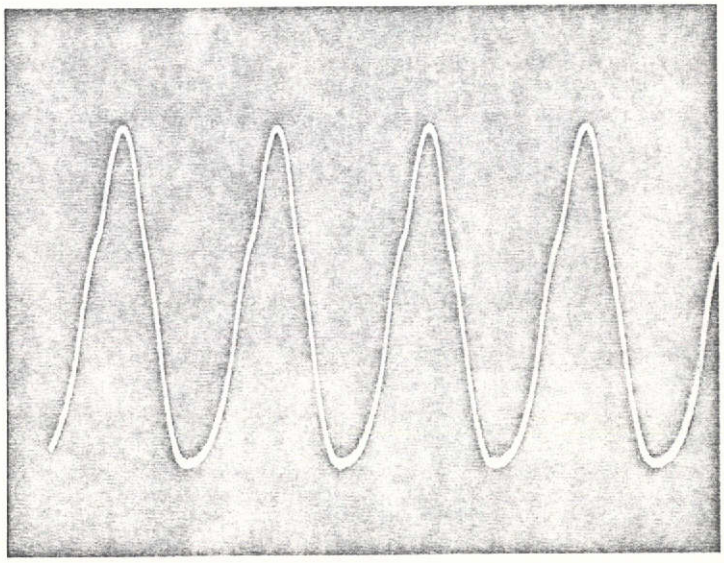

Figure 76 Sound Pressure Waveform at 175 dB

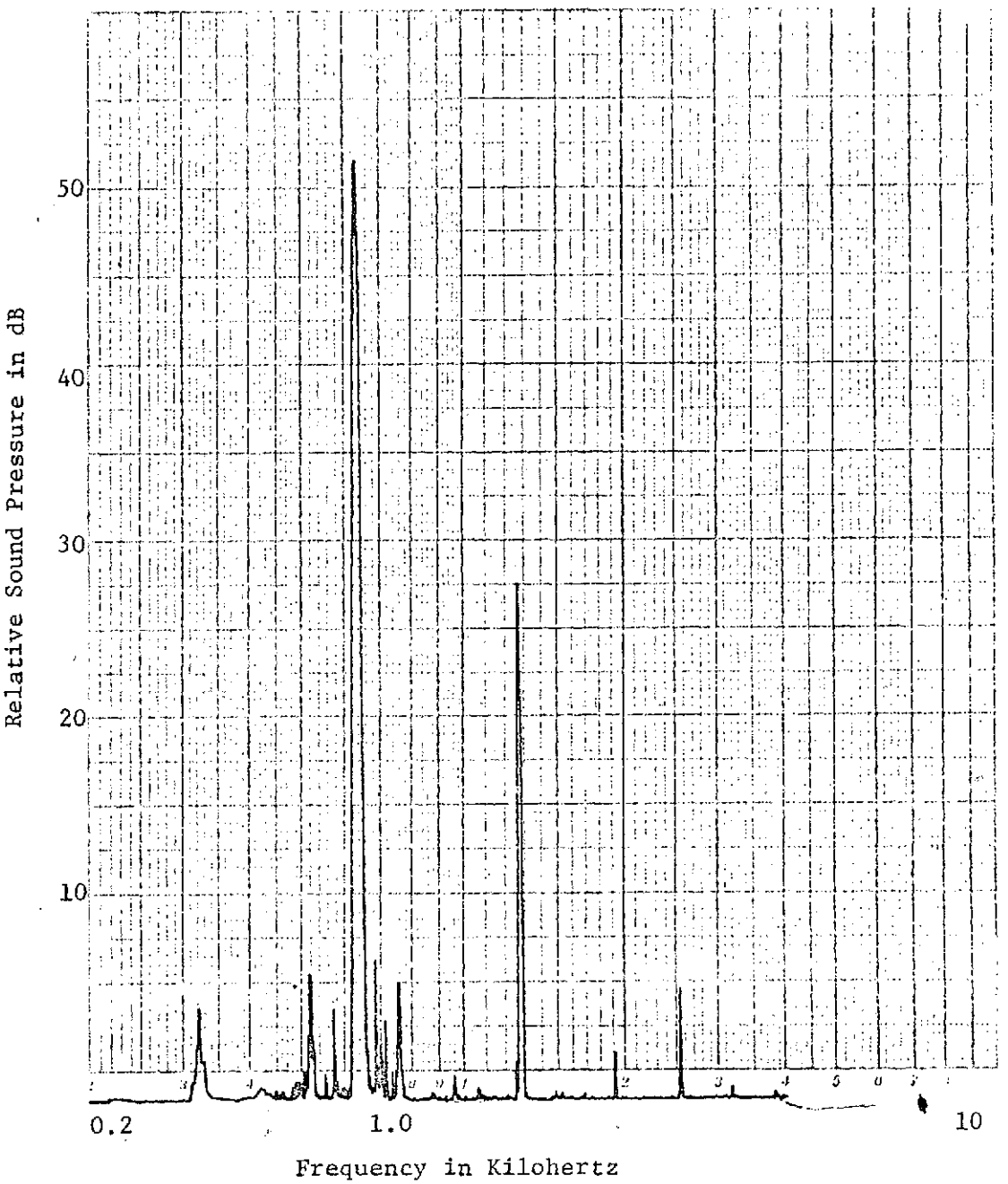

Figure 77 Spectrum Corresponding to Waveform of Figure 74

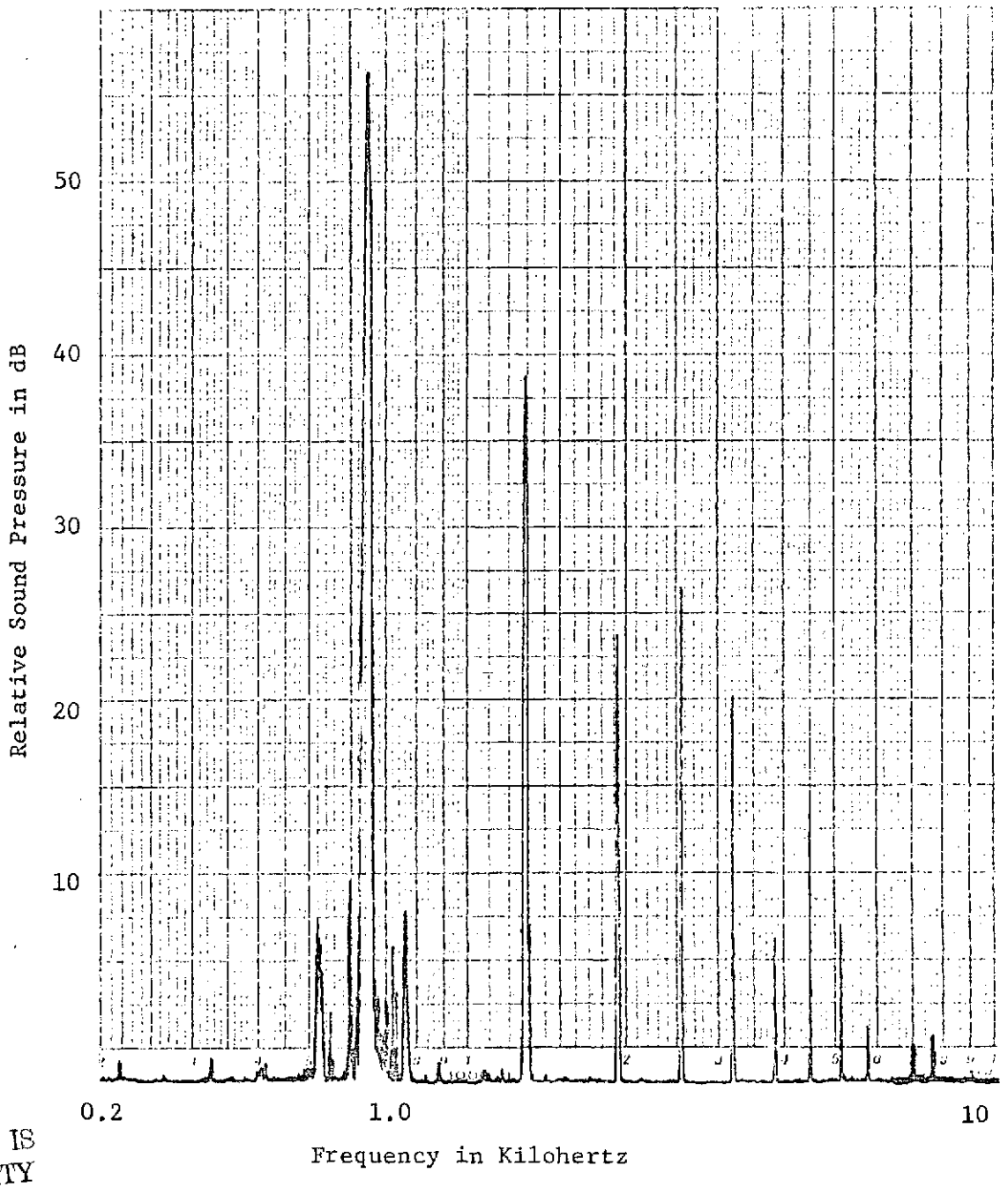

Figure 78 Spectrum Corresponding to Waveform of Figure 75

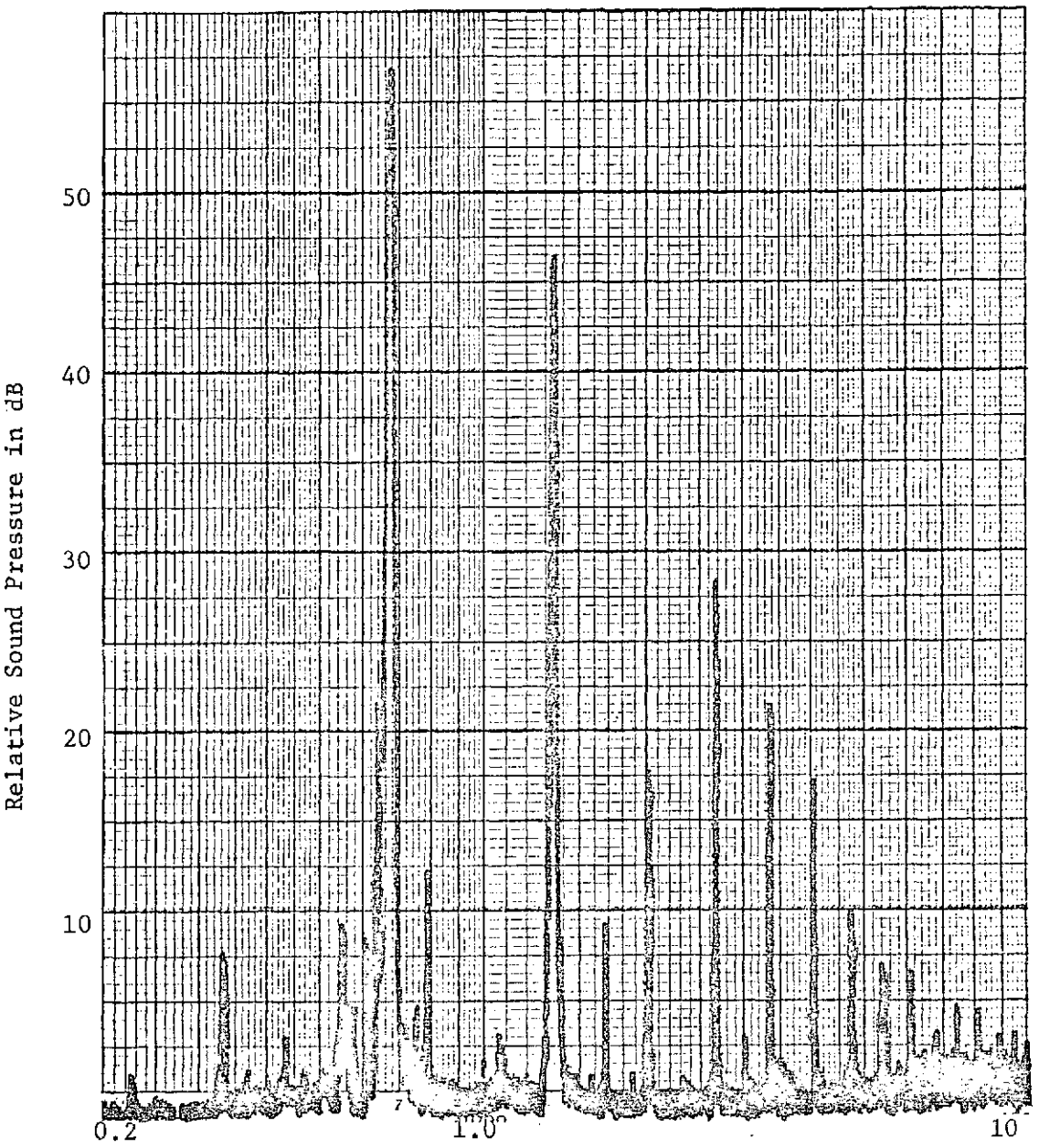

Figure 79 Spectrum of Subharmonic Generation

Subharmonic generation is of no importance to the practical applications of this study due to their low amplitudes and are pointed out here for interest only. The phenomenon could possibly be of interest at much higher amplitudes associated with instabilities in rocket engines and other combustion processes. Subharmonics of blade passage frequency have also been observed in gas turbine engines with supersonic rotor blade tips. This phenomenon has been labeled by the aircraft engine industry as "multiple pure tone" or "buzzsaw" and may bear some relationship to our subharmonic observations. Fractional harmonics have also been frequently observed in large sonar systems (see, for example, Figure 1 of Reference 16), but this has been attributed to nonlinear bubble oscillations due to cavitation. It was shown by Shalis in Reference 35 that the sudden appearance of fractional harmonics and rapid growth of harmonic distortion was a sensitive indication of the presence of ultrasonic cavitation. These and other observations have brought up the question as to whether or not the results reported by McCluney in Reference 34 were a result of cavitation (his studies were in a liquid medium). The fact that we have produced subharmonics in an acoustic waveguide in a gaseous medium would tend to support the premise that McCluney's subharmonics were not cavitation-induced and that we were both observing the same nonlinear phenomenon.

In the concluding phase of this study, we examined the behavior of two 30-inch liners made from glass fiber and woven sintered metal. The glass fiber liner was made from one-inch thick Ownes Corning Type 705 "Fiberglas," the same type of liner studied in the linear region and reported in Chapter V. The metal liner consisted of a 10-inch

diameter cylindrical shell formed from "Feltmetal" manufactured by the Brunswick Corporation. This material was an experimental type denoted by the manufacturer as "7 mesh wire B wool, 35 Rayl." It was supported in the duct by three outer rings forming a liner material consisting of the thin layer of Feltmetal and a one-inch air gap in front of the wall.

Overall sound pressure level measurements and spectra were taken upstream and downstream of both liners for the plane wave case and for the m=1, n=1 mode. Over the limited frequency range (350-550 Hz) that plane waves could be generated at high intensities, the attenuation of both liners was low (less than 6 dB) and did not vary with intensity up to 162 dB indicating that the liner materials were behaving in a linear manner. The waveform and corresponding harmonic spectra are, however, considerably altered in passing through the liner as was observed in the earlier plane wave tests reported in this chapter. Typical upstream and downstream waveforms are shown in Figures 80 and 81 for the fiberglass liner at 443 Hz. The downstream waveform has lost its sawtooth shape, but a portion of the steep wavefront remains.

Greatly enhanced attenuation was obtained for both liners for the spinning mode case as was observed earlier in Chapter V for low amplitudes. Attenuation versus frequency for the fiberglass and feltmetal liners at 160 dB upstream sound pressure level for the m=1, n=1 mode are shown in Figures 82 and 83. The performance of the fiberglass liner is better than the feltmetal; however, environmental considerations rule out the use of fiberglass in many duct liner applications. The attenuation for the fiberglass liner

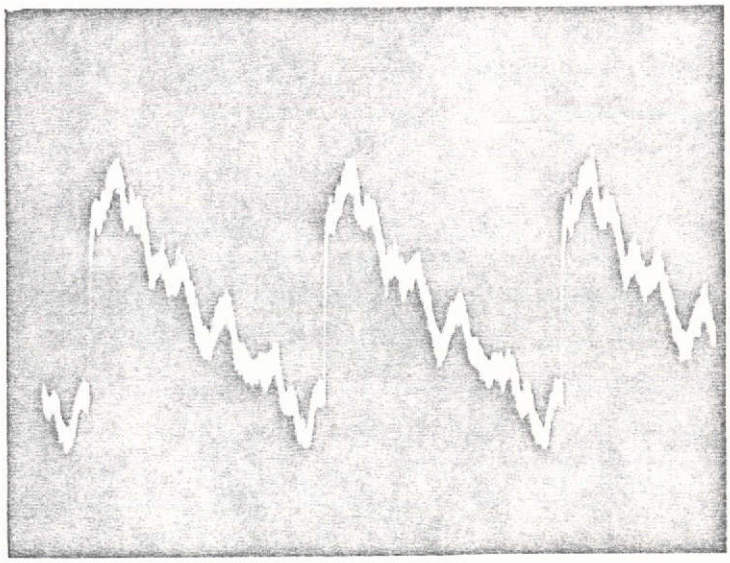

Figure 80 Typical Waveform Upstream of Liner

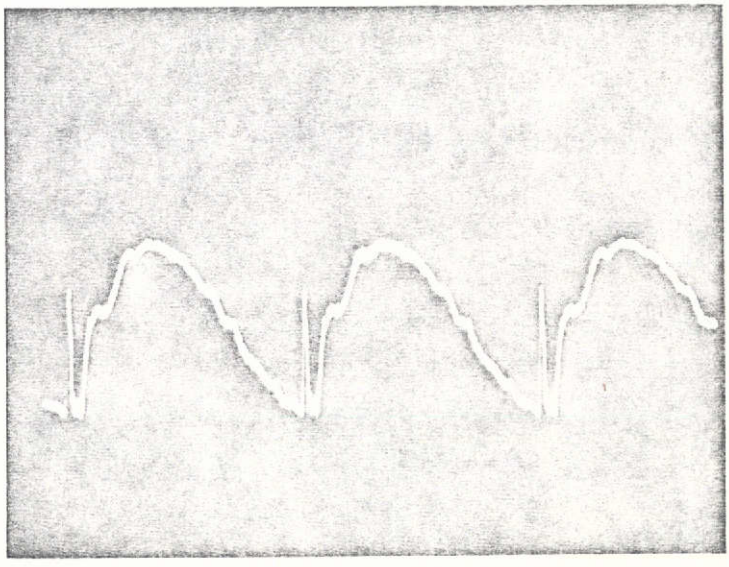

Figure 81 Typical Waveform Downstream of Liner

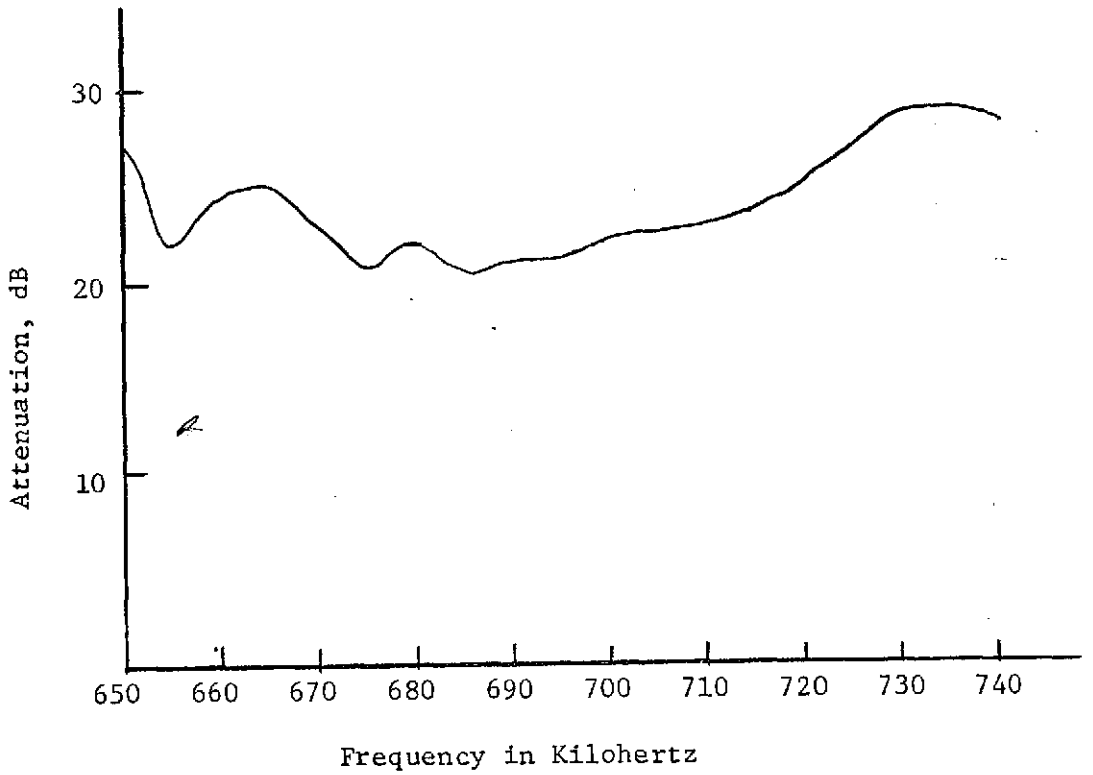

Figure 82 Attenuation Versus Frequency for 30 Inch Fiberglass Liner at 160 dB Upstream Sound Pressure Level for m=1, n=1 Mode

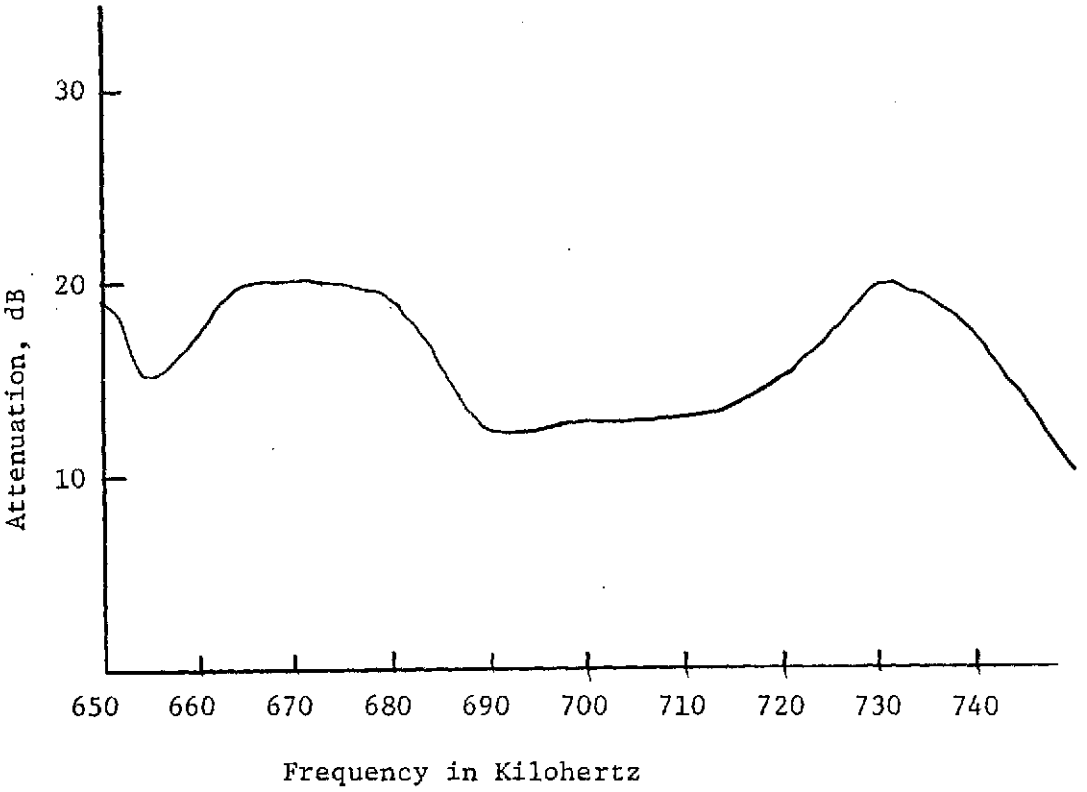

Figure 83 Attenuation Versus Frequency for 30 Inch Feltmetal Liner at 160 dB Upstream Sound Pressure for m=1, n=1 Mode

is similar to that obtained for the 24-inch liner at low amplitudes shown in Figure 43. Linearity of the feltmetal liner was checked by measuring the attenuation at 650, 660 and 670 Hz at upstream sound pressure levels of 140, 150, 160 and 170 dB. The maximum variation in attenuation with amplitude at any frequency was 2-1/2 dB indicating linear behavior of the liner materials.

It had been speculated prior to these experiments that for the plane wave case, the various harmonics generated by the cumulative distortion process would possibly couple to higher order modes when the harmonic frequencies are above the associated mode cutoff frequencies. This would lead to the dispersion phenomena disrupting the sawtooth formation, even for the plane wave case. This possibility was substantiated by the difficulties encountered in generating plane waves above the various mode cut-off frequencies. Previous studies of finite amplitude effects have been restricted to ducts of considerably smaller diameter where coupling of the harmonics to higher order modes is unlikely (see, for example, Reference 14). The observations of sawtooth waveforms with steep wavefronts reported in this chapter indicate that coupling of the harmonics to higher order modes does not take place to any significant degree. To further substantiate this, we measured mode shapes (radial amplitude plots like those presented in Chapter V for several of the harmonics in the plane wave high intensity propagation experiments). A typical set of mode shapes is shown in Figure 84. These measurements were taken upstream of the 30-inch fiberglass liner at 408 Hz at a sound pressure level of 161 dB. It can be seen from the curves that the fundamental, second harmonic and third harmonic are essentially

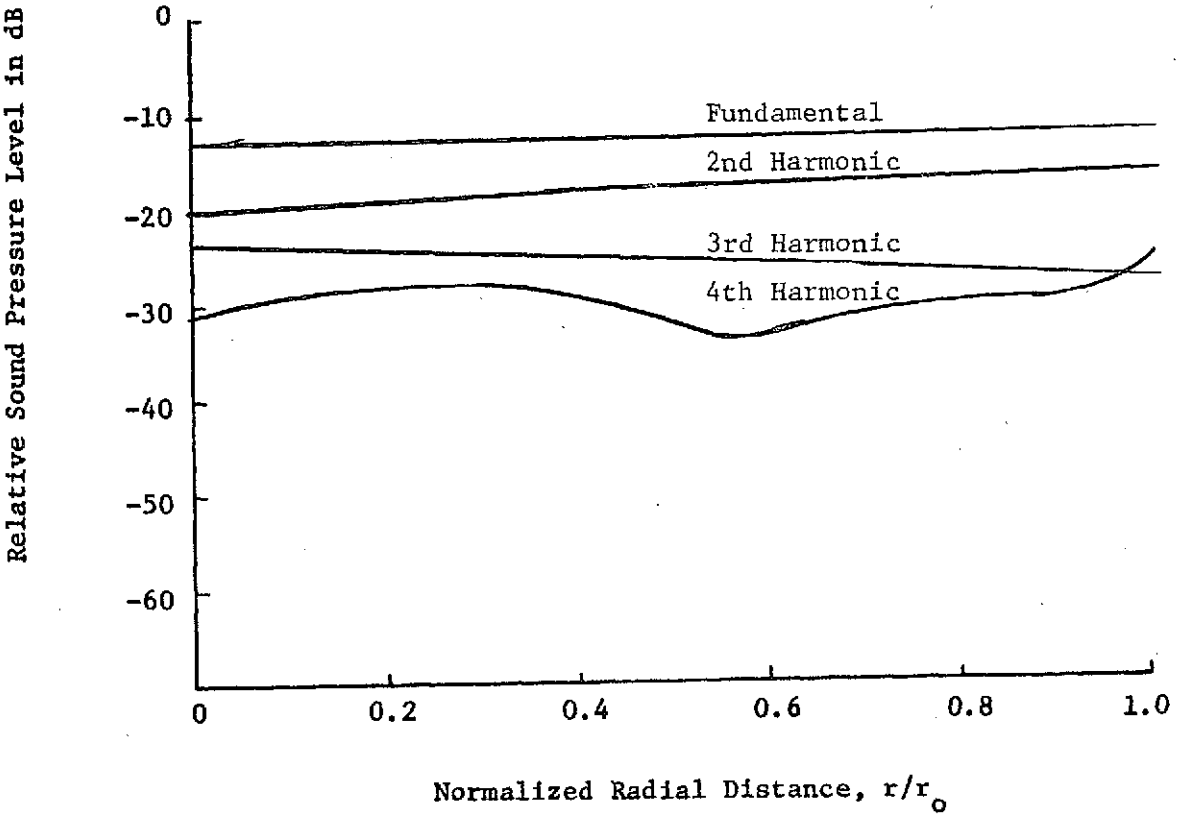

Figure 84 Harmonic Mode Shapes for a Plane Wave Fundamental

plane waves but that there is some higher order content in the fourth harmonic. This small degree of coupling to higher order modes is not serious enough to prevent the observation of plane wave finite amplitude effects but probably accounts for the slightly less than perfect sawtooth waveshapes illustrated throughout this chapter. The same measurements were also performed for the m=1, n=1 higher order mode case, and a typical set of mode shapes is shown in Figure 85. The frequency was 646 Hz, and the sound pressure level was 170 dB. It should first be noted that the levels of the harmonics are much lower than the fundamental at most values of r/r_o, and this would be expected since we have already seen that no progressive distortion occurs for higher order modes. It should also be noted that, in this case, the harmonics mode shapes bear no resemblance to that of the fundamental. This is also to be expected since there is no reason to believe that the phase and amplitude characteristics of these harmonics are in any way related to those of the fundamental as opposed to the plane wave case where the harmonics are actually generated due to the presence of the high amplitude fundamental wave and are largely plane and amplitude coherent with the fundamental.

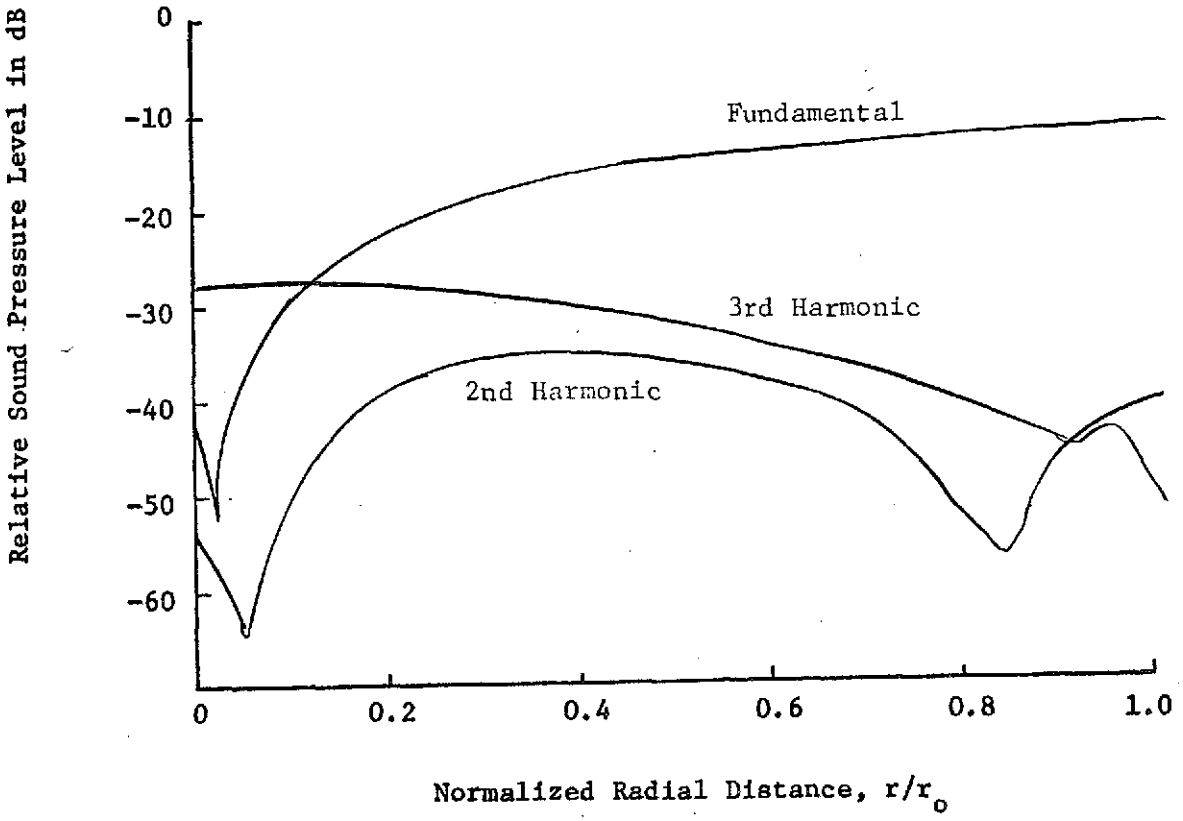

Figure 85 Harmonic Mode Shapes for a Spinning Wave Fundamental

CHAPTER VII

SUMMARY, CONCLUSIONS AND RECOMMENDATIONS

The basic objective of this project has been to study the characteristics of acoustic wave propagation in cylindrical ducts with particular emphasis on the addition of acoustically absorbent duct liners. The direction in which the research was pursued was dictated by the ultimate applications of the results; that is, the use of absorptive duct liners to reduce radiated noise from jet engines, other large air moving systems and exhaust systems for internal combustion engines. This research topic is extremely broad since it involves the presence and interaction of a number of complicated physical phenomena. It has been the subject of a number of other research efforts at The Pennsylvania State University and at many other research organizations, notably within the aircraft industry and the National Aeronautics and Space Adminstration. The work reported in this thesis should, therefore, be considered a contribution, but not the ultimate answer, to a complicated problem.

We have stated earlier that, in a real situation, complications result from the presence of higher order modes, finite wall impedance, variations in duct geometry, high intensity nonlinear effects, and the presence of flow. The present study has necessarily been restricted to constant diameter cylindrical ducts without flow so that we could isolate and understand separately the effects of plane waves and higher order modes at low and high amplitudes; first, for the hard-walled case and then in the presence of a finite wall impedance.

The thesis begins with a largely tutorial chapter on linear wave guide theory in order to give the reader an easy understanding of this topic which is very difficult to obtain from available textbooks. This treatment as well as the experiments reported later are restricted to hollow cylindrical ducts or wave guides. Rectangular waveguides could be treated using the same theoretical methods; however, this geometry has also been given considerably more attention in the literature in both acoustics and electromagnetics and is not discussed here. The dispersive nature of higher order mode propagation is then discussed in detail since it is essential in understanding the experimental results for higher order modes at high amplitudes. The chapter concludes with a formulation of the eigenvalue problem for a cylindrical duct with finite wall impedance.

The next chapter (III) is a largely theoretical discussion of the aspects of nonlinear acoustics which are applicable to the high intensity duct experiments reported later. An experiment performed with spherical waves in water is described which illustrates that nonlinear effects can sometimes be deliberately controlled and that theoretical nonlinear analyses can sometimes produce incorrect answers.

A brief description of the basic properties of sound absorbing materials is presented next in Chapter IV with adequate references for the reader who wishes to pursue this topic in more detail. The problems associated with a proper theoretical formulation of the characteristics of absorbing materials and even of measuring these characteristics are discussed. The question of the validity of the local reaction assumption is also discussed. It is pointed out

that misconceptions in the past on this subject are probably due to an incorrect interpretation of Snell's law. It is also pointed out that the local reaction assumption is, in itself, a violation of Snell's law. It is, however, highly desirable that sound absorbing materials used for duct liners be locally reacting since most of the theoretical work to date is based on that assumption. If further research indicates that this assumption is incorrect, then the theoretical formulation must include extended reaction behavior. It can be readily concluded from Chapter IV that rigorous theoretical work on the properties of sound absorbing materials is in its infancy and that much work remains to be done. It is anticipated that activity in this area will continue in our own laboratory and in many other organizations. The more general consideration of the absorption and reflection of sound waves at the boundary between two media with different acoustical properties is a subject of interest to a group of researchers much larger than the people to which this thesis is directed. In underwater acoustics, the absorptive properties of the bottom of the ocean are of great importance in many propagation problems. In seismic exploration, the acoustical properties of the layers forming the earth's crust are the subject of extensive research and in investigations of sound propagation in air over the surface of the earth, sound attenuation due to ground absorption is an important factor. Additional studies of our present topic can possibly be aided from knowledge learned in these other related fields.

In the next chapter, our experimental program to evaluate the performance of absorptive liners at low acoustic amplitudes is

described. From both a physical description of the sound field and the experimental results, it can be concluded that a downstream anechoic termination is highly desirable, or even necessary, in a test setup to evaluate duct liners. It is demonstrated first in this chapter that several higher order modes can be generated with a high degree of modal purity for the hard-wall case using a spinning mode synthesizer. Measured mode shapes agreed well with those predicted from the theory of Chapter II.

Liner performance was then studied by measuring the sound field upstream and downstream of the liners and also within the liners themselves for plane waves and higher order modes. It was found that, in some cases, higher order mode attenuation was so great that downstream mode shapes were masked by residual plane wave content and only minimum attenuations could be estimated. A good set of attenuation curves were, however, obtained for one- and two-foot liners for the plane wave and first spinning mode (m=1, n=1). It can be concluded from these data that for the liner materials used, the spinning mode is attenuated much more rapidly than the plane wave, and that there is approximately linear relationship between liner length and attenuation for the plane wave but not for the spinning wave. It was also observed that mode shapes within the liner could be considerably different from those allowed for the hard-wall case. This is not surprising since the boundary conditions are quite different for the two cases.

It can also be concluded that a lined duct in a real situation, for example, in a jet aircraft engine, air conditioning system and

exhaust systems for internal combustion engines, can behave quite differently from the usual textbook prediction based on plane wave theory.

The high intensity experiments reported in Chapter VI represent the most unique aspects of this study. Plane waves were generated up to 162 dB and spinning modes were generated up to 175 dB in a 12-inch diameter duct for both the hard-wall and lined cases. The uniqueness of the plane wave experiments is the scale on which they were performed. Previous experiments were done with considerably smaller diameter tubes where the possibility of coupling of the harmonics to higher order modes was slight. In our case, all of the harmonics were above allowed mode cutoff frequencies but, nevertheless, remained in a plane wave state coherent in phase velocity with the fundamental. The wave steepening effect was observed as predicted by the Bessel-Fubini solution.

The results for high intensity spinning modes were surprising at first, since no wave steepening or progressive distortion occurred and the wave remained sinusoidal up to 170 dB throughout the duct. It later became obvious that this is the proper result since the dispersion prevents progressive distortion. The only distortion observed was non-progressive and was only obvious at 175 dB.

The results for the lined case were also surprising since no nonlinearity in liner behavior could be detected up to the maximum obtainable levels. Flow resistance measurements of the types of materials used (see Filmer, Reference 1) indicate that nonlinear behavior should be expected at the sound pressure levels which were generated. Nonlinear flow resistance apparently does not have a

significant effect on absorption coefficient versus amplitude, at least for the materials tested here.

It should, however, be noted that there is still a significant nonlinear effect taking place when a finite amplitude plane wave propagates in a lined duct. Our studies show that, at a given frequency, the liner attenuation is independent of amplitude. The acoustic wave is, however, experiencing progressive distortion which causes a continual shift of energy into the higher harmonics where the liner has different absorption characteristics than at the original fundamental frequency. The high amplitude liner attenuation will then be increased over the low amplitude value if the plane wave attenuation is an increasing function of frequency. The reverse will be true if the attenuation is a decreasing function. This effect is qualitatively apparent in the high intensity plane wave experiments with liners presented in the last chapter. The harmonic spectra are altered drastically in the presence of a liner from those expected and observed for the hard-walled case. A quantitative evaluation of the behavior of the harmonics in propagating through the liner section would require knowledge of the high frequency plane wave absorption characteristics of the liner since the harmonics remain plane, even though their frequencies are above various higher order mode cut-off frequencies. The difficulties of determining high frequency plane wave attenuation characteristics of lined ducts experimentally, are obvious from the work reported in Chapter V; however, these characteristics could be determined theoretically from the lowest order solution to the boundary value problem for a lined duct which was described in Chapter II. The logical approach to a further study

of this particular nonlinear effect would therefore be to study the decay of the various harmonics in propagating through a liner and to compare this with theoretically determined high frequency liner attenuation. It is highly possible that liners deliberately designed to have special high frequency plane wave absorption characteristics could be utilized to exploit the frequency conversion of finite amplitude effects to best advantage. No attempt was made to do this in our present study and the excess absorption due to this effect was slight in this case. The effect will be much more pronounced at amplitudes higher than employed in the present study and it should be pointed out that, although the sound pressure levels generated in this program are impressively high (160-175 dB re 0.0002 μbar), there are practical situations where much larger amplitudes are encountered. A notible example is the exhaust system of internal combustion engines. Fortunately, laboratory simulation of these conditions with our present facilities could be accomplished since, although sound pressure levels are much higher, the total sound power required is no greater since duct diameters are much smaller for the internal combustion engine exhaust.

Our present capability of generating up to approximately 10,000 watts of acoustic power is adequate to generate the moderate sound pressure levels required for jet engine duct studies (160-175 dB) as well as the much larger levels (over 180 dB) necessary to study large amplitude wave behavior in internal combustion engines with correspondingly smaller duct diameters.

The results of the work reported here have also inspired several other recommendations for future study. The most urgent

in terms of providing practical design criteria to both the aircraft and air conditioning industries is an extension of the work on the evaluation of liners in the linear region. This should include the measurement of a much larger variety of liner materials and refinement of the measurement techniques. Emphasis should be placed on comparison of measurements with theory and modification of the theory, if necessary, to account for extented reaction. The recent theoretical work of Zorumski and Mason (Reference 36) is a firm starting point in this regard. An accurate theoretical method for predicting the performance of duct liners would be extremely valuable to noise control engineers. Anyone who has attempted to use presently available prediction methods (see, for example, Reference 29) and checked his results experimentally will appreciate the possibility of having an accurate prediction method at his disposal. It should be noted that the present methods are restricted to plane waves.

A further restriction in present theoretical treatments of lined ducts is that the duct has an infinite longitudinal dimension. In practical duct treatments, liner length is severely restricted and the impedance discontinuities at the duct walls between the treated and untreated sections could result in a discrepancy between theory and experiment. The effects of finite liner length should, therefore, be an important area of investigation.

In most practical situations, ducts are not anechoically terminated and it is obvious that this aspect of the problem is another logical extension of the present work. The radiation from a duct abruptly terminated into a free field has been the subject of several theoretical studies (References 37, 38 and 39) and includes

the plane wave case and extensions to higher order modes. These theoretical treatments are all restricted to the linear region. Our laboratory is at present uniquely equipped to study experimentally the free field radiation from an unflanged cylindrical duct in both the linear and nonlinear regions and this is recommended as an important extension of the work reported here. The results of the recommended work of duct radiation in the linear region will hopefully verify the past theoretical work or inspire further analytical work on this subject. The recommended nonlinear studies of the radiation of high intensity plane waves and higher order modes from an unflanged circular duct will have results which cannot be anticipated from present knowledge. In both the plane wave and higher order mode cases, the wave will abruptly encounter a situation where it is no longer in a wave guide situation but will be spherically diverging. For the plane wave case, it will be in the shock condition which is difficult if not impossible to achieve for a spherically diverging, initially sinusoidal source. This shock condition can be produced by an explosive spherical source but the spectrum is broad-band and unrelated to the problem which we are investigating. The question is directed to how this acoustically produced shock wave will behave as it spherically diverges.

For the higher order mode case, the situation is even more speculative. The wave progresses down the duct without distortion but at very high amplitude. It will encounter a condition at the exist where the linear wave equation does not even allow its existence.

It also suddenly encounters a condition where there is no longer any dispersion and progressive distortion is again demanded

by the medium. There will also be a backward reflection, as in the linear case, which will limit the amount of energy which penetrates into the radiated field from the unflanged duct, but this should not prevent a substantial amount of radiated acoustic energy. If, in fact, substantially high transmission of higher order modes do not contribute to the radiation from aircraft ducts, then the work of many researchers in the field is of no avail.

The behavior of high intensity acoustic waves, for both the plane wave and higher order mode cases, radiating from an unflanged circular duct, are the most interesting extensions of this project for future study. The many unanswered questions with regard to propagation of sound in lined ducts in the linear region should, however, be given considerable future attention.

REFERENCES

1. Roger D. Kilmer, "Evaluation and Prediction of the Sound Absorbing Characteristics of Composite Acoustic Absorbers for Normally Incident Plane Waves," Master's Thesis in Mechanical Engineering, The Pennsylvania State University, 1974.

2. Barry Wyerman, "Absorption Characteristics of Glass Fiber Materials at Normal and Oblique Incidence," Master's Thesis in Engineering Acoustics, The Pennsylvania State University, 1974.

3. Eugen J. Skudrzyk, The Foundations of Acoustics, Springer-Verlag, 1971.

4. E. T. Copson, An Introduction to the Theory of Functions of a Complex Variable, Oxford University Press, 1935.

5. R. B. Lindsay, Mechanical Radiation, McGraw-Hill, 1960.

6. P. M. Morse, Vibration and Sound, Second Edition, McGraw-Hill, 1948.

7. Wesley Nyborg, "Acoustic Streaming," Physical Acoustics, Vol. II, Part B, edited by Warren P. Mason, Academic Press, 1965.

8. B. E. Noltigk, "The Effects of Intense Ultrasonics in Liquids," Encyclopedia of Physics, Vol. XI/2, Edited by S. Flugge, Springer-Verlag, 1962.

9. D. T. Blackstock, "Propagation of Plane Sound Wave of Finite Amplitude in Nondissipative Fluids," Journal of the Acoustical Society of America, 34, 9-30 (1962).

10. M. J. Lighthill, "Viscosity Effects in Sound Waves of Finite Amplitude," Surveys in Mechanics, edited by G. K. Batchelor and R. M. Davies, Cambridge University Press, 1956.

11. Horace Lamb, The Dynamical Theory of Sound, Page 179, Dover reprint (1960).

12. R. T. Beyer, "Nonlinear Acoustics," Physical Acoustics, Vol. II, Part B, edited by Warren P. Mason, Academic Press, 1965.

13. E. Fubini-Ghiron, "Anomalie nella propagazeone di onda acustiche di grande amprezza (Anomalies in the Propagation of Acoustic Waves of Great Amplitude) Alta Frequenze 4, 530-581 (1935). Translation available from Physics Department, Michigan State University.

14. A. L. Thuras, R. T. Jenkens and H. T. O'Neil, "Extraneous Frequencies Generated in Air Carrying Intense Sound Waves," Journal of Acoustical Society of America, 6, 173-180 (1935).

15. L. J. Black, "A Physical Analysis of Distortion Produced by the Nonlinearity of the Medium," Journal of the Acoustical Society of America, 12, 266-267 (1940).

16. O. H. McDaniel, "Harmonic Distortion of Spherical Sound Waves in Water," Journal of the Acoustical Society of America, 38, 644-647 (1965).

17. Oliver H. McDaniel, "Reply to Comments on 'Harmonic Distortion of Spherical Sound Waves in Water,'" Journal of Acoustical Society of America, 40, 257-258 (1966).

18. D. T. Blackstock, "On Plane, Spherical and Cylindrical Sound Wave of Finite Amplitude in Lossless Fluids," Journal of Acoustical Society of America, 36, 217-219 (1964).

19. Joseph B. Keller and Martin H. Millman, "Finite-Amplitude Sound Wave Propagation in a Waveguide," Journal of Acoustical Society of America, 49, 329-333 (1971).

20. C. Zwikker and C. W. Kosten, Sound Absorbing Materials, Elsevier, 1949.

21. J. S. Pyett, "The Acoustic Impedance of a Porous Layer at Oblique Incidence," Acustica 3, 375 (1953).

22. C. B. Officer, Introduction to the Theory of Sound Transmission, McGraw-Hill, 1958.

23. David A. Bies, "Acoustical Properties of Porous Materials," Chapter Ten in Noise and Vibration Control, edited by Leo L. Beranek, McGraw-Hill, 1971.

24. K. Attenborough, "The Prediction of Oblique-Incidence Behavior of Fibrous Absorbents," Journal of Sound and Vibration, 14, 139-142, (1971).

25. K. Attenborough and L. A. Walker, "Scattering Theory for Sound Absorption in Fibrous Media," Journal of Acoustical Society of America, 49, 1331-1338 (1971).

26. D. J. Sides and K. A. Mulholland, "Variation of Normal Layer Impedance with Angle of Incidence," Journal of Sound and Vibration, 14, 139-142 (1971).

27. V. Twersky, "On Scattering of Waves by Random Distributions. I. Freespace Scatterer Formalism," Journal of Mathematical Physics, 3, 700 (1962).

28. T. F. W. Embleton, "Mufflers," Chapter Twelve in Noise and Vibration Control, edited by Leo L. Beranek, McGraw-Hill, 1971.

29. Theodore J. Schultz, "Wrappings, Enclosures, and Duct Linings," Chapter Fifteen in Noise and Vibration Control, edited by Leo L. Beranek, McGraw-Hill, 1971.

30. R. A. Mangiarotty, "Acoustic-Lining Concepts and Materials for Engine Ducts," Journal of Acoustical Society of America, 48, 783-794 (1970).

31. John M. Seiner, "The Design and Development of a Spinning Mode Synthesizer," M.S. Thesis in Aerospace Engineering, The Pennsylvania State University, September, 1969.

32. W. T. Fiala, J. J. Hilliard, J. A. Renkus, and J. J. Van Houten, "Electropneumatic Acoustic Generator," Journal of the Acoustical Society of America, 30, 956-964 (1965).

33. M. A. Breazeale and Laszlo Adler, "Parametric Oscillations in a Resonant Ultrasonic Wave System," Nonlinear Acoustics, Proceedings of a Conference Held at Applied Research Laboratory, University of Texas, 10-11 November, 1969, AD 719936.

34. W. E. McCluney, "An Investigation of Subharmonic Generation in an Ultrasonic Resonant Cavity," Masters Thesis, Department of Physics, University of Tennessee, 1966.

35. Edward V. Shalis, "Ultrasonic Cavitation Threshold Measurements in an Anechoic Tank," Master's Thesis, Department of Physics, The Pennsylvania State University, 1968.

36. William E. Zorumski and Jean P. Mason, "Multiple Eigenvalues of Sound-Absorbing Circular and Annular Ducts," Journal of the Acoustical Society of America, 55, 1158-1165 (1974).

37. H. Levine and J. Schwinger, "On the Radiation of Sound from an Unflanged Circular Pipe," Phys. Rev., 73, 383 (1948).

38. L. A. Vajnshtejn, "The Theory of Sound Waves in Open Tubes," Zhurnal Tekh. Fiz. 19, 911-930 (1949).

39. D. Lansing, J. Drischler and C. Pusey, "Radiation of Sound from an Unflanged Circular Duct with Flow," Presented at the 79th Meeting of the Acoustical Society of America, April 21-24, 1970.

VITA

Oliver Herbert McDaniel was born [redacted] He graduated from Congers High School in Congers, New York in June, 1952. In January, 1957, he received a B.S. in Electrical Engineering from Clemson University of Clemson, South Carolina and in June, 1966, an M.S. in Physics from Adelphi University of Garden City, New York.

From January, 1957, through December of 1958 Mr. McDaniel was employed as a research engineer with the Republic Aircraft Corporation. From January of 1959 to December of 1963 he was employed as a dynamics engineer for the Grumman Aircraft Engineering Corporation. In January, 1964, he accepted a position as a research assistant at the Applied Research Laboratory of The Pennsylvania State University and in January, 1970, joined the Department of Mechanical Engineering of The Pennsylvania State University as a Research Assistant and currently holds that position.

Mr. McDaniel is a member of the Acoustical Society of America and the Society of Sigma Xi.